THE INFLUENCE OF MULTI-WALLED CARBON NANOTUBES ON SINGLE-PHASE HEAT TRANSFER AND PRESSURE DROP CHARACTERISTICS IN THE TRANSITIONAL FLOW REGIME OF SMOOTH TUBES

Kersten Grote
B.Eng.(Hons.) (Pretoria)

UNIVERSITEIT VAN PRETORIA
UNIVERSITY OF PRETORIA
YUNIBESITHI YA PRETORIA

Thesis submitted to the University of Pretoria in candidature
for the degree of Masters in Engineering

November 2012

Abstract

The influence of multi-walled carbon nanotubes on single-phase heat transfer and pressure drop characteristics in the transitional flow regime of smooth tubes.

Author: Kersten Grote

Supervisor: Prof JP Meyer (University of Pretoria)

Co-supervisor: Dr TJ McKrell (MIT)

Department: Mechanical and Aeronautical Engineering

Degree: Master of Engineering (Mechanical Engineering)

Summery: There are in general two different types of studies concerning nanofluids. The first one concerns itself with the study of the effective thermal conductivity and the other with the study of convective heat transfer enhancement. The study on convective heat transfer enhancement generally incorporates the study on the thermal conductivity. Not many papers have been written on the convective heat transfer enhancement and even fewer concerning the study on multi-walled carbon nanotubes in the transitional flow regime. In this paper the thermal conductivity and viscosity was determined experimentally in order to study the convective heat transfer enhancement of the nanofluids. Multi-walled carbon nanotubes suspended in distilled water flowing through a straight, horizontal tube was investigated experimentally for a Reynolds number range of a 1 000 - 8 000, which included the transitional flow regime. The tube was made out of copper and has an internal diameter of 5.16 mm. Results on the thermal conductivity and viscosity indicated that they increase with nanoparticle concentration. Convective heat transfer experiments were conducted at a constant heat flux of 13 kW/m^2 with 0.33%, 0.75% and 1.0% volume concentrations of multi-walled carbon nanotubes. The nanotubes had an outside diameter of 10 - 20 nm, an inside diameter of 3 - 5 nm and a length of 10 - 30 μm. Temperature and pressure drop measurements were taken from which the heat transfer coefficients and friction factors were determined as a function of Reynolds number. The thermal conductivities and viscosities of the nanofluids were also determined experimentally so that the Reynolds and Nusselt numbers could be determined accurately. It was found that heat transfer was enhanced when comparing the data on a Nusselt number as a function of Reynolds number graph but comparing the results on a heat transfer coefficient as a function of average velocity graph the opposite effect was observed. Performance evaluation of the nanofluids showed that the increase in viscosity was four times the increase in the thermal conductivity which resulted in an inefficient nanofluid. However, a study on the performance evaluation criterion showed that operating nanofluids in the transition and turbulent flow regime due to the energy budget being better than that of the distilled water.

Keywords: Nanofluids, multi-walled carbon nanotubes, transition, convective heat transfer, performance evaluation

PUBLICATIONS IN JOURNALS AND CONFERENCES

Articles in refereed Journals

1. Meyer J.P., McKrell T.J. and Grote K.; The influence of carbon nanotubes on single-phase heat transfer and pressure drop characteristics in the transitional flow regime of smooth tubes, *International Journal of Heat and Mass Transfer*, 58(1-2):597-609, 2013

Conference Papers

1. Meyer J.P. and Grote K.; Nanotubes as heat transfer medium in high performance aerospace heat exchangers, International Aerospace Symposium of South Africa (IASSA), Pretoria, 17 - 18 September 2012.
2. Meyer J.P., Grote K. and McKrell T.J.; Heat transfer characteristics of multi-walled carbon nanotubes in the transitional flow regime, Proceedings of the 3rd International Forum on Heat Transfer (IFHT2012), Nagasaki, Paper no: 9, 13-15 November 2012.

Acknowledgements

The funding obtained from the NRF, TESP, University of Stellenbosch/University of Pretoria, SANERI/SANEDI, CSIR, EEDSM Hub and NAC is acknowledged and duly appreciated.

Contents

List of Figures

List of Tables

Nomenclature

D	Internal diameter of tube	m
L	Length of tube	m
P	Perimeter of tube	m
R	Thermal resistance	°C/W
T	Temperature	°C
$T(x)$	Local temperature	°C
V	Velocity	m/s
ΔP	Pressure drop across the tube	Pa
$\dot{Q}_{in}$	Heat input from heater	W
$\dot{Q}_{water}$	Heat transfer to the water	W
$\dot{m}$	Mass flow rate	kg/s
$\dot{q}$	Heat flux	W/m^2
c_p	Specific heat at constant pressure	J/kg·K
d	Particle diameter	m
f	Darcy-Weisbach friction factor	
h	Convective heat transfer coefficient	W/m^2 °C
$h(x)$	Local convective heat transfer coefficient	W/m^2 °C
k	Thermal conductivity	W/m°C
x	Axial distance	m

Greek Symbols

α	Thermal diffusivity	
δ_t	Thermal boundary layer thickness	
μ	Dynamic viscosity	kg/m·s

ϕ	Volume concentration	
ρ	Density	kg/m^3

Non-dimensional Numbers

Gr	Grashof number
Gz	Graetz number
Nu	Nusselt Number
Pe	Peclet Number
Pr	Prandtl Number
Ra	Rayleigh number
Re	Reynolds Number

Subscripts

avg	Average
b	Bulk
bf	Base fluid
d	Diameter of particle
e	Exit
i	Inlet
lam	Laminar
m	Mean
nf	Nanofluid
p	Particle
si	Inner surface
so	Outer surface
$trans$	Transition
$turb$	Turbulent
w	Wall
x	Local value

Chapter 1

Introduction

1.1 Background

There is an exponential growth in communication, electronics and computing technologies. Together with a steady decrease in their size and an enhanced rate of operation and storage of data, challenges arise in their thermal management. The conventional method is to increase the cooling rate by increasing the heat transfer surface area, but this approach requires, however, an undesirable increase of the thermal management system (Murshed et al., 2011). On a large scale, such as power generation, chemical production, air-conditioning and transportation, one requires more efficient cooling systems with greater cooling capacities and decreased size (Ding et al., 2006; Das et al., 2006). Research is being done on microscale heat transfer; however, the conventional fin-and-microchannel technology appears to be inadequate for next generation technologies (Das et al., 2006).

The low heat transfer performance of conventional fluids such as water, engine oil and ethylene glycol hinders the performance enhancement and the compactness of heat exchangers, since the thermal conductivity of these fluids play an important role on the heat transfer coefficient between the heat transfer medium and the heat transfer surface (Murshed et al., 2011; Trisaksri and Wongwises, 2007; Kakaç and Pramuanjaroenkij, 2009). Thermal conductivity of a fluid plays a vital role in the development of energy-efficient heat transfer equipment, but they have order-of-magnitude smaller thermal conductivity than metallic or nonmetallic particulates. Table 1.1 shows the thermal conductivities of commonly used liquids and materials at room temperature. When comparing the thermal conductivity of water (0.61 W/m·℃) with that of multi-walled carbon nanotubes (MWCNT), the thermal conductivity of the carbon nanotubes (3 000 W/m·℃) is about 5 000 times larger than that of the water.

By the introduction of solid particles, the thermal conductivity of the fluid is improved thereby improving its capability of energy exchange (Trisaksri and Wongwises, 2007; Xuan and Roetzel, 2000). Suspensions of millimeter- or micrometer-sized particles are well known but have not been of interest for practical applications due to erosion, fouling, increased pressure drop and sedimentation of the flow channel (Trisaksri and Wongwises, 2007; Xuan and Roetzel, 2000; Wang and Mujumdar, 2007; Daungthongsuk and Wongwises, 2007; Webb and Kim, 2005). The recent advance in materials technology has made it possible to produce nanometer-sized particles that can overcome these problems. The nanoparticles have a much larger relative surface area,

	Material	k [W/m·℃]			**Material**	k [W/m·℃]
1	Toluene	0.13		12	ZnO	15
2	Engine oil	0.145		13	Al_2O_3	40
3	Kerosene	0.15		14	MgO	43
4	Ethylene glycol	0.25		15	Fe	80.2
5	Water	0.61		16	Si	148
6	SiO_2	1.38		17	Al	237
7	ZrO_2	2		18	Au	317
8	Fe_3O_4	7.2		19	Cu	401
9	TiO_2	8.3		20	Ag	429
10	CeO_2	9		21	SiC	490
11	CuO	13.5		22	MWCNT	3000

Table 1.1: Thermal conductivities (Murshed et al., 2011) of commonly used liquids and materials at room temperature

compared with those of millimeter- or micrometer-sized particles which significantly improves heat transfer capabilities, the stability of the suspension and rheological properties (Yang et al., 2005; Wang and Mujumdar, 2007; Daungthongsuk and Wongwises, 2007). Fluids that have nanometer-sized particles suspended in them are termed "nanofluids" and are deemed the next generation heat transfer fluid (Xuan and Roetzel, 2000; Wang and Mujumdar, 2007). Nanofluids have attracted great interest from the research community due to their enhanced thermal performance and application in numerous fields such as microelectronics, microfluidics, medical and transportation (Murshed et al., 2011).

There are different methods in producing nanoparticles. The first method is primarily used to produce oxide particles, such as Al_2O_3 and CuO, and is called the inert gas condensation process giving particle sizes of 2 - 200 nm. In this process the material is evaporated in a low-density inert gas after which they are condensed and deposited by thermophoretic diffusion on a cold finger. Oxygen is then introduced to produce oxides. The major problem with this method is its tendency to form agglomerates and its unsuitability to produce pure metallic nanopowders (Das and Choi, 2009). Another method is the Laser vapour deposition technique which is used to produce SiC nanoparticles from SiH_4 and C_2H_4. A method for producing reasonable quantities of single walled and multi walled carbon nanotubes is the arc discharge method. This procedure uses a low voltage high current power supply to produce an arc across a 1 mm gap between two graphite electrodes in an inert gas (either He or Ar) atmosphere (O'Connell, 2006). The one electrode evaporates as cations followed by deposition at the cathode. Nanotubes produced by this synthesis method need extensive purification before use. Other methods for producing CNTs is the Laser ablation synthesis, which is similar to the arc discharge method. In order to produce MWCNT the anode is made out of pure graphite. Other methods for producing CNTs is the chemical vapour deposition method, high-pressure carbon monoxide synthesis and the flame synthesis (O'Connell, 2006). Shown in Figure 1.1 is an image of a single walled and multi walled carbon nanotube.

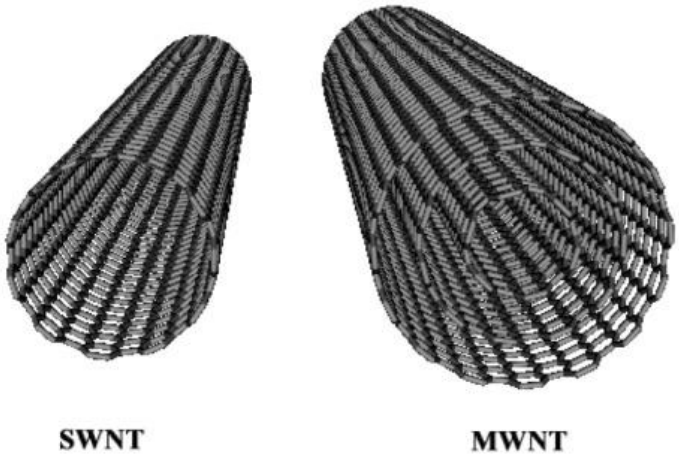

Figure 1.1: Molecular structures of a single-walled carbon nanotube (SWNT) and of a multi-walled carbon nanotube (MWNT)
(From http://www-ibmc.u-strasbg.fr/ict/vectorisation/nanotubes eng.shtml)

Once the particles have been produced the next step is to disburse them in the fluid. There are two ways one can do this, namely the one-step method and two-step method. In the one-step method the problem of agglomeration can be reduced to a good extend by using a direct evaporation condensation method. This is done by condensing the metal vapour directly into a low vapour pressure field. This method is very successful in producing pure Cu nanoparticles (Das and Choi, 2009). The disadvantage of this method is that it is limited to low vapour pressure fields and oxidation of pure metals. But it has excellent control over particle size and gives stable nanofluids (Das and Choi, 2009).In the two-step method the particles are disbursed into the fluid after production and then sonicated together with a surfactant to break up the formed agglomerates and create a stable suspension.

1.2 Previous work

Pak and Cho (1998) did experiments with $\gamma{-}Al_2O_3 - water$ and $TiO_2 - water$ nanofluids for fully turbulent flow and got a 45% enhancement in the heat transfer coefficient with the $\gamma{-}Al_2O_3 - water$ nanofluid at a volume concentration of 1.34% and for the $TiO_2 - water$ nanofluid, a 75% enhancement in the heat transfer coefficient at a volume concentration of 2.78%. But at the same concentration, the heat transfer enhancement for the $TiO_2 - water$ nanofluid was less than that of the $\gamma{-}Al_2O_3 - water$ nanofluid.

Li and Xuan (2002) used $Cu - water$ nanofluid in their experiments and tested in the laminar and turbulent flow regimes. Compared with water, the convective heat transfer coefficient of the nanofluid was increased by about 60% for a volume concentration of 2% for the same Reynolds number.

Wen and Ding (2004) performed experiments at the entrance region under laminar flow condition using $\gamma{-}Al_2O_3 - water$ nanofluids. For a volume concentration of 1.6%, the local heat transfer coefficient was around 45% higher than that of water only. This enhancement decreased

to around 14% further away from the entrance.

Yang *et al.* (2005) did experiments with $graphite - water$ nanofluids under laminar flow conditions. For a 2.5 wt%, they experienced an increase in heat transfer of 22% over the base fluid at a temperature of 50°C and 15% at a temperature of 70°C.

Ding *et al.* (2006) tested *MWCNT-water* nanofluids in the entrance region of laminar flow. They experienced a maximum enhancement in heat transfer of over 350% at a Reynolds number of 800 and an axial distance of approximately 110 times the tube diameter for 0.5 wt% of MWCNTs.

Heris *et al.* (2007) tested $Al_2O_3 - water$ nanofluids under laminar flow range conditions. They had heat transfer enhancement and found that as the particle volume concentration increases so does the enhancement. They tested volume concentrations of 0.2 vol% up to 2.5 vol%.

Murshed *et al.* (2008) did experiments with $TiO_2 - water$ nanofluids under laminar flow conditions. They found for a volume concentration of 0.8 vol% and at position x/D = 25 that the local heat transfer coefficient of the nanofluid was about 12% and 14% higher than deionised water at a Reynolds number of 1 100 and 1 700 respectively.

Garg *et al.* (2009) also tested *MWCNT-water* nanofluids. Their experiment was concerned about the preparation and the enhancement in the laminar flow range using *MWCNT-water* nanofluids. They had a maximum heat transfer enhancement of 32% at a Reynolds number of 600.

Kim *et al.* (2009) used two different nanofluids in their experiments. They tested in the laminar and turbulent flow range. The two nanofluids they used were $\gamma{-}Al_2O_3 - water$ and amorphous carbonic water. In laminar flow, the $\gamma{-}Al_2O_3 - water$ nanofluids had a heat transfer enhancement of around 14% whereas the amorphous carbonic nanofluid showed enhancement of around 7%. In turbulent flow, the $\gamma{-}Al_2O_3 - water$ nanofluids had an increase of around 20% and the amorphous carbonic nanofluid showed no enhancement.

Anoop *et al.* (2009) did experiments with $\gamma{-}Al_2O_3 - water$ nanofluids with different particle sizes in the laminar flow range. They showed that there is larger heat transfer enhancement with a smaller particle size than a larger one. At a Reynolds number of 1 550 for the 45 nm particle size, the enhancement was around 25% whereas for a 150 nm particle size the enhancement was 11%.

Amrollahi *et al.* (2010) did experiments with functionalized MWCNT-water in laminar and turbulent flow at the entrance region. Under laminar flow the heat transfer coefficient is increased by 25% for a concentration of 0.12 wt% at 20C. In the turbulent flow regime the heat transfer enhancement increases between 5-25% for different temperatures and particle concentrations.

Liu and Liao (2010) tested CNT's suspended in an aqueous drag-reducing fluid for the turbulent flow range. At high temperatures the heat transfer enhancement for 1.0 wt% increases by about 40% compared to that of water.

Duangthongsuk and Wongwises (2010) tested $TiO_2 - water$ nanofluids for the turbulent flow

Author	**Flow Range**	**Nanofluid**	**Results**
Pak and Cho (1998)	Turbulent	$\gamma - Al_2O_3 - water$ $TiO_2 - water$	45% enhancement 75% enhancement
Li and Xuan (2002)	Laminar and turbulent	*Cu-water*	60% enhancement
Wen and Ding (2004)	Laminar	$\gamma - Al_2O_3 - water$	45% enhancement for developing flow
Yang *et al.* (2005)	Laminar	*Graphite-water*	22% enhancement at 50°C 15% enhancement at 70°C
Ding *et al.* (2006)	Laminar	*MWCNT-water*	350% enhancement at the entrance region
Murshed*et al.* (2008)	Laminar	$TiO_2 - water$	12% and 14% enhancement at the entrance region
Garg *et al.* (2009)	Laminar	*MWCNT-water*	32% enhancement
Kim *et al.* (2009)	Laminar and turbulent	$\gamma - Al_2O_3 - water$ *A/C-water*	14% enhancement, laminar 7% enhancement, laminar
Anoop *et al.* (2009)	Laminar	$\gamma - Al_2O_3 - water$	25% enhancement for 45 nm 11% enhancement for 150 nm
Amrollahi *et al.* (2010)	Laminar and turbulent	Functionalized *MWCNT-water*	25% enhancement in laminar flow and 2-25% enhancement in turbulent flow
Liu and Liao (2010)	Turbulent	aqueous drag-reducing fluid with CNT	40% enhancement
Duangthongsuk and Wongwises (2010)	Turbulent	$TiO_2 - water$	26% enhancement for 1 vol% -14% enhancement for 2 vol%
Ferrouillat *et al.* (2011)	Turbulent	$SiO_2 - water$	50% enhancement for 18.93 vol%

Table 1.2: Comparison of flow range, type of nanofluid and enhancement of previous work

range. At a volume concentration of 1%, the heat transfer enhancement was approximately 26% whereas at a volume concentration of 2%, the heat transfer enhancement was reduced by 14%.

Ferrouillat *et al.* (2011) tested $SiO_2 - water$ nanofluids for the entire flow range but only considered results for the turbulent flow range. At a volume concentration of 18.9%, the heat transfer enhancement was approximately 50% for a Reynolds number greater than 1 000.

Table 1.2 summarises the previous work found in literature. It shows which flow range was tested in, what type of nanofluid was used and the percentage enhancement in heat transfer over that of the base fluid water.

1.3 Problem statement and objectives

Evaluating the literature shows that there are few works (Pak and Cho, 1998; Li and Xuan, 2002; Wen and Ding, 2004; Ding et al., 2006; Heris et al., 2007; Murshed et al., 2008; Yang et al., 2005; Garg et al., 2009; Kim et al., 2009; Anoop et al., 2009; Amrollahi et al., 2010; Liu and Liao, 2010; Daungthongsuk and Wongwises, 2010) that have reported on convective heat transfer characteristics of nanofluids, especially CNT nanofluids (Ding et al., 2006; Garg et al., 2009; Amrollahi et al., 2010; Liu and Liao, 2010). All of the studies considered in literature either test in the laminar (Li and Xuan, 2002; Wen and Ding, 2004; Ding et al., 2006; Heris et al., 2007; Murshed et al., 2008; Yang et al., 2005; Garg et al., 2009; Kim et al., 2009; Anoop et al., 2009; Amrollahi et al., 2010) or high turbulent flow range (Pak and Cho, 1998; Li and Xuan, 2002; Kim et al., 2009; Amrollahi et al., 2010; Liu and Liao, 2010; Daungthongsuk and Wongwises, 2010) and very few tested in the transitional flow range (Liu and Yu, 2011).

It is normally advised when designing heat transfer equipment to remain outside the transitional flow regime due to the uncertainty and flow instability of this region. Large pressure variations are also encountered in this region since the pressure gradient required to pump the fluid in laminar and turbulent flow could vary by an order of magnitude. As more and more sophisticated heat transfer enhancement techniques are being used in heat exchangers, the mass flow rates have slowly decreased over the years for a specific heat transfer rate and these days a lot of heat transfer equipment has started operating close to or in the transitional flow range. Thus there is a need for more design information in transitional flow. In the recent works of Meyer and Olivier (Olivier, 2009; Olivier and Meyer, 2010; Meyer and Olivier, 2011a,b), the heat transfer coefficients and pressure drops were measured for transitional flow in smooth and enhanced tubes with different types of inlets. They showed that the heat transfer and pressure drop characteristics are stable and that there is a smooth transition from laminar to turbulent flow. They also showed that if heat transfer occurs, the type of inlet has no influence on the heat transfer coefficients, friction factors and on the critical Reynolds number.

However, no work has thus far be conducted to investigate the influence of the use of MWCNTs on single phase heat transfer and pressure drop characteristics in the transitional flow regime of smooth tubes. Therefore, the purpose of this study is to experimentally measure, for a few low concentrations of MWCNTs suspended in water, the heat transfer and pressure drop characteristics of nanofluids in the transitional flow regime in a horizontal smooth tube.

Hence the separate objectives of this study will be:

- to obtain heat transfer coefficient and friction factor data for Reynolds numbers between 1 000 and 8 000 spanning the entire flow range for smooth tubes using water and three different concentrations of *MWCNT-water* nanofluids as the working fluid.
- to develop new heat transfer correlations for the transitional flow regime for smooth tubes using *MWCNT-water* nanofluid as the working fluid.

These objectives will be met by means of an experimental system specifically designed for capturing the required information. The system is designed in such a way that it can accommodate various *MWCNT-water* nanofluid concentrations.

1.4 Layout of thesis

The thesis starts off by looking at the different mechanism of energy transport in nanofluids, followed by a summary of previous literature of convective heat transfer and pressure drop using nanofluids. This forms part of the literature survey in Chapter 2. In Chapter 3 the experimental setup, test section, calibration of instruments are discussed. The method of data reduction, uncertainty analysis of the experimental setup and validation of the test section are discussed in Chapter 4. The preparation and properties of the *MWCNT-water* nanofluids are discussed in Chapter 5. Heat transfer and friction factor results are discussed in Chapter 6 which is followed by the performance evaluation of the *MWCNT-water* nanofluids. The last chapter will contain a summery of the work done and proposed recommendations for future work. Appendix A discusses different experimental setups, from which the current setup is based. Appendix C looks at the different preparation methods of nanofluids and Appendix D discusses the properties of water and nanofluids as found in literature. Appendix B gives the full uncertainty analysis of the heat transfer coefficients and friction factors of water.

Chapter 2

Literature study

2.1 Introduction

The chapter starts off with a literature review on transitional flow where water is used as the working fluid after which the different energy modes in nanofluids are discussed. First the enhancement in the thermal conductivity is explored followed by the influence it has on the enhancement in convective heat transfer. Studies found in literature on convective heat transfer enhancement follow in the next section after which the pressure drop in nanofluids is discussed. This chapter ends with a summery on the convective heat transfer enhancement using nanofluids.

2.2 Transitional flow in horizontal smooth tubes

It generally is accepted that the onset of transitional flow in horizontal smooth tubes starts at Reynolds number of about 2 300 (Olivier and Meyer, 2010). Although this is an accepted value the onset of transition generally depends on the inlet condition used.

Tam and Ghajar (1997) did experimental work in the transitional flow regime for smooth horizontal tubes with three different inlet configurations. They discovered that the transitional flow range depends on the inlet configuration. For isothermal flow the transitional flow range for a reentrant inlet configuration is for a Reynolds number range of 2 870 - 3 500, for a square-edged inlet configuration the range is 3 110 - 3 700 and for a bell-mouth inlet configuration the range is 5 100 - 6 100. When considering the effect of heating, the onset of transition is delayed due to the stabilising effect that heating has on the flow.

Heat transfer results by Ghajar and Tam (1994) showed that secondary flow effects had an influence on the transitional flow regime. The onset of transition for the reentrant inlet configuration started at a Reynolds number of 2 000 and stayed constant throughout the length of the tube. The end of the transition varied from a Reynolds number of 6 400 near the inlet, to 8 000 near the exit of the tube. For the square-edged inlet configuration the onset of transition started at a Reynolds number of 2 200 and stayed constant throughout the length of the tube. The end of transition varied from a Reynolds number of 7 500 near the inlet, to 8 100 near the exit of the tube. The onset of transition for the bell-mouth inlet configuration varied from a Reynolds number of 3 800 near the inlet, to 3 900 near the exit of the tube. The end of the transition

varied from a Reynolds number of 9 500 near the inlet, to 10 000 near the exit of the tube. This variation from inlet to outlet is due to the variation in fluid properties. Since the tube was heated the fluid was heated along the axial length with the effect of viscosity decreasing and hence an increase in Reynolds number.

Adiabatic results by Olivier and Meyer (2010) also show that different inlets delay the onset of transition. For the reentrant inlet condition, transition appeared to differ very little from the fully developed value, while the square-edged and bell-mouth inlet conditions delayed the onset of transition quite considerably. There was also a difference in the delay of transition for the bell-mouth inlet when considering two different tube sizes in that the larger tube delays the transition more than the smaller one. The possible reason for the difference is that the bell-mouths had different contraction ratios for each tube and they were manufactured at different dates. This could mean that their internal roughness might have been different due to different manufacturing techniques, which has an effect on transition.

The reason for the delay in transition when considering different inlet conditions is due to the amount of turbulence that the different inlets generate. Heat transfer results indicated, however, that transition is independent of the type of inlet used. The effect of heat transfer, which induces secondary flows, actually dampens the effect of the turbulence generated at the inlet, thus almost nullifying its presence. Also the transition from laminar to turbulent flow happens much smoother than it does for the adiabatic case.

In a recent study by Ghajar *et al.* (2010) they tested the effect of the friction factor in the transitional flow regime for water in 12 different mini-and microtubes. The results showed that for a tube range of 2 083 - 838 μm the onset of transition increased from a Reynolds number of 1 500 for a tube diameter of 2 083 μm, to a Reynolds number of 2 200 for a tube diameter 838 μm. The end of transition for the that specific tube range stayed constant at a Reynolds number of 4 000.

For a tube range of 732 - 337 μm the onset of transition decreased from a Reynolds number of 2 300 for a tube diameter of 732 μm, to a Reynolds number of 1 300 for a tube diameter of 337 μm. The end of transition also shifted to a lower Reynolds number. For the tube diameter of 732 μm the end of transition was at a Reynolds number of 3 000 and for a tube diameter of 337 μm the end of transition was at a Reynolds number of 1 700. The reason for the shift in transition to lower Reynolds numbers for the tube range of 732 - 337 μm is that the surface roughness may be beginning to influence the friction factor. They suggested that the onset of transition in mini-and microtubes is due to the relative roughness of the tubes, which lowers the Reynolds numbers for the onset of transition.

The early onset of transition was also experienced by Meyer and Olivier (2011a; 2011b). They did experimental work in the transitional flow regime using enhanced tubes. The results indicated when using the enhanced tubes that the onset of transition shifts to lower Reynolds numbers due to the fin-height-to-diameter ratio. With the imposed roughness in the tubes a secondary transition occurred between a Reynolds number of 3 000 and 10 000. This secondary transition was explained by the effective rotation the fins bring about the fluid. When considering heat transfer, transition appeared to occur at roughly the same Reynolds numbers which was in agreement with their previous study using different inlet geometries (Olivier and Meyer, 2010). This was due to the secondary flow which influences the growing boundary layer to such an extent that it negates any disturbance of the inlet. It was also observed that the roughness

during heat transfer had little or no effect on the transition region.

2.3 Different modes of energy transports in nanofluids

There are two different types of studies concerning nanofluids. The first one concerns itself with the study of the effective thermal conductivity and the other with the study of convective heat transfer enhancement. In the study of the effective thermal conductivity, correlations are developed for the thermal conductivity, which are then used in the study of heat transfer enhancement. The thermal conductivity of the nanofluid is a function of both the thermal conductivity of the nanoparticle and base fluid as well as the volume fraction, surface area, shape of the nanoparticle, the distribution of the dispersed particles and the thermal conductivity of the nanolayer (Kakaç and Pramuanjaroenkij, 2009; Xuan and Roetzel, 2000). The heat transfer coefficient of the nanofluid depends upon a number of factors such as thermal conductivity and heat capacity of the base fluid and nanoparticles, the flow pattern, the viscosity of the nanofluid, the volume fraction of the suspended particles, the dimensions and the shape of these particles as well as on the flow structure (Xuan and Roetzel, 2000). The methods, which are mentioned above, consider the nanofluid as a single phase fluid. The size of the dispersed particles presents some difficulty in analysing the interaction between the fluid and the solid particles during heat transfer (Kakaç and Pramuanjaroenkij, 2009).

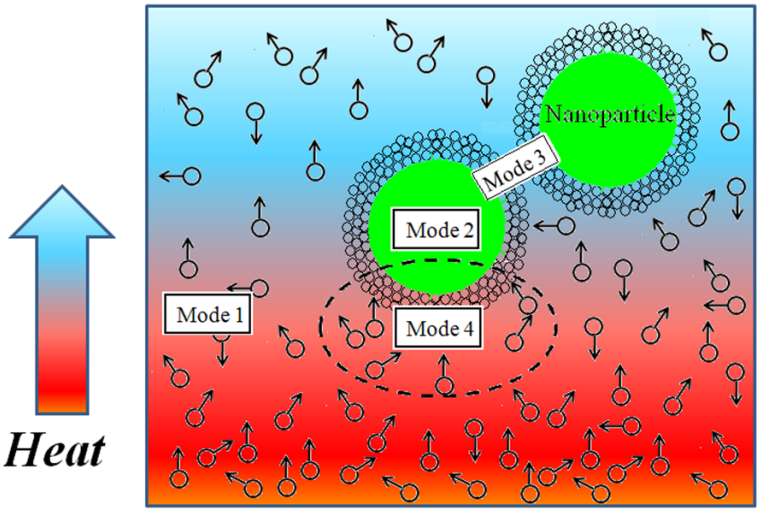

Figure 2.1: Modes of energy transport in nanofluids

Jang and Choi (2004) derived four modes of heat transport in nanofluids as shown in Figure 2.1. The first mode of heat transport is the collision between base fluid molecules, which physically represents the thermal conductivity of the base fluid. The second mode is the thermal diffusion in nanoparticles. The thermal diffusion is carried by phonon's which are created at random, propagate in random directions through the particles and are scattered by each other or by defects in the particles, thus justifying the macroscopic description of heat transport (Keblinski et al., 2002). The third mode is Brownian motion, which is the collision between nanoparticles. This enables direct solid to solid transport of heat from one to another, but it is a very slow process and can be neglected (Jang and Choi, 2004; Keblinski et al., 2002). Brownian motion could, however, have an important indirect role in producing particle clustering which significantly could enhance the thermal conductivity, since the particles are much closer together and thus enhance consistent phonon heat transfer among the particles (Keblinski et al., 2002). The last mode is the thermal interactions of the nanoparticles with the base fluid molecules, which translates into conduction at the macroscopic level. Hence the nanolayer that forms, works as a thermal bridge between the liquid base fluid and the solid nanoparticles and this will enhance the effective thermal conductivity (Kakaç and Pramuanjaroenkij, 2009).

2.4 Convective heat transfer in nanofluids

Pak and Cho (1998) performed experiments on $\gamma{-}Al_2O_3 - water$ and $TiO_2 - water$ for five different volume concentrations ranging from 1.0% - 10% for both nanofluids. The Reynolds number and Prandtl number range was from $10^4 - 10^5$ and $6.5 - 12.3$ respectively. They investigated the hydrodynamic and convective heat transfer characteristics of the nanofluids. The convective heat transfer coefficient increased with increasing Reynolds number and volume concentration. The enhancement for the $TiO_2 - water$ nanofluid was less than for the $\gamma{-}Al_2O_3 - water$ nanofluid at the same volume concentration. They found that the percentage increase in the convective heat transfer coefficient was much greater then the percentage increase for the effective thermal conductivity at the different volume concentrations. The reason for this was attributed to the enhanced mixing caused by the submicron particles near the walls. Equation 2.1 was developed, with a maximum deviation of 4.8%, by curve fitting the experimental data.

$$Nu_{nf} = 0.021 Re^{0.8} Pr^{0.5} \tag{2.1}$$

Xuan and Li (2000) developed, through numerical analysis, a correlation (Equation 2.2) for a constant wall temperature boundary condition.

$$Nu_{nf} = \frac{\Sigma_{m=1}^{\infty} X(\bar{x})/[X(0) - X'(0)/Pe^*]}{\Sigma_{m=1}^{\infty}[X(\bar{x})/[X(0) - X'(0)/Pe^*]]/\beta_m^2} \tag{2.2}$$

where

$$X(\bar{x}) = m_2 e^{m_2 + m_1 \bar{x}} - m_1 e^{m_1 + m_2 \bar{x}}$$

$$X'(\bar{x}) = m_1 m_2 (e^{m_2 + m_1 \bar{x}} - e^{m_1 + m_2 \bar{x}})$$

$$m_{1,2} = \frac{Pe^* \pm \sqrt{Pe^{*2} + 4\beta_m^2 (L/R)^2}}{2}$$

The eigenvalues β_m are determined from the following equation:

$$J_0(\beta_m)$$

also L and R are the length and radius of the tube respectively.

The enhanced performance of the nanofluid results from not only its high thermal conductivity but also from the chaotic movement of the particles which increases the effect of thermal dispersion, i.e. energy exchange rates are increased in the fluid. The introduction of the Peclet number is there to describe such effects of thermal dispersion caused by the microconvective and microdiffusion of the suspended nanoparticles (Xuan and Li, 2003). The Peclet number is defined as

$$Pe_d = \frac{V_{avg} d_p}{\alpha_{nf}} \tag{2.3}$$

where the thermal diffusivity is given by

$$\alpha_{nf} = \frac{k_{nf}}{(\rho c_p)_{nf}} \tag{2.4}$$

Xuan and Roetzel (2000) came up with the general form of the Nusselt number:

$$Nu_{nf} = f\left(Re, Pr, \frac{k_p}{k_{bf}}, \frac{(\rho c_p)_p}{(\rho c_p)_{bf}}, \phi, dimensions\, and\, shape\, of\, particles,\ flow\, structure\right)$$

The objective of their study was to derive a correlation for predicting convective heat transfer of nanofluids with two different approaches. The one approach is to consider the nanofluid as a single-phase fluid and the other approach is to consider it as a two-phase fluid. In the single-phase fluid approach, one assumes that there exists no motion slip between the ultra fine particles ($<$ 100 nm) and the base fluid and the local thermal equilibrium between the nanoparticles and the base fluid is upheld (Xuan and Roetzel, 2000). This means all equations of continuity, motion and energy for the base fluid can also be used for the nanofluid. The thermal properties though are those of the nanofluid. The increase in the heat transfer rate can be approximated by the following ratio:

$$\frac{h_{nf}}{h_{bf}} \approx \left(\frac{k_{nf}}{k_{bf}}\right)^c$$

where the exponent c is a constant which depends on the flow pattern. In the two-phase fluid approach several factors such as gravity, Brownian diffusion and friction force between the base fluid and nanoparticles may coexist in the main flow of the nanofluid. This means that the slip velocity between the base fluid and the particles may not be zero. Chaotic movement of the particles increases the effect of thermal dispersion. Thermal dispersion flattens the temperature distribution and makes the temperature gradient between the base fluid and wall steeper, which increases the heat transfer rate between the fluid and the wall (Xuan and Roetzel, 2000). A correlation, which is shown in Equation 2.5 was developed by taking the thermal dispersion into account.

$$Nu_{nf} = [1 + C^* Pe^n f'(0)]\theta'(0) Re^m \tag{2.5}$$

where the exponent m and n depend on the flow pattern and C^* is an unknown constant which should be determined by matching experimental data. The case of $C^* = 0$ corresponds to zero thermal dispersion. f and θ are the dimensionless velocity and dimensionless temperature respectively. Equation 2.5 indicates that the heat transfer enhancement of the nanofluid increases with an increase in the Peclet number.

Li and Xuan (2002) performed experiments for a *Cu-water* nanofluid in the laminar and turbulent flow regime for volume concentrations of 0.3%, 0.5%, 0.8%, 1.0%, 1.2%, 1.5% and 2.0%.

The Reynolds number range that they tested was from 800 - 25 000. They discovered that the nanofluid behaves more like a two-phase fluid, since the thermal dispersion plays an important role in the heat transfer enhancement. Hence experimental data is correlated by using the two-phase flow methodology presented by Xuan and Roetzel (2000). They proposed Equation 2.6 to correlate the experimental data for the nanofluid, under a constant heat flux boundary condition.

$$Nu_{nf} = c_1(1 + c_2\phi^{m_1}Pe_d^{m_2})Re^{m_3}Pr^{0.4} \tag{2.6}$$

The case of $c_2 = 0$ refers to zero thermal dispersion, which corresponds to the case of a pure base fluid. By fitting the experimental, the constants m_1, m_2, m_3 can be determined. Two correlations were developed for laminar (Equation 2.7) and turbulent (Equation 2.8) flow:

- for laminar flow

$$Nu_{nf} = 0.4328(1 + 11.285\phi^{0.754}Pe_d^{0.218})Re^{0.333}Pr^{0.4} \tag{2.7}$$

- for turbulent flow

$$Nu_{nf} = 0.0059(1 + 7.6286\phi^{0.6886}Pe_d^{0.001})Re^{0.9238}Pr^{0.4} \tag{2.8}$$

Xuan and Li (2003) studied the heat transfer performance of single-phase flow, *Cu-water* nanofluid, in tubes for the turbulent flow regime (10 000 < Re < 25 000) and for volume concentrations of 0.3%, 0.5%, 0.8%, 1.0%, 1.2%, 1.5% and 2.0%. They based their correlation on the one developed by Li and Xuan (2002) which is shown in Equation 2.6. Here again the case of $c_2 = 0$ refers to zero thermal dispersion, which corresponds to the case of a pure base fluid. By fitting the experimental data the following correlation (Equation 2.9), for a constant heat flux boundary condition, was developed:

$$Nu_{nf} = 0.0059(1 + 7.6286\phi^{0.6886}Pe_d^{0.001})Re^{0.9238}Pr^{0.4} \tag{2.9}$$

Wen and Ding (2004) performed experiments on $\gamma - Al_2O_3 - water$ nanofluids at constant heat flux boundary conditions for a Reynolds number range of 500 - 2 100 and for volume concentrations of 0.6%, 1.0% and 1.6%. The focus on the study was in the entrance region. The results show that the use of nanofluids significantly improves the convective heat transfer, especially at the entrance region and at higher Reynolds numbers. The local heat transfer coefficient can be approximated by k/δ_t, where δ_t is the thickness of the thermal boundary layer. Hence an increase in k and/or decrease in δ_t increases the convective heat transfer coefficient. A large enhancement in the heat transfer coefficient can be attributed to a decrease in the thermal boundary layer. One possible reason for the decrease of the thermal boundary layer is particle migration in nanofluids due to shear action, viscosity gradient and Brownian motion in the cross-section of the tube. Particle migration is expected to be more significant in the entrance region due to a larger velocity gradient. The non-uniform particle concentration also has an influence on the local thermal conductivity and viscosity, which results in a higher Nusselt number.

Yang *et al.* (2005) did experimental work under a constant heat flux boundary condition and

a laminar Reynolds number range of 5 - 110 for a 2% weight concentration *graphite-water* nanofluid. They discovered that the increase in the heat transfer coefficient of the nanofluid is much less than that predicted from a conventional correlation. They suspect that as the nanofluid is heated, the fluid viscosity decreases and the velocity profile ceases to be parabolic. As the shear rate changes, the nanoparticles align with the velocity. This can decrease the thermal conductivity of the fluids if the nanoparticle-nanoparticle interactions responsible for the enhanced heat transfer are disrupted. Another possible reason is the reduction of particles in the near-wall fluid phase, which leads to a lower thermal conductivity layer near the wall. Equation 2.10 was developed from their experimental work.

$$Nu_{nf} = 1.86 Re^{1/3} Pr^{1/3} (D/L)^{1/3} (\mu_b/\mu_w)^{0.14} \tag{2.10}$$

Maiga *et al.* (2006) did numerical work on $\gamma - Al_2O_3 - water$ nanofluids in the turbulent flow regime. The Reynolds number range was between $10^4 - 5 \cdot 10^5$ and a constant heat flux boundary condition was enforced. The volume concentrations that were tested, were 1%, 2.5%, 5%, 7.5% and 10%. In their work they assumed negligible motion slip as well as the thermal equilibrium between the phases. The nanofluid mixture may then be considered as a single-phase fluid. Hence a classical theory that is developed for a conventional single phase fluid can be applied to a nanofluid. This assumption is of course only valid if particle suspension is assured and that the spatial distribution can approximately be considered as uniform. They developed Equation 2.11 which exhibits maximum, mean and a standard deviation of relative error of 19%, 12% and 6% respectively.

$$Nu_{nf} = 0.085 Re^{0.71} Pr^{0.35} \tag{2.11}$$

Heris *et al.* (2006) performed experiments with *CuO-water* and $Al_2O_3 - water$ nanofluids in the laminar flow regime for volume concentrations ranging from 0.2 - 3.0%. The Reynolds number range was set between 650 - 2 050 and the tests were performed under a constant wall temperature boundary condition. Results indicated that the heat transfer enhancement for the $Al_2O_3 - water$ nanofluid was higher than that of the *CuO-water* nanofluid, even though *CuO* nanoparticles have a higher thermal conductivity. This is due to the large *CuO* particle size and high viscosity of the *CuO-water* nanofluid, which both affect the heat transfer coefficient. Therefore increasing the heat transfer rate is not only dependent on the thermal conductivity but also on the dispersion and chaotic movement of nanoparticles, Brownian motion, particle migration and the viscosity of the nanofluid. Chaotic movement and fluctuations of the nanoparticles, especially near the tube wall, leads to an increase in the energy exchange rate and increases the heat transfer rate between fluid and tube wall.

Ding *et al.* (2006) concerned themselves with the convective heat transfer of suspensions of MWCNTs for volume concentrations of 0.1%, 0.25% and 0.5%. They performed the experiments for a Reynolds number range of 800 - 1 200 under a constant heat flux boundary condition. Results indicate that there is a significant increase in the heat transfer rate with the presence of MWCNT and the increase is more considerable at high MWCNT concentrations. They discovered that there are a few possible reasons for the enhancement of the heat transfer rate. Firstly, the large enhancement may be attributed to a decrease in the thermal boundary layer thickness or an increase in the effective thermal conductivity. Secondly, MWCNT nanofluids exhibit a significant shear thinning behaviour so the effective thermal conductivity under dynamic shear conditions may therefore be higher than the measured effective thermal conductivity under static

conditions. Thirdly, MWCNT are likely to form structures which have an effective particle size much larger than the volume based equivalent particle diameter. This leads to a high Peclet number and a significant further enhancement on the thermal conduction. Fourthly, the presence of MWCNTs affects the development of the boundary layer. It is suggested that the delay in the boundary layer development is a mechanism for heat transfer enhancement in particulate flows. The fifth reason is the particle re-arrangement due to non-uniform shear-rate across the tube cross-section. Lastly, there is a high heat transfer enhancement due to the high aspect ratio of the MWCNTs.

Williams *et al.* (2008) did experiments with $Al_2O_3 - water$ and $ZrO_2 - water$ nanofluids in a horizontal tube for Reynolds number ranges of 9 000 - 63 000. They tested particle concentrations of 0.9 - 3.6 vol% and 0.2 - 0.9 vol% for Al_2O_3 and ZrO_2 respectively and the results were compared with predictions made using the traditional single-phase heat transfer correlations for fully developed turbulent flow. They observed no abnormal heat transfer enhancement and found that convective heat transfer behaviour of nanofluids can be predicted by means of the traditional correlations and models, as long as the effective nanofluid properties are used. Therefore using nanofluids as enhanced coolants depend largely on the trade-off between increase in thermal conductivity and increase in viscosity.

Kim *et al.* (2009) did convective heat transfer tests with two different types of nanofluids. An $Al_2O_3 - water$ nanofluid, which had a volume concentration of 3%, was produced with the two-step method whereas the amorphous carbonic nanoparticle laden *(A/C)-water* nanofluid, which had a volume concentration of 3.5%, was produced by the one-step method. They performed the tests under a constant heat flux boundary condition for a Reynolds number range of 800 - 6 500. Results show that there was a significant increase in the effective thermal conductivity of the $Al_2O_3 - water$ nanofluid whereas no significant increase was seen with the *(A/C)-water* nanofluid. They gave two reasons for the convective heat transfer enhancement of nanofluids: thermal conductivity enhancement and the delaying and disturbance of the thermal boundary layers. In the laminar flow regime there was an increase in the heat transfer coefficient for both nanofluids, whereas in the turbulent flow regime only the $Al_2O_3 - water$ nanofluid showed an increase in the convective heat transfer coefficient. The reason for this is that in the laminar flow regime the changes of the boundary layer had a much more dominant effect on enhancing the convective heat transfer than the thermal conductivity, hence why both nanofluids showed an increase in the convective heat transfer coefficient. In the turbulent flow regime the enhancement of the thermal conductivity played a much more important role in enhancing the convective heat transfer, hence why only the $Al_2O_3 - water$ nanofluid showed an increase in the convective heat transfer coefficient.

Anoop *et al.* (2009) tested the effect of particle size on the heat transfer with an $Al_2O_3 - water$ nanofluid. The Reynolds number range they tested was from 500 - 2 000 and a constant heat flux boundary condition was used. The particle sizes were 45 nm and 150 nm and tested concentrations were 1 wt%, 2 wt%, 4 wt%, 6 wt%. From the viscosity and thermal conductivity measurements it was discovered that as the particle size decreased the effective thermal conductivity increases. The viscosity is the same for both particle sizes at low concentrations but at higher concentrations the viscosity increases sharply for the smaller particle size. It was shown that the $Al_2O_3 - water$ nanofluid has a higher heat transfer coefficient as compared with the base fluid. Furthermore, it was found that the smaller particle size has a greater magnitude of enhancement as compared with the larger particle size. They concluded that the enhancement

of heat transfer was due to particle migration effects and/or thermal dispersion and not solely due to the thermal conductivity enhancement. The following correlation was developed for the entrance region, since the highest heat transfer enhancement was observed in the entrance region:

$$Nu_x = 4.36 + \left[a \cdot x_+^{-b} \cdot (1 + \phi^c) \cdot exp(-d \cdot x_+^{-b})\right] \cdot \left[1 + e \cdot \left(\frac{d_p}{d_{ref}}\right)^{-f}\right] \tag{2.12}$$

where

$$x_+ = \frac{x}{D \cdot Re \cdot Pr}$$

and also $a = 6.219 \cdot 10^{-3}$, $b = 1.1522$, $c = 0.1533$, $d = 2.5228$, $e = 0.57825$, $f = 0.2183$ and $d_{ref} = 100$ nm.

Garg *et al.* (2009) did experimental work under a constant heat flux boundary condition. *MWCNT-water* was the working fluid, with a nanoparticle weight concentration of 1%, and they tested three different Reynolds numbers (600, 900 and 1 200). Experimental work was focused on the sonication time when preparing the nanofluid and it was found that there is an optimal sonication time for a certain nanofluid concentration which has an effect on the heat transfer enhancement. They found that the viscosity decreases with shear rate and thermal conductivity of *MWCNT-water* nanofluids increases with temperature. This leads to a non-uniform viscosity and thermal conductivity enhancement in the radial direction which results in a higher heat transfer coefficient. Another reason for enhancement is that fluids who exhibit shear thinning behaviour have a higher heat transfer then fluids that do not exhibit it. Since CNT-based nanofluids exhibit a shear thinning behaviour it is possible that it is a major mechanism behind the high heat transfer enhancement.

Amrollahi *et al.* (2010) studied the effects of water based functionalized MWNT on the heat transfer. They tested four different mass fractions (0.1 wt%, 0.12wt%, 0.2wt% and 0.25wt%) under constant heat flux boundary condition. The three Reynolds numbers tested were 1 592, 3 490 and 4 778. Results showed that the suspended particles enhance the convective heat transfer coefficient by about 25% for laminar flow and in turbulent flow between 2-25%. The enhancement in the heat transfer coefficient, in turbulent flow, decreases with increasing temperature. At 33°C, for a Reynolds number of 4 778 the enhancement is only 2% whereas at 20°C the enhancement is 25%. This was attributed to (1) in turbulent flow there is not enough time to better heat transfer between nanofluid and heater, (2) in high temperature the agglomeration happen more rapidly than low temperature, and (3) depletion of particles in the near-wall fluid phase

Liu and Liao (2010) did experimental work on an aqueous drag-reducing fluid with carbon nanotubes added. 1 wt% to 4.0 wt% of CNT were suspended in an alkali/deionized water mixture. They tested under a constant heat flux boundary condition for a Reynolds number range from 3 000 to 50 000. For CNT suspended in deionized water, the results indicate that with increase in nanoparticle concentration and fluid temperature the convective heat transfer coefficient is enhanced. Due to the nature of the experimental results, the heat transfer characteristics of the nanofluid can be treated as conventional fluid and predicted by conventional correlations when both the fluid temperature and the CNT mass concentration are comparatively low. The nanometer effect will appear with both the increase of CNT mass concentration and the fluid temperature. A high fluid temperature accelerates the irregular heat movement

(Brownian movement) of nanoparticles in the base fluid. The collision between the nanoparticles and the base fluid get much more intense, which makes more effective enhancing efficiency in the heat transfer of the nanofluid.

Duangthongsuk and Wongwises (2010) tested five samples of $TiO_2 - water$ nanofluids, with volume concentrations ranging from 0.2% to 2.0%. They did their experimental work for Reynolds number range of 3 000 to 18 000. They discovered that the Nusselt number of nanofluids is higher than that of water for volume concentrations less then 1.0 vol%. For a volume concentration of 2.0% the heat transfer coefficient was 14% smaller than that of water. The reason for the decrease in heat transfer performance is that the effect of the viscosity increase overcomes the effect of the thermal conductivity enhancement. This is due to the fact that an increase in viscosity of the fluid leads to an increase in the boundary layer thickness, which results in a decrease in the heat transfer performance. Another reason for the decrease in the heat transfer performance is that at higher volume concentrations the particles may combine together, which causes the overall size to become bigger and leads to a lower heat transfer rate. They proposed the following equation for predicting the heat transfer coefficient of nanofluids for a volume concentration of less than 1.0%

$$Nu_{nf} = 0.074 Re_{nf}^{0.707} \cdot Pr_{nf}^{0.385} \cdot \phi^{0.074} \tag{2.13}$$

Liu and Yu (2011) studied $\gamma - Al_2O_3 - water$ nanofluids in the transitional flow regime under a constant heat flux boundary condition. The tests were done for a Reynolds number range of 600 - 4 500 and four nanofluid volume concentrations of 1%, 2%, 3.5% and 5%. The results indicate that heat transfer is enhanced in the laminar flow regime. They discovered that in the transition and the early stages of fully developed turbulent flow that presence of nanoparticles causes a deterioration of the heat transfer compared with water. This was due to the suppression of turbulence. In the fully turbulent flow the difference in the measured Nusselt number between nanofluids and water tends to diminish as a result of the alleviated suppression of turbulence. They suggested that nanofluids should be operated in either the laminar region or the fully developed turbulent region with sufficiently high Reynolds numbers for the sake of enhanced heat transfer performance.

Ferrouillat *et al.* (2011) did experimental work on $SiO_2 - water$ nanofluids for three different volume concentration of 2.3%, 7.95% and 18.93%. The tests were done for a Reynolds number range of 200 - 10 000 under a constant wall boundary condition for heating and cooling. They observed that for the turbulent regime there was significant enhancement for the Nusselt number compared with the base fluid. Also as the volume concentration increased so did the enhancement in heat transfer. They split up their results into three different part. The first part was the turbulent flow regime which started at a Reynolds number of a 1 000. The reason for the early start of turbulence is due to the fact that they inserted thermocouples into the flow. The second part was characterised as the laminar flow regime and its flow range was from 200 $<$ Re $<$ 1 000. The last part was for Reynolds numbers less than 200. In this flow range the heat transfer results showed longitudinal conduction effects. They observed large scattering in their results for Reynolds numbers less than 1 000 and hence only considered the fully turbulent flow regime in their analysis. When considering the heating and cooling effect on nanofluids it was observed that the cooling condition resulted in equal or better heat transfer performance characteristics than the heating condition. Like Williams *et al.* (2008) they also observed that the heat transfer can be predicted by using conventional heat transfer correlations.

2.5 Friction factors of nanofluids

In the pressure drop experiment by Pak and Cho (1998) they only used dilute concentrations (< 3 vol%) from a practical point of view. They found that the friction factors coincide well with Kays' prediction regardless of the volume concentration, implying that the pumping power can be estimated well with a well-known correlation if the volume concentration of the particles is less then 3%. Also the effect of particle size on the friction factor was not seen with two different particle sizes as long as the volume concentration was less then 3%.

Li and Xuan (2002) and Xuan and Li (2003) used four samples of nanofluids of volume fractions of 1%, 1.2%, 1.5% and 2.0%. They discovered that for the dilute nanofluids there was no significant augmentation in pressure drop as compared with water. This implies that the friction factor correlation for the single-phase flow can be extended to the dilute nanofluids.

Ko *et al.* (2007) performed adiabatic experiments with *MWCNT-water* nanofluid for a Reynolds number range of 1 000 - 100 000 and a volume fraction ranging from 0.06% - 0.22%. They used two different methods in preparing the nanofluids. The one method was to use a surfactant, sodium dodecyl sulfate, in conjunction with MWCNT and then sonicate the mixture to make a well-dispersed and homogenous suspensions. They referred to this type of nanofluid as the pristine CNT nanofluid. In the other method they treated the MWCNT with nitric/sulphuric acid. This method attaches hydrophilic functional group onto the surface of the CNTs. The treated CNTs were then added into distilled water and sonicated to produce a well-dispersed and homogenous suspensions.

The results from the viscosity measurement indicate that at a given shear rate the viscosity of the pristine CNTs nanofluid increases with increasing CNT volume fraction. What is also observed is the shear thinning behaviour of the nanfluids. The CNT, which are initially entangled, are rearranged along the flow direction under the shear stress and consequently the viscosity of the solution decreases with shear rate. Another observation that was made is that at a given shear rate the viscosity of the treated CNTs is lower then that of the pristine CNTs. The reason for this is that the acid soften the CNTs making them more flexible. When looking at the friction factor of the two different types of nanofluids it is observed that treated CNTs in laminar flow show only a slight increase in friction factor as compared with water where as the pristine CNTs have a much large increase. The friction factor for both methods also increase with increasing volume concentration in laminar flow. In turbulent flow both types of nanofluids tend towards the friction factor of the distilled water. This is due to the viscosity decreasing under high shear loads.

Williams *et al.* (2008) found that there was an increase in viscosity as the particle loading increased, they also noted that the viscosity ratio μ_{nf}/μ_{bf} is independent of the temperature. The friction factor results were compared against predictions of theory which is either determined from the Blasius relation for a Re $< 30\ 000$

$$f = 0.316Re^{-0.25} \tag{2.14}$$

or the McAdams relation for a Re $> 30\ 000$

$$f = 0.184Re^{-0.2} \tag{2.15}$$

The temperature- and loading-dependent measured properties of the specific nanofluid were used and it was found that theory predicted the results to within $\pm 20\%$.

Duangthongsuk and Wongwises (2010) tested five nanofluid samples under turbulent flow conditions. Results show that the pressure drop and friction factor of the nanofluids increase with an increase in Reynolds number and that there is a small increase with increase in particle concentrations. They developed a new correlation to predict the friction factor of nanofluids

$$f_{nf} = 0.961\phi^{0.052} \cdot Re^{-0.375} \tag{2.16}$$

Liu and Yu (2011) firstly discovered that the friction factor for nanofluids in laminar flow shows an increasing trend with the volume concentration and is generally higher than that of pure water at the same Reynolds number. Secondly, the entrance region in nanofluids is prolonged due to the shear-induced nanoparticle migration which results in a maximum concentration of particles at the centerline of the tube and decreasing concentration towards the wall. Hence the local viscosity of the nanofluid is greater in the centerline region than in the near-wall region, this results in a non-parabolic velocity profile. The profile is flattened at the centre with a steeper gradient near the wall, which is interpreted as a prolonged entrance region effect in nanofluids. Thirdly, the onset of transition to turbulence is delayed in nanofluids. At the onset of transition the friction factor falls below that of water and persists until fully developed turbulence begins after which the data for both nanofluids and water collapse together. This phenomenon can be described by the fact that the addition of small particles can modify the turbulent structures by changing the turbulent kinetic energy of the base fluid. The changes in the turbulent structure depend on the Kolmogorov microscale. The Kolmogorov microscale represents the finest structure in turbulence at which the kinetic energy, η, is dissipated by viscosity and can be estimated as:

$$\eta \approx \frac{\nu}{u_\tau^2} \tag{2.17}$$

where the wall shear velocity u_τ is defined as $u_\tau = \sqrt{\tau_w/\rho_f}$, ν is the kinematic viscosity, τ_w is the shear stress of the fluid evaluated at the wall and ρ_f is the density of the fluid. The critical parameter, which is defined as $d_p/\eta \approx 0.1$ for gas-solid flows, shows that the turbulence intensity is enhanced for values above the critical value and reduced for values below. A smaller critical value is expected for liquid-solid flows where the interaction between the liquid and solid particles is much more intensive. Hence for values much less than 0.1 the particles-fluid interaction will dampen the instability and reduce the turbulence intensity and Reynolds stress in the flow, delaying the transition to turbulence.

Ferrouillat *et al.* (2011) tested three volume concentrations of $SiO_2 - water$ nanofluids for a flow range of $200 < \text{Re} < 10\,000$. They found that for a Reynolds number less than 1 000 the results correlate quite well with Poiseuille's law. For a Reynolds number range of 1 000 - 2 300 Poiseuille's law under predicts the results. For $\text{Re} > 2\,300$ Colebrook correlation predicted the results better than Blasius. The greatest difference between the experimental results and the Colebrook correlation was observed for the 18.93 vol% nanofluids.

2.6 Summary on the convective heat transfer

In this section, the literature discussing the enhancement in heat transfer is summarised in Table 2.1. The columns of the table consist of the authors that did the study, the type of

experimental setup used, if a correlation was developed, the nanofluid used and in which flow range the nanofluid was tested. The entries are arranged according to the date of publication, first row being the earliest publication and the last row the most recent publication. Table 2.1 shows that small diameters and short lengths were used as the test section. This is due to the high cost of nanoparticles. The majority of nanofluids that were tested were with metal oxide particles whereas only two studied CNT particles. The most popular nanofluids that were tested are the $Al_2O_3 - water$ and $Cu\text{-}water$ nanofluids. Only one study was on the $MWCNT\text{-}water$ nanofluid and it was tested in the laminar flow regime. Most of the studies listed either tested in the laminar or the turbulent flow regime and only one study, by (Liu and Yu, 2011), was done in the transitional flow regime, using $\gamma - Al_2O_3$ particles.

Author(s)	**Geometry and Boundary Conditions**	**Correlation**	**Fluid, Range and Enhancement**
Pak and Cho (1998)	Experimental study; Stainless steel tube of ID 10.66 mm and a length of 4 800 mm; constant heat flux boundary condition	$Nu_{nf} = 0.021 Re^{0.8} Pr^{0.5}$	$\gamma - Al_2O_3 - water$ and $TiO_2/water$ nanofluid $10^4 < \text{Re} < 10^5$ 45% enhancement for $\gamma - Al_2O_3 - water$ and 75% enhancement for $TiO_2/water$ nanofluid
Xuan and Li (2000)	Numerical study; constant wall temperature boundary condition	$Nu_{nf} = \frac{\Sigma_{m=1}^{\infty} X(\bar{x})/[X(0) - X'(0)/Pe^*]}{\Sigma_{m=1}^{\infty} [X(\bar{x})/[X(0) - X'(0)/Pe^*]]/\beta_m^2}$	
Xuan and Roetzel (2000)	Numerical study	$Nu_{nf} = [1 + C^* Pe^n f'(0)]\theta'(0) Re^m$	
Li and Xuan (2002)	Experimental study; Brass tube of ID 10 mm and a length of 800 mm; constant heat flux boundary condition	$Nu_{nf} = 0.4328(1 + 11.285\phi^{0.754Pe} Pe_d^{0.218}) Re^{0.333} Pr^{0.4}$ $Nu_{nf} = 0.0059(1 + 7.6286\phi^{0.6886} Pe_d^{0.001}) Re^{0.9238} Pr^{0.4}$	$Cu\text{-}water$ nanofluid $800 < \text{Re} < 25\,000$ 60% enhancement
Xuan and Li (2003)	Experimental study; Brass tube of ID 10 mm and a length of 800 mm; constant heat flux boundary condition	$Nu_{nf} = 0.0059(1 + 7.6286\phi^{0.6886} Pe_d^{0.001}) Re^{0.9238} Pr^{0.4}$	$Cu\text{-}water$ nanofluid $10\,000 < \text{Re} < 25\,000$ 60% enhancement
Wen and Ding (2004)	Experimental study; Copper tube of ID 4.5 mm and a length of 970 mm; constant heat flux boundary condition	No developed correlation	$\gamma - Al_2O_3 - water$ nanofluid $500 < \text{Re} < 2\,100$ entrance region 45% enhancement

Author(s)	**Geometry and Boundary condition**	**Correlation**	**Fluid, Range and Enhancement**
Yang *et al.* (2005)	Experimental study; Tube of ID 4.57 mm and a length of 457 mm; constant heat flux boundary condition	$Nu_{nf} = 1.86 Re_{nf}^{1/3} \cdot Pr_{nf}^{1/3} \cdot (D/L)^{1/3} \cdot (\mu_b/\mu_w)^{0.14}$	*graphite-water* nanofluid $5 < \text{Re} < 110$ 22% enhancement
Ding *et al.* (2006)	Experimental study; Copper tube of ID 4.5 mm and a length of 970 mm; constant heat flux boundary condition	No developed correlation	*MWCNT-water* nanofluid $800 < \text{Re} < 1\,200$ 350% enhancement
Maiga *et al.* (2006)	Numerical study; Tube of ID 10 mm and a length of 1 000 mm; constant heat flux boundary condition	$Nu_{nf} = 0.085 Re_{nf}^{0.71} \cdot Pr_{nf}^{0.35}$	$\gamma - Al_2O_3 - water$ nanofluid $10^4 < \text{Re} < 5 \cdot 10^5$
Heris *et al.* (2006)	Experimental study; Copper tube of ID 6 mm and a length of 1 000 mm; constant wall temperature boundary condition	No developed correlation	$Al_2O_3 - water$ and CuO-*water* nanofluid $650 < \text{Re} < 2\,050$
Williams *et al.* (2008)	Experimental study; Stainless steel tube of ID 9.4 mm and a length of 2 819 mm; constant heat flux boundary condition	Use traditional correlations	$Al_2O_3 - water$ and $ZrO_2 - water$ nanofluid $9\,000 < \text{Re} < 63\,000$
Kim *et al.* (2009)	Experimental study; Stainless steel tube of ID 4.57 mm and a length of 2 000 mm; constant heat flux boundary condition	No developed correlation	$Al_2O_3 - water$ and A/C-*water* nanofluid $800 < \text{Re} < 6\,500$ 14% enhancement for $Al_2O_3 - water$ and 7% enhancement for A/C-*water* nanofluid

Author(s)	**Geometry and Boundary condition**	**Correlation**	**Fluid, Range and Enhancement**
Anoop *et al.* (2009)	Experimental study; Copper tube of ID 4.75 mm and a length of 1 200 mm; constant heat flux boundary condition	$Nu_x = 4.36 + \left[a \cdot x_+^{-b} \cdot (1+\phi^c) \cdot exp(-d \cdot x_+^{-b})\right] \cdot \left[1 + e \cdot \left(\frac{d_p}{d_{ref}}\right)^{-f}\right]$ where $x_+ = \frac{x}{D \cdot Re \cdot Pr}$ and the constants are given in Equation 2.12	$Al_2O_3 - water$ nanofluid $500 < \text{Re} < 2\,000$ 25% enhancement for 45 nm and 11% enhancement for 150 nm particle size
Garg *et al.* (2009)	Experimental study; Copper tube of ID 1.55 mm and a length of 914 mm; constant heat flux boundary condition	No developed correlation	*MWCNT-water* nanofluid $600 < \text{Re} < 1\,200$
Amrollahi *et al.* (2010)	Experimental study; Copper tube of ID 11.42 mm and a length of 1 000 mm; constant heat flux boundary condition	No developed correlation	*FMWCNT-water* nanofluid $1\,592 < \text{Re} < 4\,778$ 25% enhancement in laminar flow and 2-25% enhancement in turbulent flow
Liu and Liao (2010)	Experimental study; Copper tube of ID 25.6 mm and a length of 1 080 mm; constant heat flux boundary condition	No developed correlation	*CNT-water* nanofluid $3\,000 < \text{Re} < 50\,000$ 40% enhancement

Author(s)	**Geometry and Boundary condition**	**Correlation**	**Fluid, Range and Enhancement**
Duangthongsuk and Wongwises (2010)	Experimental study; Copper tube of ID 8.13 mm and a length of 1 500 mm; tube-in-tube Heat exchanger, heating of the nanofluid	$Nu_{nf} = 0.074 Re_{nf}^{0.707} \cdot Pr_{nf}^{0.385} \cdot \phi^{0.074}$	$TiO_2 - water$ nanofluid 3 000 < Re < 18 000 26% enhancement for 1 vol% and -14% enhancement for 2 vol%
Liu and Yu (2011)	Experimental study; Stainless steel tube of ID 1.09 mm and a length of 306 mm; constant heat flux boundary condition	No developed correlation	$\gamma - Al_2O_3 - water$ nanofluid 600 < Re < 4 500 19% enhancement for 5 vol% in the entrance region
Ferrouillat *et al.* (2011)	Experimental study; Copper tube of ID 4 mm and a length of 500 mm; constant wall temperature boundary condition	Use traditional correlations	$SiO_2 - water$ nanofluid 200 < Re < 10 000 50% enhancement for 18.9 vol%

Table 2.1: Summary of previous literature

2.7 Conclusion

Literature shows that there is an enhancement in heat transfer when working with nanofluids. The enhancement mainly depends on the thermal conductivity and heat capacity of the base fluid and nanoparticles, the flow pattern, the viscosity and density of the nanofluid, the volume fraction of the suspended particles, the dimensions and the shape of these particles as well as on the flow structure. The thermal conductivity of the nanofluid is a function of both the thermal conductivity of the nanoparticle and base fluid as well as the volume fraction, surface area, shape of the nanoparticle, the distribution of the dispersed particles and the thermal conductivity of the nanolayer. Many studies were done on the convective heat transfer enhancement of nanofluids containing metallic oxide particles and only a few containing MWCNT. The correlations were mainly developed for nanofluids containing metallic oxide particles and then only for the laminar or turbulent flow regime.

Studies on the friction factor in nanofluids indicate that there is a pressure increase which is also directly related to the particle concentration. The penalty in pumping power is the greatest in the laminar flow regime but decreases as one enters the turbulent flow regime due to the shear thinning behaviour of the nanofluids. The pumping power can be reduced by proper preparation of the nanofluid. Literature showed that by treating the CNT with acid softens them, which makes them flexible and allows them to align up with the shear in the fluid.

There has been very little literature reported on the pressure losses and heat transfer enhancement in the transitional flow regime for nanofluids. Thus a study on MWCNT nanofluids in the transitional flow regime and developing a correlation for prediction purposes is of a great interest.

Chapter 3

Experimental setup and test section

3.1 Introduction

In this chapter the experimental set-up, test section and the preparation of the nanofluid will be discussed. The entire experimental set-up was built from the ground up to accommodate nanofluid testing. The experimental system and test section design was based on the experimental set-up's used in other studies (Appendix A).

3.2 Experimental set-up

Shown in Figure 3.1 was the experimental set-up used. An electronically controlled magnetic gear pump (*Item* 1) was used to pump the working fluid at a stable flow rate. A bypass loop, which was controlled via a gate valve (*Item* 11), was added to control the flow rate. In order to protect the equipment a pressure relief valve (*Item* 2), which wass rated at 350 kPa, and a non-return valve (*Item* 3) were incorporated into the system. The inlet and exit thermocouples (*Item* Ti and Te respectively) were attached to the system rather then the test section, since this will avoid any influence that the test section has on the readings. The test section (*Item* 5) was connected to the system via rubber hosing, so as to prevent axial conduction. The flow rate through the test section was measured via a Coriolis flow meter (*Item* 6), which was placed after the test section. After the flow meter the fluid was cooled back to the inlet temperature ($\approx$ 20°C) via the cooling loop that consists out of a simple tube-in-tube heat exchanger (*Item* 7), chiller (*Item* 8) and a centrifugal pump (*Item* 9), before it was pumped back up to the 22 *litre* storage tank (*Item* 10). Just after and before the storage tank there are three ball valves (*Item* 4) that allow the system to be flushed and cleaned easily. The test section, pump and flow meter all lie in the same plane, this was done so that gravitational effects were prevented. The storage tank lied 0.5 m above the test section in order to ensure that the pump never ran dry. The system and storage tank were kept small to ensure that the volume of MWCNTs (which was very expensive) used was kept to a minimum.

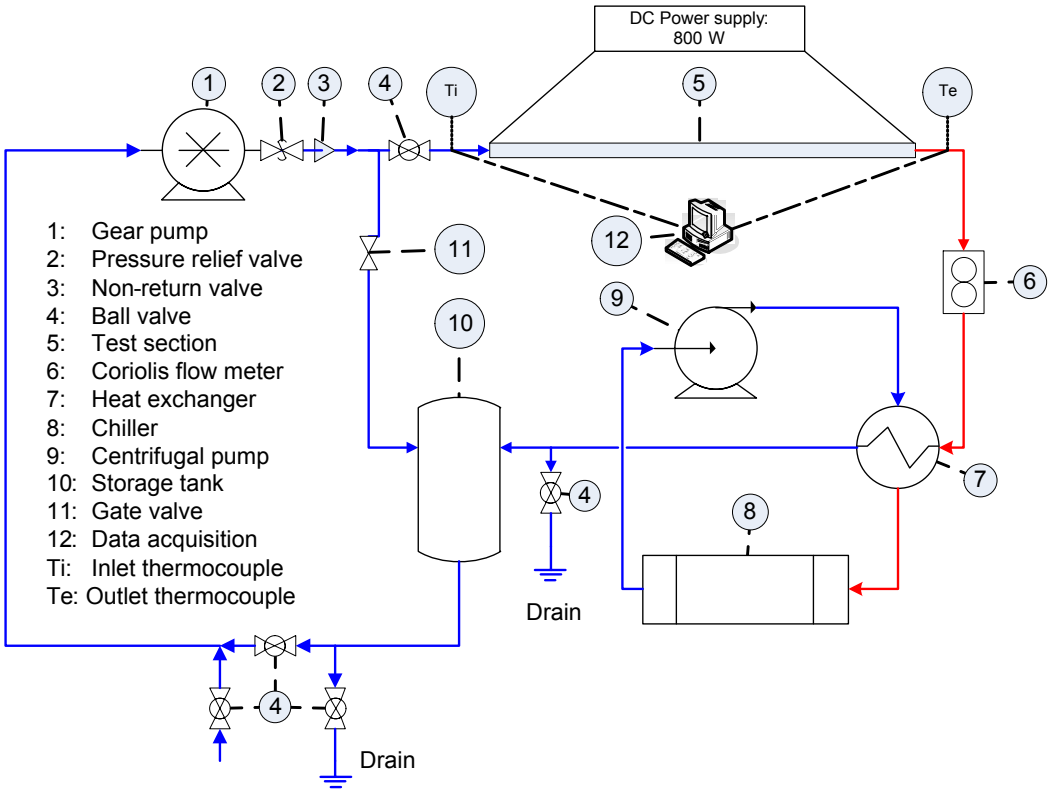

Figure 3.1: Schematic presentation of the experimental setup

3.3 Test section

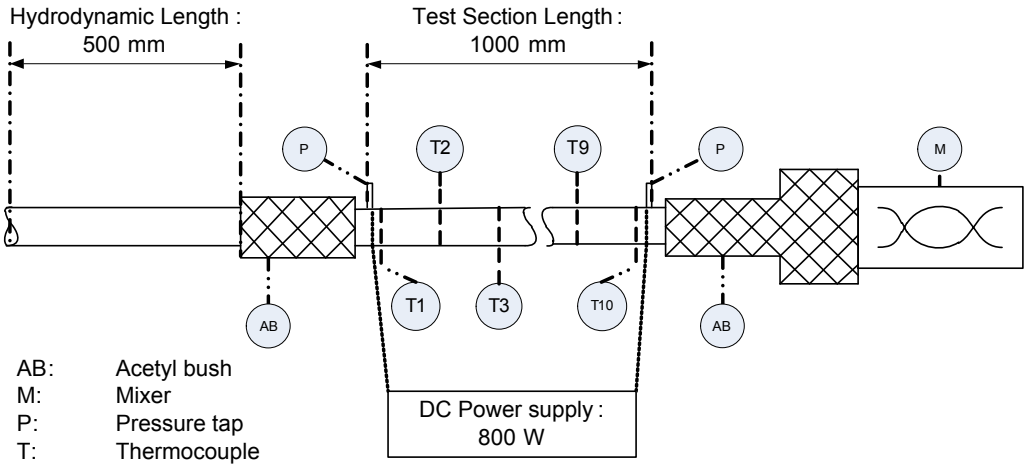

Figure 3.2: Schematic of the test section

Shown in Figure 3.2 is a schematic of the test section used in this study. The test section was made from 1 m hard drawn copper and had an internal diameter of 5.16 mm and an external diameter of 6.44 mm. The entire test section consists out of a hydrodynamic entry section, a heat transfer test section and a mixer (*Item* M), where all three sections are separated by

acetal bushes (*Item* AB). The acetal bushes are used to thermally insulate the mixer and inlet sections from the heat transfer test section. Acetal has a thermal conductivity of 0.23 W/m°C (compared with the thermal conductivity of 401 W/m°C of the copper test section), which acts as a good insulating material to prevent axial conduction from the heat transfer test section. Care was taken with the inner diameter of the acetal bushes to ensure a smooth connection so that the boundary layer was influenced as little as possible.

The hydrodynamic entrance length was designed according to the correlation given by Durst *et al.* (2005) to ensure that the laminar flow is fully developed:

$$\frac{L}{D} = \left[(0.619)^{1.6} + (0.0567 \cdot Re)^{1.6}\right]^{1/1.6} \tag{3.1}$$

Due to the size constrictions on the experimental setup a maximum developing length of 500 mm was chosen. Which results in $L/D = 96$ at a Reynolds number of 1 700.

Coriolis mass flow meters were used to measure the flow rates. The flow meters had a factory-calibrated uncertainty of 0.05%. One flow meter with a maximum flow rate of 0.0682 kg/s was used for all experiments.

A mixer was attached at the outlet of the test section, after the acetal bush, to ensure a uniform temperature distribution is measured. The mixer has a length of 100 mm and an internal diameter of 14.46 mm. The design was adapted from the work done by Galaktionov *et al.* (2003). The mixing plates have a length of 25 mm and are twisted by a half revolution. Four of these plates are arranged inside the tube in an alternating pattern. By constructing the mixer in this fashion it is ensured that the thermal layer is split and mixed a few times resulting in a temperature distribution throughout the cross-section that is uniform.

Two pressure taps were soldered at the beginning and the end of the heat transfer test section (*Item* P). They have an internal diameter of 4 mm and are 1 m apart. The reason for the small diameter is so that the overall flow is not disturbed (Rayle, 1949), since a large hole could lead to a localised eddy forming which results in an error in pressure readings (Olivier, 2009). Care was also taken to clean the holes of any burrs, since burrs may cause a local pressure increase, that may have formed. Nylon tubing was then used to connect the pressure tap to the pressure transducer. The pressure transducer used had an accuracy of 0.08% at full scale, in this case full scale being 17 kPa. Hence the differential pressure accuracy at all Reynolds numbers was 13.6 Pa. The pressure transducer was calibrated with the aid of a water manometer which has an accuracy of 50 Pa. Eight points were captured for the calibration. The calibration done and the calibration given by the supplier of the pressure transducer differ by 1%. The pressure range of the experiments was from 155 Pa to 8.2 kPa.

The heat transfer test section is heated via a constantine wire which is connected to an 800 W power supply. The constantine wire has a resistively of $5 \cdot 10^{-7}\Omega$. The diameter of the wire was 0.24 mm and 20 m of it was used. The wire was wrapped tightly and uniformly at a constant pitch around the test section. In order to achieve a power input of 212 W ($\approx$ 13 000 W/m^2) an input voltage of 210 V and an input current of 1.01 A were required and where measured via the power supply. The power was supplied via a DC power supply which was rated at 800W and controlled electrically through the computer. The test section was insulated with 60 mm thick insulation having a thermal conductivity 0.041 W/m°C. The estimated relative heat loss, which

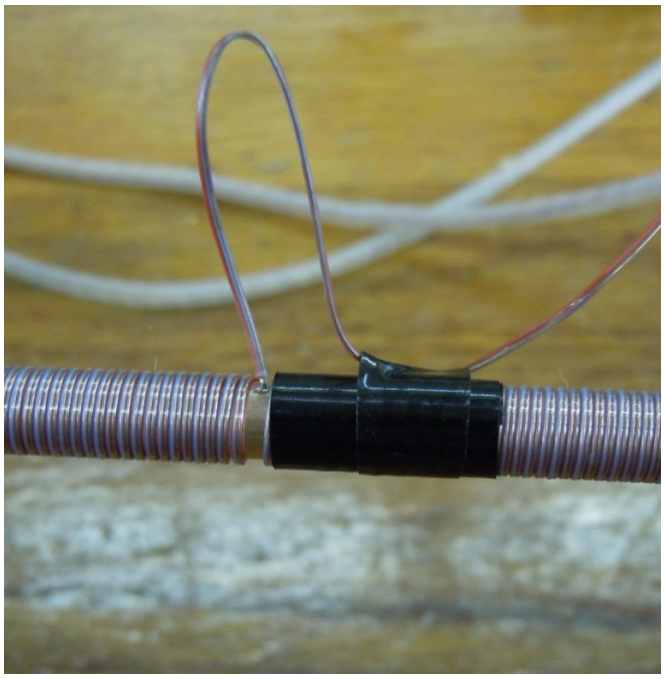

Figure 3.3: Attached thermocouple

was determined from an energy balance, to the environment was around 1.1% at the lowest Reynolds number and 0.3% at the highest Reynolds number.

There were in total 16 T-type thermocouples, 13 were evenly spaced along the tube wall of the heat transfer test section to measure the wall temperature (*Item* T). Two were used to measure the inlet and outlet temperatures and the last one was used to measure the ambient temperature. In order to attach the thermocouple to the test section a small pilot indentation of 1 mm diameter was drilled into the test section. The test section was then heated up and the thermocouple end was placed into the hole and secured via a drop of solder. Shown in Figure 3.3 is the attached thermocouple with the tightly wrapped heating wire. It can be seen from the Figure that the heating wire is wrapped very close to the thermocouple, this is done to achieve a constant heat flux throughout the heat transfer test section.

The thermocouples were calibrated prior to attaching them to the test section. This was done by inserting the thermocouples into a thermal bath along with a reference thermocouple and logging a range of temperatures. The calibration was done separately for the station, inlet, outlet thermocouples and the ambient. The station thermocouples were calibrated from 50°C down to 20°C in increments of 2°C. The inlet and outlet thermocouples were calibrated from 60°C down to 16°C in increments of 2°C. A linear curve fit was used to fit the data of the thermocouples and the reference. To determine the accuracy of the thermocouples the maximum relative error approach was used. A value of 0.04°C was added to the error to account for discrepancy of the reference. On average the accuracy of the thermocouples was calculated to be 0.08°C but an accuracy of 0.1°C was chosen for the thermocouples uncertainties (see Section 4.3) as this was more of a conservative approach.

3.4 Conclusion

The description of the flow loop,test section, calibration of the pressure transducer and thermocouples was discussed. The experimental setup was designed and built to be able to test multiple concentrations of nanofluids. The test section was a single tube heated by a constantine wire to create a constant heat flux boundary condition. The pressure transducer was calibrated and compared with the factory calibration and differed by 1%. The thermocouples were calibrated via a thermal bath and a reference thermocouple, which was used a reference temperature. The thermocouples were calibrated to an uncertainty of 0.1℃.

Chapter 4

Data analysis and validation

4.1 Introduction

In this chapter the methodology of determining the heat transfer coefficient and friction factor are described. The experimental procedure and data reduction are discussed with the experimental results being validated for water only against those published in literature. The average Nusselt number is compared with well known laminar and turbulent heat transfer models. Lastly the adiabatic pressure drop results are compared to well known laminar and turbulent flow equations. The purpose of this validation is to ensure that the experimental setup can take accurate measurements with water before any tests are done on *MWCNT-water* nanofluids.

4.2 Data reduction

4.2.1 Heat transfer coefficient

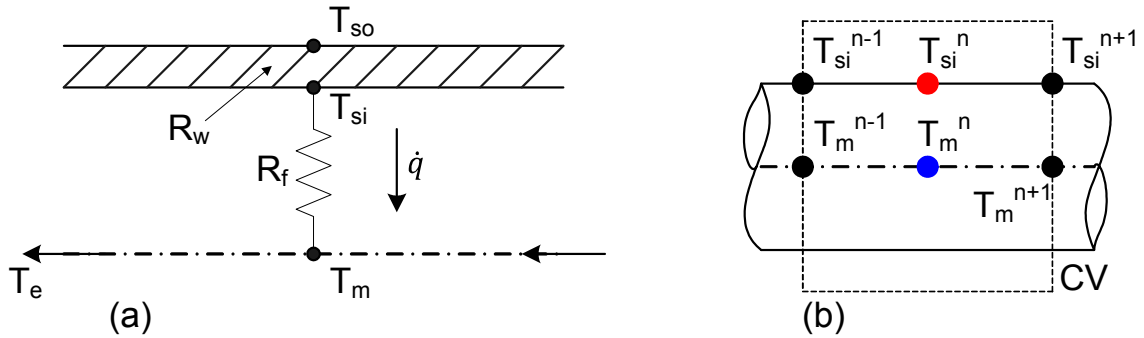

Figure 4.1: Schematic of the (a) resistances inside the test section and (b) control volume around the mean fluid temperature

Shown in Figure 4.1a is the schematic of the test section showing the thermal resistances from which the local heat transfer coefficient, $h(x)$, is calculated.

$$h(x) = \frac{\dot{q}_{in}}{T_{si}(x) - T_m(x)} \tag{4.1}$$

The heat flux, $\dot{q}_{in}$, was determined from the electrical energy input, $\dot{Q}_{in} = V \cdot I$, and the inner surface area, $A_s = \pi \cdot D \cdot L$. The electrical energy input remained constant at 212 W throughout the measurements thus resulting in a constant heat flux ($\approx$ 13 000 W/m^2). The equation of the heat flux is given below:

$$\dot{q}_{in} = \frac{V \cdot I}{\pi \cdot D \cdot L} \tag{4.2}$$

In order to determine the local heat transfer coefficient the local mean temperature has to be determined first. This is done by drawing a control volume (CV) around the mean temperature (see Figure 4.1b) and using the conservation of energy principal. The CV uses the surface temperature as its border. The energy transported by the fluid through the cross section must equal the energy that would be transported through the same cross section if the fluid were at a constant temperature T_m (Çengel, 2006).

$$\dot{q} \cdot P \cdot dx = \dot{m} \cdot c_p \cdot dT_m \tag{4.3}$$

where $P = \pi \cdot D$

$$\frac{dT_m}{dx} = \frac{\dot{q} \cdot \pi \cdot D}{\dot{m} \cdot c_p} \tag{4.4}$$

Integrating both sides with respect to x:

$$\int dT_m = \int \frac{\dot{q} \cdot \pi \cdot D}{\dot{m} \cdot c_p} dx \tag{4.5}$$

$$T_m(x) = T_i + \frac{\dot{q} \cdot x \cdot \pi \cdot D}{\dot{m} \cdot c_p} \tag{4.6}$$

The inner local surface temperature, $T_{si}(x)$, was determined from the measurements of the outside wall temperature, T_{so}, and the heat transfer and resistance through the tube wall:

$$T_{si}(x) = T_{so}(x) - \dot{Q}_{in} \cdot R_w \tag{4.7}$$

where

$$R_w = \frac{ln(D_{so}/D_{si})}{2 \cdot \pi \cdot k_{Cu} \cdot L} \tag{4.8}$$

The thermal conductivity of the copper was obtained from Abu-Eishah (2001) and is given by

$$k_{Cu} = a \cdot T_{Cu}^b \cdot e^{cT_{Cu} + d/T_{Cu}} \tag{4.9}$$

where the constants $a = 82.56648$, $b = 0.262301$, $c = -4.06701 \cdot 10^{-4}$ and $d = 59.72934$. T_{Cu} is the mean temperature of the copper tube in Kelvins.

To obtain the average heat transfer coefficient, Equation 4.1 is averaged along the length of the tube. This is done by taking the mean of all the local heat transfer coefficients.

$$h_{avg} = \frac{h(x_1) + ... + h(x_n)}{n} \tag{4.10}$$

where n is the number of CVs.

The average Nusselt number can then be calculated as follows:

$$Nu_{avg} = \frac{h_{avg} \cdot D}{k} \tag{4.11}$$

where k is the thermal conductivity of the working fluid, determined at the bulk fluid temperature, $T_b = (T_i + T_e)/2$, For water the thermal conductivity was determined from the equations developed by Popiel and Wojtkowiak (1998).

4.2.2 Reynolds number and Prandtl number

The average Reynolds number and Prandtl number were calculated based on the viscosity, thermal conductivity and specific heat determined at the bulk fluid temperature, T_b, using the equations developed by Popiel and Wojtkowiak (1998).

- Reynolds number:

$$Re = \frac{4 \cdot \dot{m}}{\pi \cdot D \cdot \mu} \tag{4.12}$$

- Prandtl number:

$$Pr = \frac{\mu \cdot c_p}{k} \tag{4.13}$$

4.2.3 Friction factor

The Darcy-Weisbach equation is used to calculate the friction factor:

$$f = \frac{\Delta P \cdot D \cdot 2}{L \cdot \rho \cdot V_{avg}^2} \tag{4.14}$$

This is then simplified to include the mass flow rate:

$$f = \frac{\Delta P \cdot \rho \cdot \pi^2 \cdot D^5}{8 \cdot L \cdot \dot{m}^2} \tag{4.15}$$

The pressure drop was determined from the pressure drop measurements of the transducer and the mass flow rate was determined from the readings of the Coriolis mass flow meter.

4.2.4 Energy balance

The measured heat transfer of the water was compared to that of the electrical input energy, $\dot{Q}_{in}$, which was supplied by the constantine heating wire, by means of an energy balance which is given by

$$EB = \frac{\dot{Q}_{in} - \dot{Q}_{water}}{(\dot{Q}_{in} + \dot{Q}_{water})/2} \cdot 100 \tag{4.16}$$

where $\dot{Q}_{in} = 212$ W and the heat transfer to the water, $\dot{Q}_{water}$, is

$$\dot{Q}_{water} = \dot{m} \cdot c_p \cdot (T_e - T_i) \tag{4.17}$$

Although energy balances of around 3% were obtained the input energy was used for the calculations since it was the most accurate of the two.

4.3 Uncertainties

All uncertainties were calculated within the 95% confidence level. Table 4.1 lists the instruments used in the study with their uncertainties. The full uncertainty analysis (by following the procedure set out by Moffat (1988)) is found in Appendix B. The uncertainty of the heat transfer coefficient is between 1.4% for the low Reynolds number ($\approx$ 1 000) and up to 2.5% for the highest Reynolds number ($\approx$ 8 000) tested. The friction factor has an uncertainty of 18% for the lowest Reynolds number and goes down to 2% for the highest. The lowest pressure drop recorded is 155 Pa hence the uncertainty of 18% at the low Reynolds number. The uncertainties of the measurements are shown in Table 4.2 for the low Reynolds number and highest Reynolds number.

Instrument	**Range**	**Uncertainty**
Thermocouple		
Inlet/Outlet	-200 - 350 ℃	0.1 ℃
Station	-200 - 350 ℃	0.1 ℃
Coriolis flow meter	0 - 0.07 kg/s	0.1 %
Pressure transducer	0 - 17 kPa	0.16 %
Power supply	0 - 320 V	0.33 V
	0 - 12.5 A	0.04 A

Table 4.1: Ranges and accuracies of instruments used

Property	**Low *Re***	**High *Re***
$\dot{m}$	1.99 %	0.20 %
T_m	0.11 ℃	0.1 ℃
$\dot{q}_{in}$	3.49 %	3.49 %
h	1.35 %	2.45 %
Nu	2.45 %	3.19 %
Re	2.26 %	1.09 %
ΔP	17.5 %	0.3 %
f	18 %	2.0 %

Table 4.2: Uncertainties of the equations used

4.4 Experimental procedure

After the start-up of the system, it was necessary to let the system settle for at least two hours in order to reach steady-state conditions. This was due to the thermal inertia of the system being relatively slow before it got to steady-state temperatures and mass flow rates. Once the system was steady, small changes were made in the flow rates in order to achieve the desired

mass flow rates for data capturing.

Steady-state conditions were monitored visually, in that there were no observable changes in the temperatures, pressure drops, mass flow rates and energy balances. In the transition region, steady-state conditions were difficult to achieve due to the continuous fluctuations of temperatures, pressure drops and energy balances. But once the fluctuations repeated themselves periodically, measurements were taken. After the change in the mass flow rate from a high flow rate to low flow rate, it took approximately 5 - 10 min for steady state-conditions to be met. The reason for decreasing the flow rate was to ensure that very little residual heat was stored in the insulation, which has an effect on the next reading. On average, an energy balance of 3% was achieved before the data was captured. For each data point, 200 readings at a rate of 20 Hz were captured and then averaged for the post processing.

4.5 Validation of experimental setup

The heat transfer coefficients and friction factors were validated by taking measurements in the laminar and turbulent flow regimes and comparing these with published data. Adiabatic friction factors were used to validate the experiment since they disregard any influence of heat transfer on the properties. Diabatic friction factors were also measured and compared with published data. Only water was used to validate the experimental set-up.

4.5.1 Friction factor

Adiabatic friction factor

The friction factor data consisted of 82 data points spanning a Reynolds number range of 1 000 - 8 000. Measurements were taken without any heat transfer to eliminate any varying density and viscosity effects. Figure 4.2 shows the adiabatic friction factor data, which was calculated using Equation 4.15, as compared with Poiseuille flow and the Blasius equation. Comparing the laminar results with Poiseuille flow, the data is under predicted on average by 3.3% with a maximum deviation of 2.8%. For the turbulent data, Blasius correlation under predicts the data, on average, by 0.2% with a maximum deviation of 0.5%. In general the friction factors in the laminar and turbulent flow regimes compare well with the Poiseuille and Blasius equations.

When considering the transitional flow regime, transition to turbulent starts at a Reynolds number of about 3 100 rather than the conventional value of 2 300 and transition region is also very short, around 100 Reynolds number long. However on closer inspection the experimental data starts to deviate from the laminar line at a much lower Reynolds number. Shown in Figure 4.3 is the ratio of the predicted to experimental adiabatic friction factors for the laminar flow regime. The error of the experimental friction factor compared to the predicted friction factor starts to be greater then 1% after a Reynolds number of 1 700. The hydrodynamic entrance length was designed for a Reynolds number of 1 700 which seems to correlate with the current experimental results.

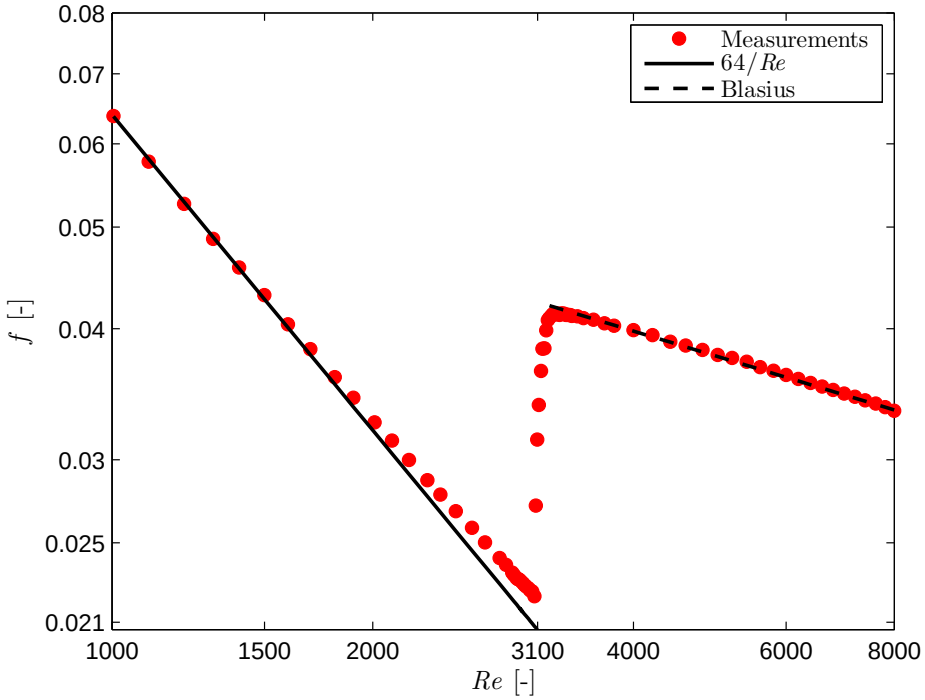

Figure 4.2: Validation of the adiabatic friction factor results

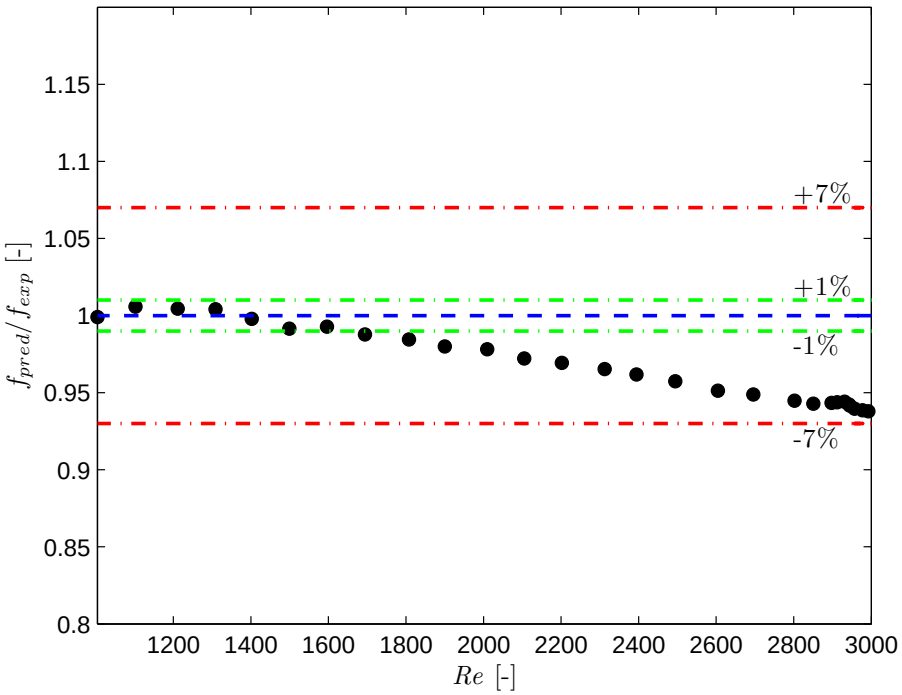

Figure 4.3: Ratio of predicted to experimental adiabatic laminar friction factor

Diabatic friction factor

Figure 4.4 shows the experimental data for the diabatic friction factor, which was calculated using Equation 4.15, as a function of the Reynolds number compared with the laminar Poiseuille equation, the Blasius equation and corrected Blasius equation as suggested by Allen and Eckert (1964). The diabatic friction factors are lower than the adiabatic friction factors in laminar and turbulent flow. Allen and Eckert (1964) proposed a viscosity correction factor, $(\mu_b/\mu_w)^{-0.25}$, to be multiplied with the Blasius equation. The turbulent results correlate fairly well with the corrected Blasius equation (on average, the data is under predicted by 0.5% with a maximum deviation of 1.9%). It should be noted that the correction factor is very close to unity (on average, it is 0.96) and the experimental data correlates with the Blasius equation very well (on average, the data is under predicted by 1.9% with a maximum deviation of 2.1%).

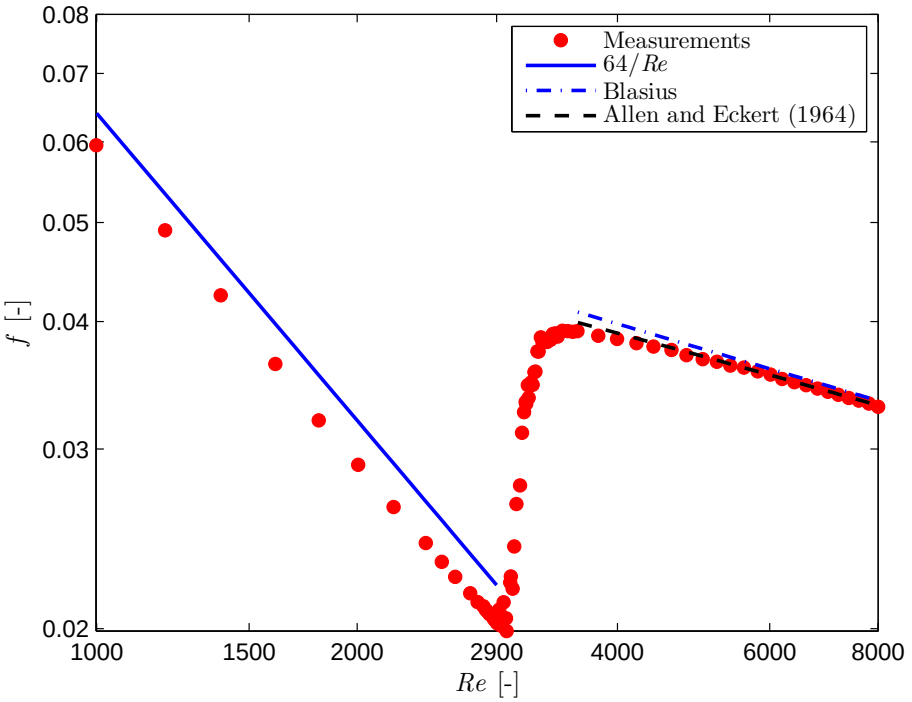

Figure 4.4: Experimental diabetic friction factors as a function of the Reynolds number

In the laminar flow regime, the same phenomenon happens as in the turbulent flow regime. Here the experimental data is under predicted by an average of 8.5% with a maximum deviation of 2.2% (however, it is within the uncertainties of 18% at low Reynolds numbers). According to Shome and Jensen (1995) and Tam and Ghajar (1997), secondary flow effects increase the friction factor, especially in tubes with uniform heat flux boundary conditions. Tam and Ghajar (1997) found that by increasing the overall heat flux, the laminar friction factors increased. The reason for this is that the wall-to-bulk temperature difference exists throughout the length of the tube (Shome and Jensen, 1995).

Metais and Eckert (1964) recommend the use of a flow map to distinguish between mixed and forced convection regimes. The map is based on the Reynolds number being a function of the Rayleigh number. Their flow map is for a constant wall boundary condition and hence cannot be used to compare the current data. Ghajar and Tam (1995) developed a new flow map for a constant heat flux boundary condition. They used the data for three different inlets to produce a new boundary between laminar, transition and turbulent forced and mixed convection. Figure 4.5 shows the flow map developed by Ghajar and Tam (1995) with the current data plotted. From the map, it can be concluded that experimental laminar values for this study are well within the laminar forced convection boundary and secondary flow effects are not present. Hence the reason for the drop in friction factor is the result of the reduction of liquid viscosity in the near-wall region due to heating (Shome and Jensen, 1995), which seems to be the dominating effect.

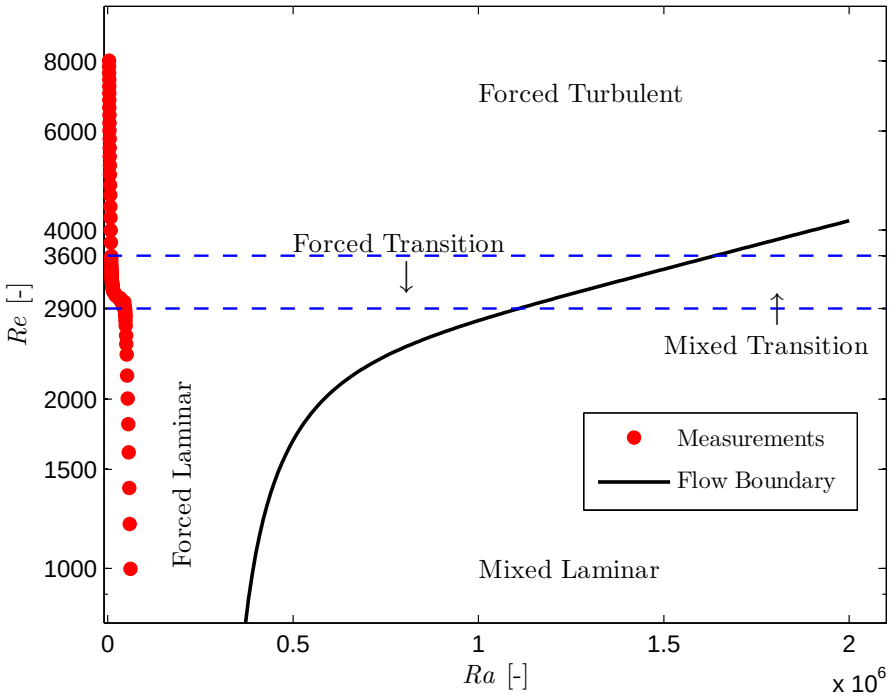

Figure 4.5: Laminar-turbulent heat transfer results on the flow regime map of Ghajar and Tam (1995)

4.5.2 Heat transfer coefficient

Laminar flow results

Experimental laminar flow data is compared to the correlations developed by Sieder and Tate (1936), Ghajar and Tam (1994) and Olivier (2009). The correlations are shown in Table 4.3.

Author(s)	Correlation	Restrictions
Sieder and Tate (1936)	$Nu = 1.86 \cdot Gz^{1/3} \cdot \left(\frac{\mu_b}{\mu_w}\right)^{0.14}$	$1\,000 \leq Re \leq 2\,000$ $0.7 \leq Pr \leq 17\,600$ $0.01 \leq \frac{\mu_b}{\mu_w} \leq 10$
Ghajar and Tam (1994)	$Nu = 1.24\left[Gz + 0.025 \cdot (Gr \cdot Pr)^{0.75}\right]^{1/3} \cdot \left(\frac{\mu_b}{\mu_w}\right)^{0.14}$	$280 \leq Re \leq 3\,800$ $40 \leq Pr \leq 160$ $1.2 \leq \frac{\mu_b}{\mu_w} \leq 3.8$
Olivier (2009)	$Nu = 2.686\left[Re^{0.105} \cdot Pr^{1.133} \cdot \left(\frac{D}{L}\right)^{0.483} + 1.082\left(Gr^{0.362} \cdot Pr^{-2.987} \cdot \left(\frac{L}{D}\right)^{0.202}\right)^{0.277}\right]^{2.226} \cdot \left(\frac{\mu_b}{\mu_w}\right)^{0.152}$	$940 \leq Re \leq 2\,522$ $4.43 \leq Pr \leq 5.72$ $0.695 \leq \frac{\mu_b}{\mu_w} \leq 0.85$

Table 4.3: Developed laminar correlations

Figure 4.6 shows the experimental data of 25 data points, in the laminar flow regime for a Reynolds number range of 1 000 - 3 000. Comparing the correlations of Sieder and Tate (1936), Ghajar and Tam (1994) and Olivier (2009) (see Figure 4.7), it was found that the correlation of Sieder and Tate (1936) under predicts the data, on average, by 13% with a maximum deviation of 19%. Ghajar and Tam (1994) under predicts the data, on average, by 5% with a maximum deviation of 7% and Olivier (2009) over predicts the data, by 75% with a maximum deviation of 4%. The correlation by Sieder and Tate (1936) was developed for both heating and cooling of the fluid and it does not take mixed convection into account. The heating of the fluid has a completely opposite effect regarding mixed convection when compared to the cooling of the fluid. The first effect on a liquid being heated, is that the liquid in the near wall region is less viscous than that in the centre, because of that the fluid velocity is larger in the near wall region. A second effect that heating has on the liquid is that secondary flow is increased due to the lesser viscous resistance. Both these effects increase the heat transfer during heating (Shome and Jensen, 1995). As discussed in Section 4.5.1 secondary flow is not present whereas the first effect, as discussed by Shome and Jensen (1995), is still present. The correlation of Olivier (2009) is not shown on Figure 4.7 due to the large over prediction when compared to the current data. The reason for the large over prediction is that the correlation was developed for a constant surface boundary condition, cooling of the fluid and is valid for lower Prandtl numbers, viscosity ratios and larger Grashof numbers. The larger Grashof numbers are due to the large tube sizes used in the study where secondary flow effects have a larger influence as compared to the current test setup. However, it can be concluded that the experimental values measured in the laminar flow regime compare well to literature especially to the correlation developed by Ghajar and Tam (1994).

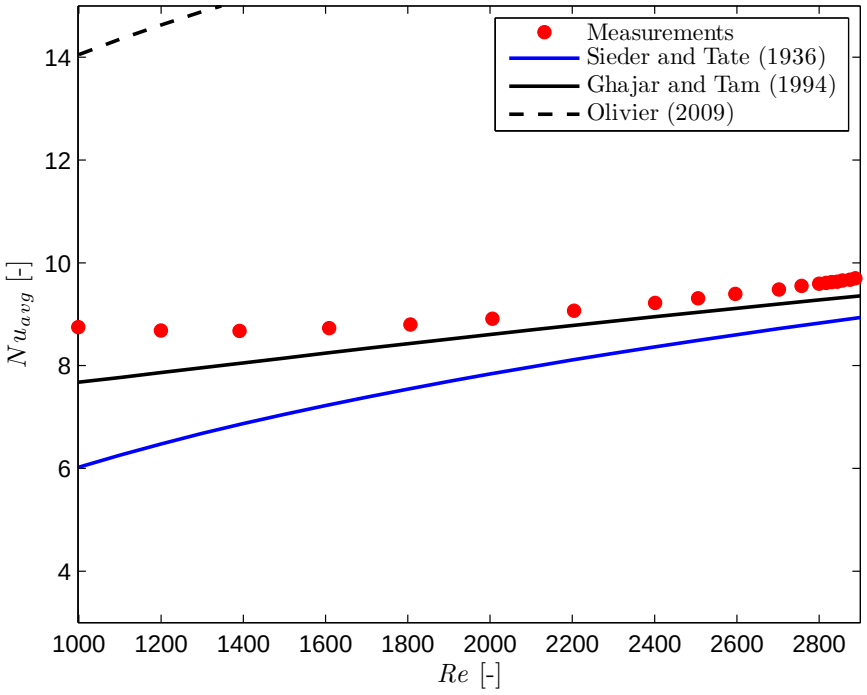

Figure 4.6: Laminar heat transfer results for water compared to literature

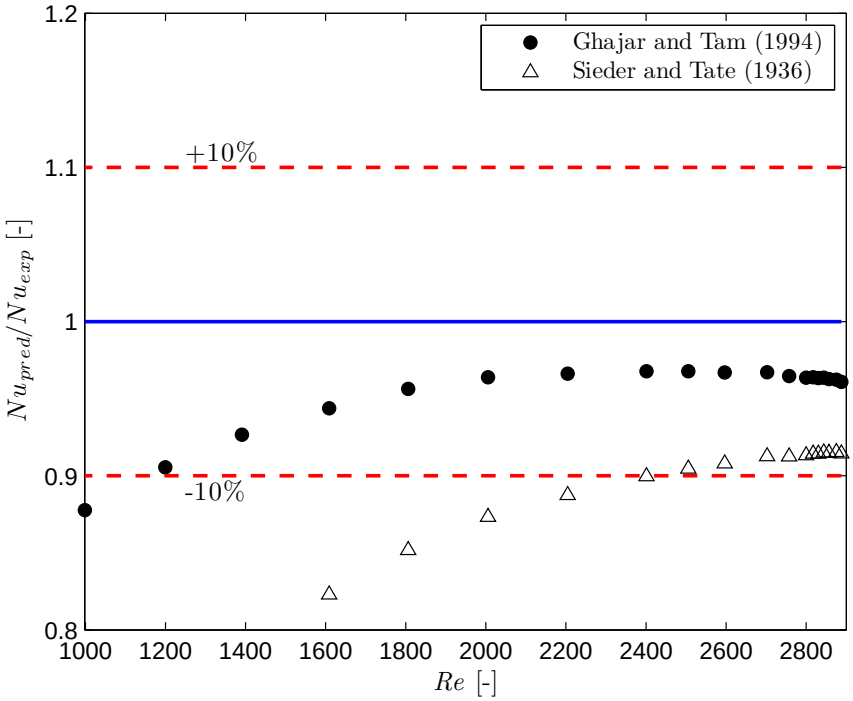

Figure 4.7: Ratio of predicted to measured Nusselt numbers as a function of the Reynolds number

Turbulent flow results

Turbulent experimental data is compared to the correlations developed by Sieder and Tate (1936), Gnielinski (1976), Ghajar and Tam (1994) and Olivier (2009). The developed correlations with their restrictions are shown in Table 4.4.

Author(s)	Correlation	Restrictions
Sieder and Tate (1936)	$Nu = 0.027 \cdot Re^{0.8} \cdot Pr^{1/3} \cdot \left(\frac{\mu_b}{\mu_w}\right)^{0.14}$	$0.7 \leq Pr \leq 17\ 600$ $Re \geq 10\ 000$
Gnielinski (1976)	$Nu = \frac{(f/8)(Re-1000)Pr}{1+12.7(f/8)^{0.5}(Pr^{2/3}-1)}$ $f = (0.79 \cdot ln\ Re - 1.64)^{-2}$	$0.5 \leq Pr \leq 2\ 000$ $3\ 000 \leq Re \leq 5{\cdot}(10)^6$
Ghajar and Tam (1994)	$Nu = 0.023 \cdot Re^{0.8} \cdot Pr^{0.385} \cdot \left(\frac{x}{D}\right)^{-0.0054} \cdot \left(\frac{\mu_b}{\mu_w}\right)^{0.14}$	$4 \leq Pr \leq 34$ $7\ 000 \leq Re \leq 49\ 000$
Olivier (2009)	$Nu = 0.026 \cdot Re^{0.788} \cdot Pr^{1/3} \cdot \left(\frac{\mu_b}{\mu_w}\right)^{0.14}$	$3.73 \leq Pr \leq 5.06$ $3\ 000 \leq Re \leq 17\ 800$

Table 4.4: Developed turbulent correlations

Shown in Figure 4.8 are the heat transfer results, of 27 data points, in the turbulent flow regime for a Reynolds number range of 3 000 - 8 000. Comparing the correlations of Sieder and Tate (1936), Gnielinski (1976), Ghajar and Tam (1994) and Olivier (2009) (see Figure 4.9), it was found that Sieder and Tate over predicts, on average, by 18% with a maximum deviation of 4%. Gnielinski over predicts the data, on average, by 5% with a maximum deviation of 5% while Ghajar and Tam under predicts the experimental data, on average, by 2% with a maximum deviation of 1%. Olivier under predicts the data, on average, by 16% with a maximum deviation of 1%. Sieder and Tate (1936) developed their correlation for Reynolds numbers greater then 10 000 over 70 years ago, hence the poor performance in predicting the current experimental data. Gnielinski (1976) modified the Petukhov and Popov equation to improve the accuracy at lower Reynolds numbers. The original correlation was developed for fluids being heated, hence why the correlation predicts the experimental values fairly well. Ghajar and Tam (1994) correlation is applicable to turbulent forced convection in the entrance and fully developed regions and also for a constant heat flux boundary condition, hence why it is in good agreement with the current data set. Olivier (2009) developed their correlation for cooling of a fluid which results in lower viscosity ratio. Hence the poor performance when predicting the current experimental data. In general, however, it can be concluded that the experimental values in the turbulent flow regime compare well to that of the literature.

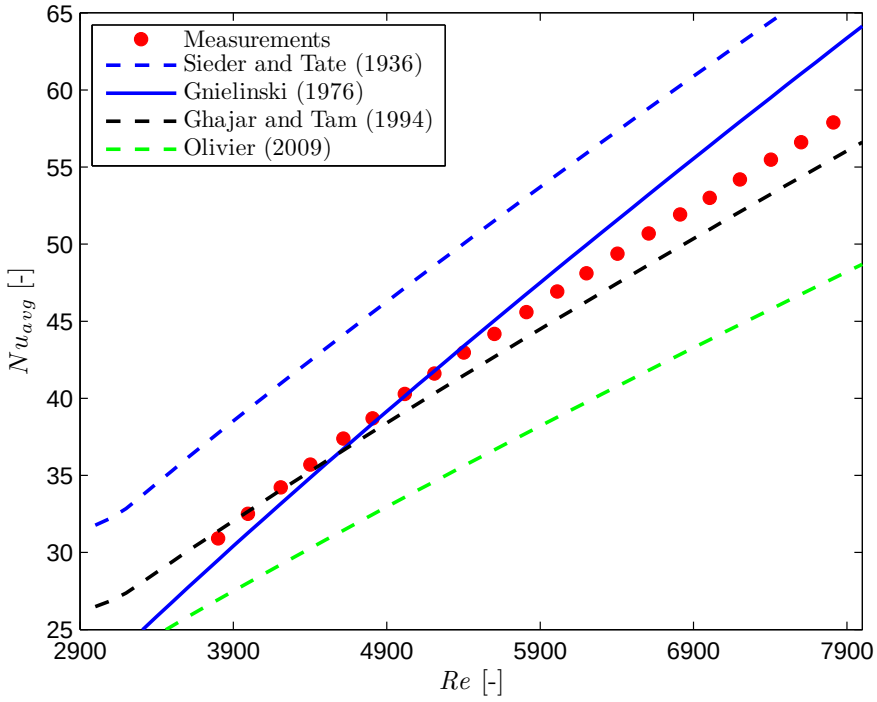

Figure 4.8: Heat transfer results for turbulent flow

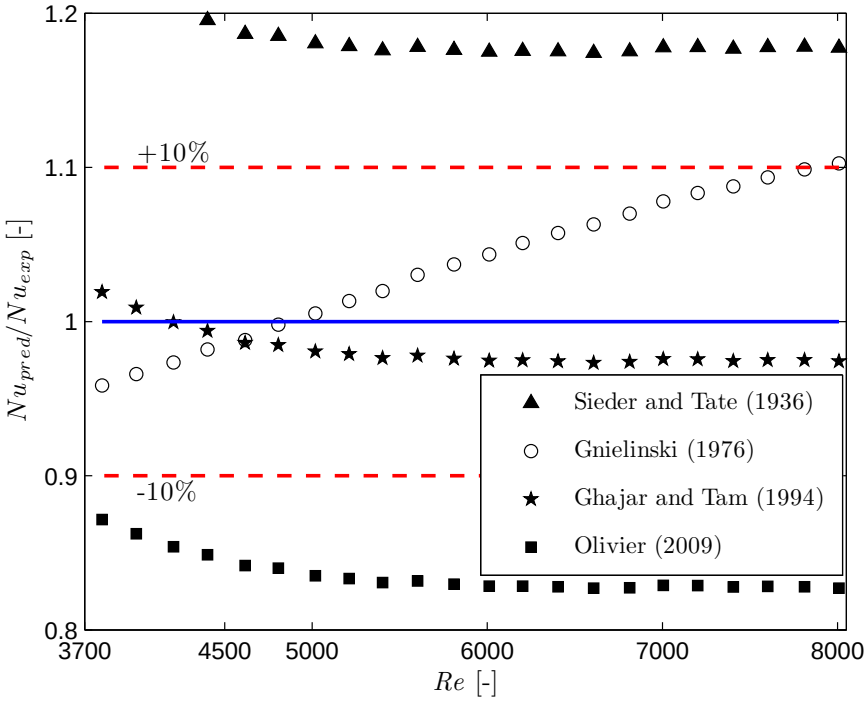

Figure 4.9: Ratio of predicted Nusselt numbers as a function of the Reynolds number

Entire flow range results

Shown in Figure 4.10 are the experimental results in terms of the average Nusselt number as a function of Reynolds number for the entire flow range. A total of 80 data points are represented and compared to Ghajar and Tam (1994) correlations for the laminar and turbulent flow regime. It can be seen from that the experimental data correlates well to the published data.

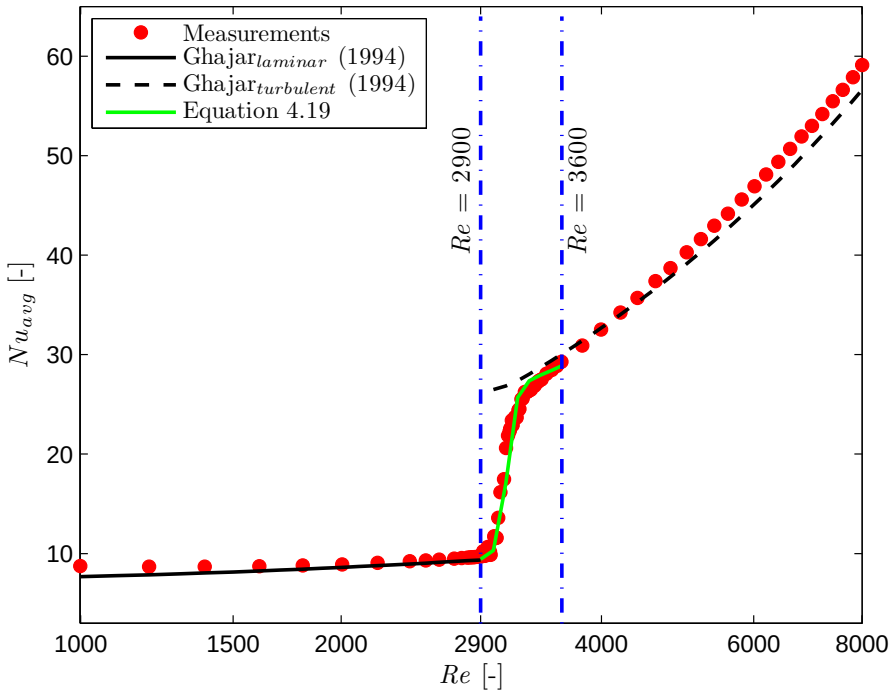

Figure 4.10: Smooth tube heat transfer results

For the transitional flow regime a new correlation was developed since the developed correlation by Ghajar and Tam (1994) are for the reentrant, square-edged or bell-mouth inlet conditions. In the current study only a fully developed flow inlet condition was used due to the size constraint on the system. To correlate the transitional flow regime, it was decided to use an equation that is similar in the form as that used by Ghajar and Tam (1994). The correlation consists of a laminar, transition and turbulent part and is given as

$$Nu_{trans} = Nu_{lam} + \left[e^{\frac{a-Re}{b}} + Nu_{turb}^{c}\right]^{c} \tag{4.18}$$

By curve fitting the data the constants a, b and c were obtained and the final equation is given as

$$Nu_{trans} = Nu_{lam} + \left[e^{\frac{Re_{trans}-Re}{36}} + Nu_{turb}^{-0.935}\right]^{-0.935} \tag{4.19}$$

Equation 4.19 is shown as the green line in Figure 4.10 and it predicts the data on average, by 5.3% with a maximum deviation of 15.5%. It can be gathered from Figure 4.10 that the onset of transition starts at a Reynolds number of about 2 900 and the length of the transitional flow

regime is around 700 Reynolds numbers long. Just as with the diabetic friction factor results, the onset of transition is delayed to much higher Reynolds numbers due to the the reduction of liquid viscosity in the near-wall region (Shome and Jensen, 1995).

4.6 Conclusion

The heat transfer coefficient for water was determined and the results were validated against published results in literature. Validation was done for flow in the laminar and turbulent flow regime, and the results show that the experimental data is under predicted, by 5% in the laminar flow regime and by 2% in the turbulent flow regime when compared to published literature. The uncertainties in the heat transfer coefficient were 1.4% for the lowest flow rate and 2.5% for the highest. In the transitional flow regime a new correlation was developed based on the works in published literature, the reason being that only a fully developed inlet condition was used throughout the experimental process.

For validating the friction factor only the adiabatic results are used in order to eliminate any density and viscosity variations due to the heating of the tube. The friction factors were compared to Poiseuille flow in laminar flow and Blasius in turbulent flow. The experimental data was under predicted on average by 3.3% in laminar flow and 0.2% in turbulent flow. The uncertainties in the friction factor were between 2% and 18%.

In general, the friction factors and Nusselt numbers in the laminar and turbulent flow regimes compare well with literature. This adds confidence in the measurement techniques and further validates the experimental set-up and data reduction methodology.

Chapter 5

Preparation and properties of *MWCNT-water* nanofluids

5.1 Introduction

In this chapter the preparation and properties of the *MWCNT-water* nanofluids are discussed. The chapter starts off with the preparation of the *MWCNT-water* nanofluids. After which a discussion on the thermal conductivity and viscosity of the *MWCNT-water* nanofluids is presented. A literature review on the preparation of nanofluids can be viewed in Appendix C.

5.2 Preparation of the *MWCNT-water* nanofluid

5.2.1 Amount of MWCNT to be disbursed into distilled water and the sonication time of the nanofluids

Three different volume concentrations, measured according to the volume of the base fluid, of MWCNTs were prepared. The MWCNTs have an outside diameter of 10 - 20 nm an inside diameter of 3 - 5 nm and a length of 10 - 30 μm, which results in an aspect ratio of 1 333. The three different volume concentrations were 0.33%, 0.75% and 1%, which were then dispersed into 10 *litres* of distilled water. In order to stabilise the three different mixtures Gum Arabic (GA) powder was dissolved into the distilled water first. Garg *et al.* (2009) used 0.25 wt% GA with 1 wt% MWCNTs, which results in 1:4 ratio. They discovered that at this ratio there is no significant change in thermal conductivity and the convective heat transfer coefficient when compared with water. A similar approach was used here, namely one part GA to four parts MWCNTs.

According to the supplier of the MWCNTs (Cheap Tubes Inc.) the sonication time for a ratio of 1:0.005 of *MWCNT/water* mixture is 2-8 minutes, when using an ultrasonic vibrator rated at 750 W, with an interruption of 10 seconds every 30 seconds at high amplitude. Garg *et al.* (2009) sonicated various samples for four different time lengths. They found that the optimum sonication time for a 1 wt% MWCNTs and 0.25 wt% GA mixture, was 40 min using a 130 W, 20 kHz ultrasonicator. The sonication times in the current study were adjusted to match the optimum sonication time of Garg *et al.* (2009). In the current study the nanofluids were soni-

Fluid	MWCNTs vol%	MWCNTs wt%	MWCNTs wt [gram]	GA vol%	GA wt%	GA wt [gram]	Sonication time [min]
1	0.33	0.69	69.3	0.13	0.17	17.3	27
2	0.75	1.58	157.5	0.29	0.39	39.4	80
3	1.0	2.10	210.0	0.39	0.53	52.5	120

Table 5.1: Mass, volume, weight percentage and sonication time for both MWCNT and GA

cated with a 24 kHz, 200 W ultrasonicator. Shown in Table 5.1 are the mass, volume, weight percentage and sonication time for both MWCNTs and GA for the three different nanofluid mixtures tested.

5.2.2 pH of the *MWCNT-water* nanofluid

For a stable nanoparticle-dispersion, the pH is a key parameter, which is related to the electrostatic charge on the particle's surface which is known as the zeta potential. At the iso-electric point, which is the point were the nanoparticle carries no net electrical charge, the nanoparticles will form agglomerations since there are no sufficient repulsive forces between the nanoparticles. As the pH moves away from the iso-electric point, the absolute value of the zeta potential of the nanoparticle surface increases so that agglomeration and collision between nanoparticles caused by Brownian motion are prevented (Lee et al., 2011).

Shown in Figure 5.1 are the measured pH of the distilled water compared with that of the *MWCNT-water* nanofluid and *GA-water* mixture. The pH of the distilled water is 7.1 and that of the *GA-water* mixture for a volume concentrations of 0.33%, 0.75% and 1.0% is 6.63, 6.37 and 7.45 respectively. The *MWCNT-water* nanofluids follow a similar trend as that of the *GA-water* mixture. At volume concentration of 0.33% the pH of *MWCNT-water* nanofluid is 8.0 and the pH then decreases to 7.74, which is the same decrease as that of the *GA-water* mixture. At a volume concentration of 1.0% the pH of the *MWCNT-water* nanofluid suddenly drops and almost equals that of water. Xie *et al.* (2003) measured the pH of their MWCNT suspension and found that the iso-electric point was at a pH of 7.3. Hence the 1.0 vol% *MWCNT-water* nanofluid has a large possibility of its nanoparticles forming agglomerations and falling out of the suspension.

The 0.33 vol% and 0.75 vol% nanofluid concentrations remained stable for 3 days whereas the 1.0 vol% only remained stable for around 24 hours due to the large possibility of its nanoparticles forming agglomerations and settling out of the suspension.

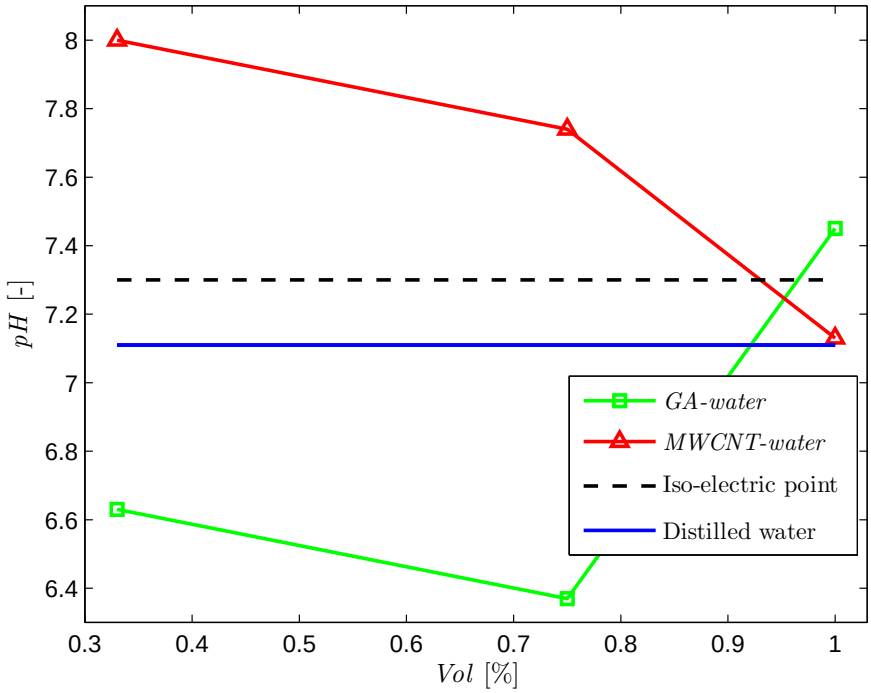

Figure 5.1: pH of the *MWCNT-water* nanofluid compared with that of *GA-water* mixture and distilled water

5.3 Properties of *MWCNT-water* nanofluid

5.3.1 Thermal conductivity of *MWCNT-water* nanofluid

The thermal conductivity was measured using a KD2 thermal property meter (Decagon Devices), which is based on the transient line heat source method. Measurements were taken for temperatures within the range of experiments conducted. The results are shown in Figure 5.2 for three different temperatures. The KD2 thermal property meter had a measurement uncertainty of ±5%. The results fall within the theory (Popiel and Wojtkowiak, 1998), which is predicted by Equation D.3, found in Appendix D.

Shown in Figure 5.3 is the measured thermal conductivity of the 0.33 vol%, 0.75 vol% and 1.0 vol% *MWCNT-water* nanofluids compared with distilled water at various temperatures. The thermal conductivities of the 0.33 vol%, 0.75 vol% and 1.0 vol% *MWCNT-water* nanofluids are 2%, 3.3% and 8% respectively greater than that of the distilled water. The increase in thermal conductivity falls to within the measurement uncertainty of the device. Xie *et al.* (2003) reported a 7% increase in thermal conductivity for MWCNTs suspended in water at a volume concentration of 1.0%, which compares very well with the measured 8% increase. Prasher *et al.* (2006a) showed that the thermal conductivity can increase due to agglomeration of the nanoparticles as compared with a well-dispersed system, which is a possible reason for the large increase in the thermal conductivity of the 1.0 vol% *MWCNT-water* nanofluid. Keblinski *et al.* (2002) also showed that particle clustering, due to Brownian motion, could enhance the thermal conductivity since the particles are much closer together and thus enhance the consistent phonon

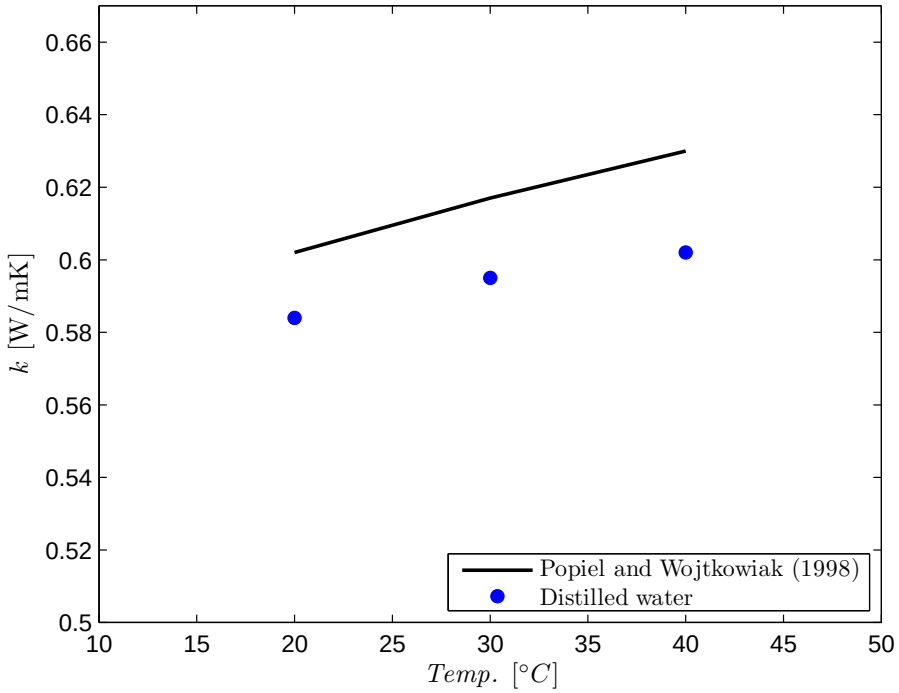

Figure 5.2: Thermal conductivity of distilled water at various temperatures

heat transfer.

Figure 5.4 shows the thermal conductivity ratios of the *MWCNT-water* nanofluid as a function of the volume concentration. For volume concentration of 0%, 0.33% and 1.0% the various thermal conductivities at different temperatures collapse approximately onto one point, except for the volume concentration of 0.75%. The enhancement of the thermal conductivity falls to within the measurement uncertainty, a possible reason being the sensitivity of the meter to natural convection. At 20C the data follows almost a straight line. This is due to that fact that natural convection in the sample is low. The scatter in the data increases with increasing temperature. From prediction models, the thermal conductivity can be written as follows (Prasher et al., 2006b):

$$\frac{k_{nf}}{k_{bf}} = 1 + C_k \phi \tag{5.1}$$

where C_k is a constant depending on the experimental data. In this case, $C_k = 7$ and is shown in Figure 5.4. Also shown is the correlation developed by Xue (2005), which can be found in Appendix D. Equation 5.1 over predicts the data for the 0.33 vol% *MWCNT-water* nanofluid concentration by 2.8%, for the 0.75 vol% *MWCNT-water* nanofluid concentration by 5.8% and under predicts the 1.0 vol% *MWCNT-water* nanofluid concentration by 7.6%.

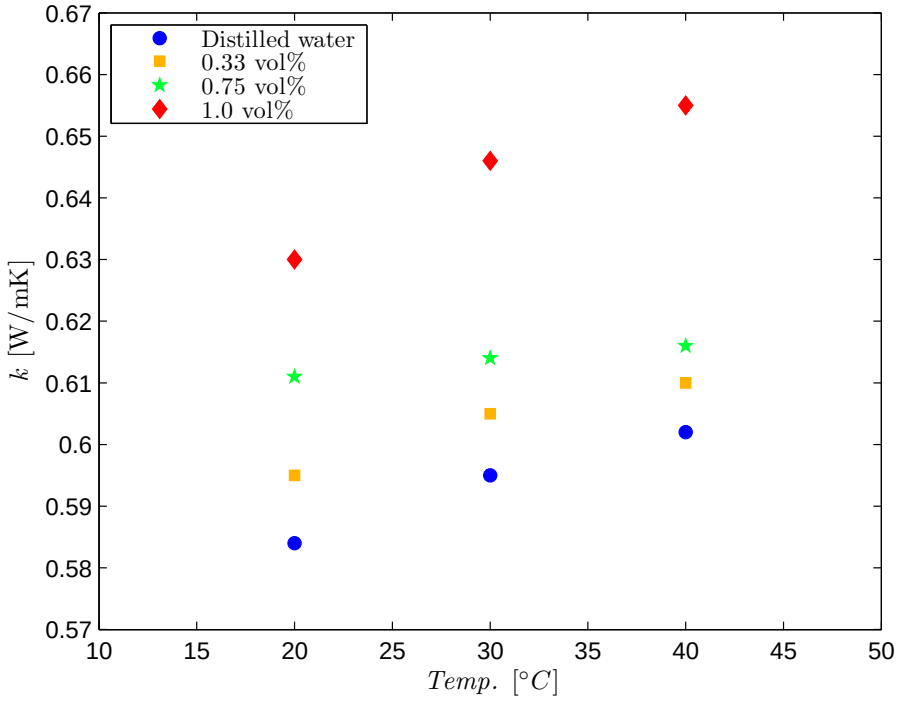

Figure 5.3: Thermal conductivity of *MWCNT-water* nanofluids compared with distilled water at various temperatures

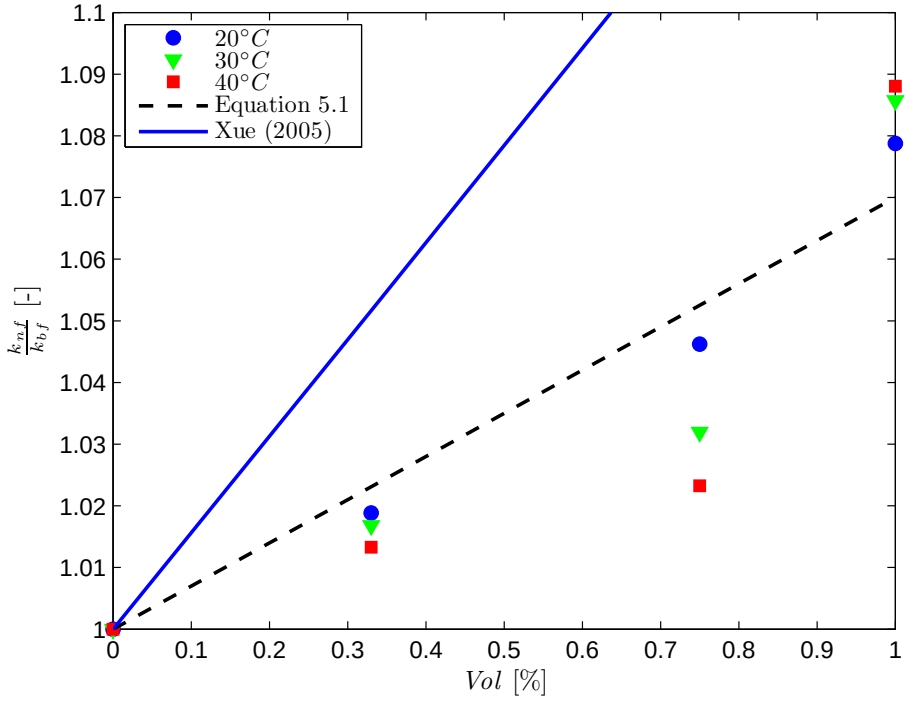

Figure 5.4: Relative thermal conductivity of the *MWCNT-water* nanofluid as a function of the volume concentration

5.3.2 Viscosity of *MWCNT-water* nanofluid

A double concentric cylinder geometry was used to measure the viscosity's of the fluids. The results of the viscosity for the distilled water are shown in Figure 5.5 where the measured viscosity of the water is compared with the experimental viscosity of water given by Popiel and Wojtkowiak (1998). The experimental results of the distilled water are on average by 23% lower when compared with the viscosity data by Popiel and Wojtkowiak (1998).

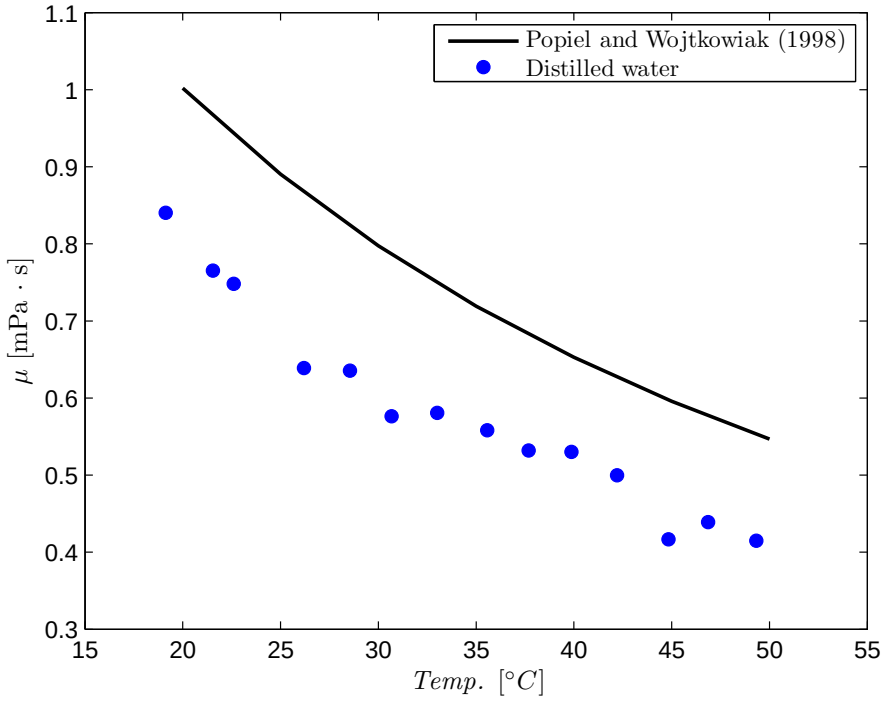

Figure 5.5: Viscosity of water results compared with theoretical water viscosity

Shown in Figure 5.6 are the measured viscosities of the three different *MWCNT-water* nanofluid concentrations compared with that of distilled water for a temperature range of 20°C - 50°C. The viscosity of nanofluids increases with increasing MWCNT concentration and decreasing temperature. There is a large increase in viscosity from 0.75 vol% to 1.0 vol%, also the gradient of the 1.0 vol% is steeper than the gradient for the 0.33 vol% and 0.75 vol%.

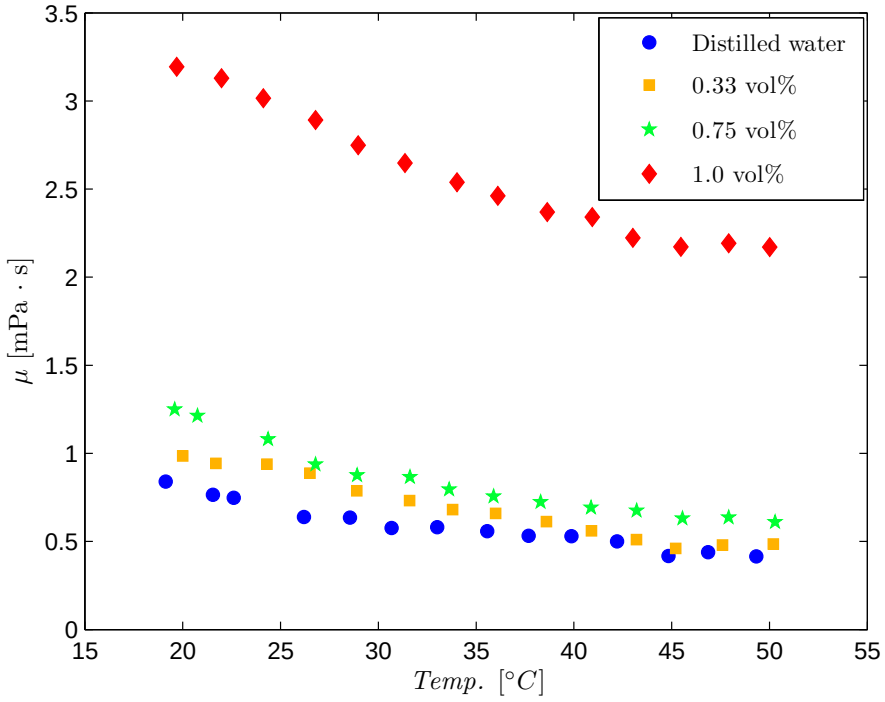

Figure 5.6: Viscosity of the *MWCNT-water* nanofluid at various volume concentrations as a function of the temperature

Shown in Figure 5.7 are plotted the viscosity ratios as a function of the volume concentrations of the *MWCNT-water* nanofluids. For volume concentration of 0%, 0.33% and 0.75% the various viscosities at different temperatures collapse approximately onto one point, except for the volume concentration of 1.0%. Also there is a linear increase from a concentration of 0 vol% up to 0.75 vol% and then suddenly a steep increase to 1.0 vol%. This trend is also seen in Figure 5.6, the gradient of the 1.0 vol% is -4·10^{-5} whereas the gradient both for the 0.33 vol% and 0.75 vol% is -2·10^{-5}. A similar phenomenon is seen in the pH of the 1.0 vol% *MWCNT-water* nanofluid in that there is sudden decrease in pH. A possible reason for the large increase in viscosity is that the nanoparticles have agglomerated after sonication due to the pH of the solution being to close to the iso-electric point (Lee et al., 2011). The black line in Figure 5.7 fits the data for all the volume concentrations and the Equation is shown below:

$$\frac{\mu_{nf}}{\mu_{bf}} = 1.78 \cdot 10^7 \cdot \phi^3 - 1.92 \cdot 10^5 \cdot \phi^2 + 498.5 \cdot \phi + 1 \tag{5.2}$$

Einstein, in 1906, developed a correlation for the viscosity of dilute suspensions (< 5 vol%) for small and rigid spherical particles (Hiemenz, 1986):

$$\frac{\mu_{nf}}{\mu_{bf}} = 1 + 2.5\phi \tag{5.3}$$

Equation 5.3 under predicts the data for the 0.33 vol% *MWCNT-water* nanofluid concentration by 16%, for the 0.75 vol% *MWCNT-water* nanofluid concentration by 30% and the 1.0 vol% *MWCNT-water* nanofluid concentration by 78%. The reason for the large under prediction by Equation 5.3 is that the correlation was developed for spherical particles. The equation can be

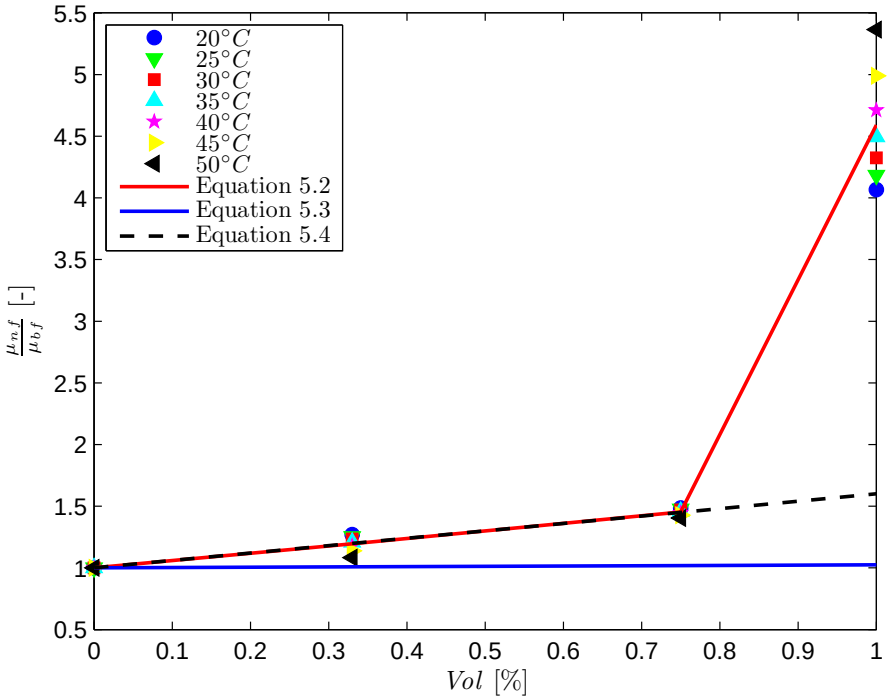

Figure 5.7: Relative viscosity of the *MWCNT-water* nanofluid as a function of the volume concentration

extended to include ellipsoidal particles (Ferouillat et al., 2011):

$$\frac{\mu_{nf}}{\mu_{bf}} = 1 + C_{\mu}\phi \tag{5.4}$$

where C_{μ} depends on the ratio of the revolution ellipsoid axes and is equal to 2.5 for spherical particles. In this case, the constant C_{μ} equal to 60 correlates the volume concentrations of 0.33% and 0.75% well. At a volume concentration of 0.33%, Equation 5.4 over predicts the viscosity by 0.24%, at a volume concentration of 0.75%, the viscosity is under predicted by 0.17% and at a volume concentration of 1.0%, the viscosity is under predicted by 65%.

5.4 Uncertainties of the *MWCNT-water* nanofluid properties compared with that of water

Table 5.2 compares the nanofluid properties with water. The uncertainty of the density and the specific heat for the nanofluid are the same as that of the water, since they largely only depend on the uncertainty of the water properties. There is slight change in the thermal conductivity of the 0.75 vol% and 1.0 vol% of the *MWCNT-water* nanofluid compared with water where as there is a bigger change when comparing the viscosity. This could be due to the coefficient of Equation 5.4 being significantly larger than that of Equation 5.1. The full uncertainty analysis can be viewed in Appendix E. The uncertainties of the density and specific heat where calculated using the Equation D.5 for the nanofluid density and Equation D.7 for the specific heat of the nanofluid.

Property	**Water**	**0.33 vol%**	**0.75 vol%**	**1.0 vol%**
Density	0.003%	0.003%	0.003%	0.003%
Specific heat	0.04%	0.04%	0.04%	0.04%
Thermal conductivity	2%	5.4%	5.4%	5.4%
Viscosity	1%	1.2%	1.5%	1.6%

Table 5.2: Uncertainties of properties for water and *MWCNT-water* nanofluid

5.5 Conclusion

The preparation of the nanofluids was based on the work found in literature with some adjustment on the sonication times. From the pH of the nanofluids it was shown that the 1.0 vol% nanofluid was very close the iso-electric point, which means that fluid can show signs of the nanoparticles agglomerating. This was further validated via the thermal conductivity and viscosity of the nanofluids. The 1.0 vol% nanofluid which exhibited the highest thermal conductivity and viscosity compared with the other nanofluids had a possibility of agglomerated nanoparticles in its suspension. The uncertainties of the *MWCNT-water* nanofluid density and specific heat was the same as that of water since they largely only depend on the uncertainty of the waters density and specific heat. There was a slight change in the thermal conductivity of the 0.75 vol% and 1.0 vol% of the *MWCNT-water* nanofluid compared with water where as there was a bigger change when comparing the viscosity to that of water. This was attributed to the large difference in the thermal conductivity and viscosity coefficient used in the newly developed correlations.

Chapter 6

Heat transfer and friction factor results of *MWCNT-water* nanofluids

6.1 Introduction

In this chapter the experimental heat transfer coefficients and friction factors of *MWCNT-water* nanofluids are determined by using the experimental thermal conductivity and viscosity properties determined in Chapter 5. The heat transfer results of the three different volume concentrations of *MWCNT-water* nanofluids were compared with the results of distilled water. Developed correlations for water found in literature are used to develop new correlations by substituting the experimental properties of nanofluids in place of the water properties. Lastly, the friction factors of the *MWCNT-water* nanofluids are also compared with that of water.

6.2 Repeatability of results and stability of nanofluids

Many experiments were conducted over a few days and were repeated a few days later without any measurable changes in results. However, the nanofluids were sonicated again before it was used after it has been standing for more than 24 hours. Agglomeration of the nanoparticles was checked via a scanning electron microscope, but according to Hiemenz (1986) it does not give a clear indication whether the particles have clustered together or not since during the drying process the particles cluster together. However, it was observed the particles had a fairly even distribution in the water. It was also observed that there was some entanglement of the particles especially for the 0.75 vol% and 1 vol% nanofluid but this could have been due to the preparation of the samples.

6.3 Heat transfer results

Three different volume concentrations of *MWCNT-water* nanofluids are experimentally tested and the results are compared to that of distilled water. The same methodology is followed in determining the heat transfer coefficient as was done for the water in Chapter 4. However, the viscosity was approximated using Equation 5.4 and the thermal conductivity was calculated

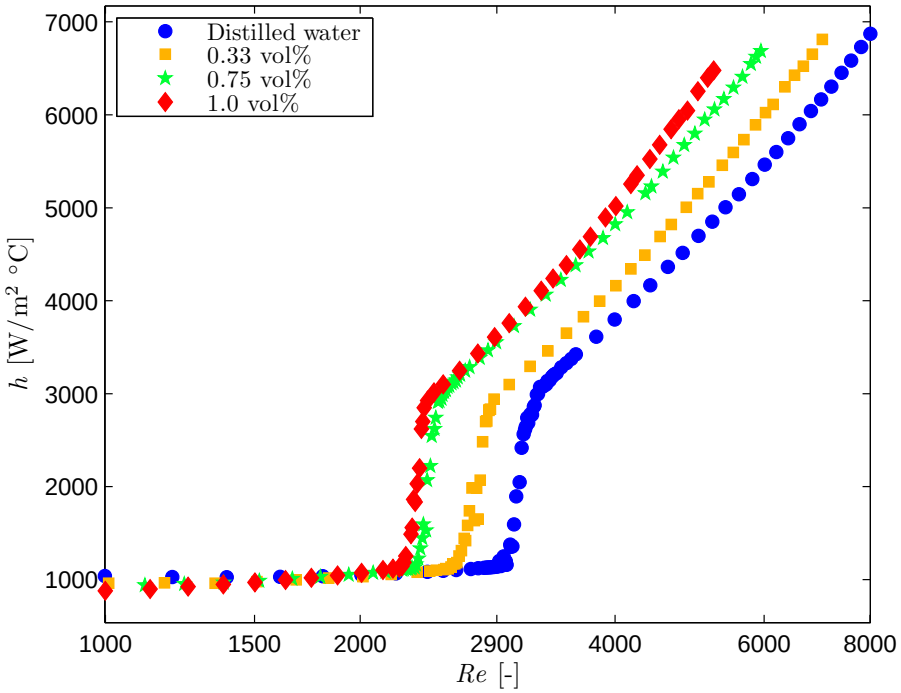

Figure 6.1: Heat transfer coefficient results of *MWCNT-water* nanofluids at average Reynolds number

using Equation 5.1.

6.3.1 Heat transfer results of *MWCNT-water* nanofluids compared to water for the entire flow range

Shown in Figure 6.1 are the averaged Nusselt numbers for the *MWCNT-water* nanofluids compared with the distilled water. For fully turbulent flow, at a Reynolds number of 5 000, the heat transfer coefficient is enhanced by 10% when using the 0.33 vol% *MWCNT-water* nanofluid, by 24% when using the 0.75 vol% *MWCNT-water* nanofluid and by 33% when using the 1.0 vol% *MWCNT-water* nanofluid.

Shown in Table 6.1 are the experimental uncertainties compared to that of distilled water at a Reynolds number of a 5 000. The uncertainty increases as the nanoparticle volume increase but is still significantly smaller than the increase in convective heat transfer coefficient enhancement. Hence one can say with certainty that there is enhancement in the convective heat transfer coefficient.

Distilled water	**0.33 vol%**	**0.75 vol%**	**1.0 vol%**
1.9%	2.0%	2.2%	2.3%

Table 6.1: Uncertainty of the working fluids at a Re = 5 000

A possible reason for the increase in the heat transfer coefficient is that the nanoparticles presented in the base fluid increase the thermal conductivity, delay and disturb the thermal boundary layer and due to the chaotic movement of the nanoparticles accelerate the energy exchange process in the fluid (Xuan and Li, 2003; Kim et al., 2009; Daungthongsuk and Wongwises, 2010). However with an increase in the effective thermal conductivity of the nanofluid, so does the viscosity increase and both increase with an increasing particle concentration (Daungthongsuk and Wongwises, 2010). The increase in the thermal conductivity leads to an increase in heat transfer performance whereas the increase in viscosity leads to an increase in boundary layer thickness, which results in a decrease in heat transfer performance (Yu et al., 2009).

Hence comparing heat transfer of a nanofluid to that of its base fluid at a constant Reynolds number is generally not the best comparison since the viscosity of the nanofluid is larger than that of its base fluid (Pak and Cho, 1998). It was proposed by Pak and Cho (1998) that a comparison of the heat transfer coefficient as a function of constant velocity comparison gives a more accurate representation of the heat transfer. Such a comparison is made in Figure 6.2. The results show that, at a constant velocity, the heat transfer coefficient of 0.33 vol% is 3.3% lower, at 0.75 vol% it is 6.6% lower and at 1.0 vol% it is 12.6% lower than that of distilled water. This trend of lower heat transfer coefficients in nanofluids compared with water was also experienced by Pak and Cho (1998), Williams *et al.* (2008) and Yu *et al.* (2009). It is, however, interesting to note that at very high velocities the heat transfer coefficients of the 0.33 vol% *MWCNT-water* nanofluid is equal that of the distilled water. This could be due to the fact that nanofluids exhibit shear thinning behaviour at high shear rates (Ding et al., 2006; Ko et al., 2007; Garg et al., 2009), which decreases the viscosity and the nanofluid then enhances the heat transfer.

Figure 6.2 also shows that the transitional flow regime for each *MWCNT-water* nanofluid is delayed which is in agreement with the work of Liu and Yu (2011). This is due to the particle-fluid interaction, which dampens the instability and reduces the turbulence intensity and Reynolds stress in the flow (Liu and Yu, 2011).

The reason for the early transition when comparing the heat transfer coefficient with the Reynolds number (see Figure 6.1) is that the viscosities of the *MWCNT-water* nanofluids are larger compared with those of distilled water. This results in the data shifting to lower Reynolds numbers and the *MWCNT-water* nanofluids showing enhancement in heat transfer.

For laminar flow, at a Reynolds number of a 1 000, the heat transfer coefficient is reduced by 7.5% when using the 0.33 vol% *MWCNT-water* nanofluid, by 11% when using the 0.75 vol% and by 15% when using the 1.0 vol% *MWCNT-water* nanofluid.

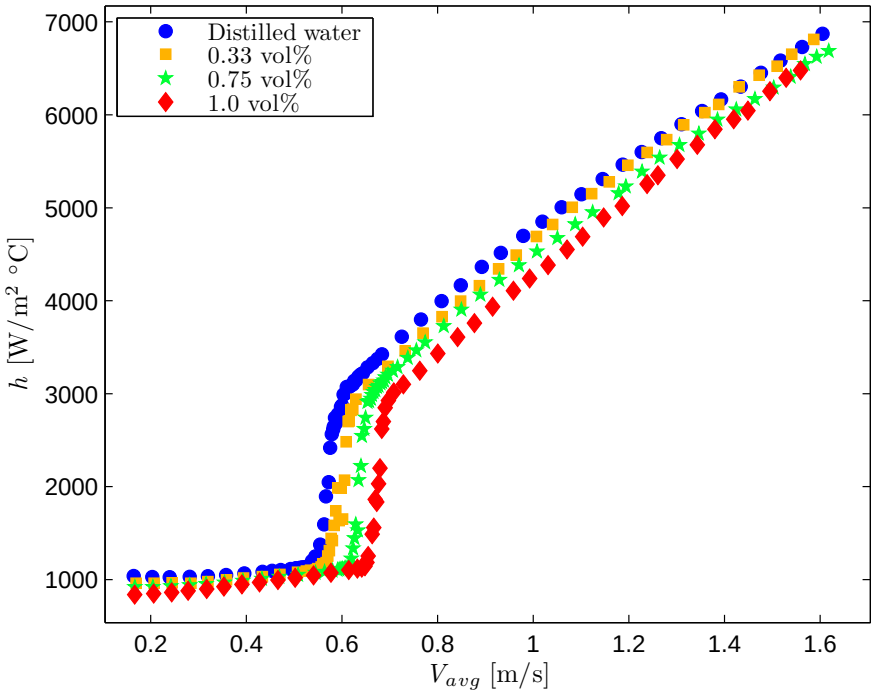

Figure 6.2: Heat transfer coefficient results of *MWCNT-water* nanofluids at constant velocity

Shown in Table 6.2 are the experimental uncertainties compared to that of distilled water at a Reynolds number of a 1 000. The uncertainties remain the same as the nanoparticle volume increase but are still significantly smaller than the decrease in the convective heat transfer coefficient. Hence one can say with certainty that there is a decrease in the convective heat transfer coefficient.

Distilled water	**0.33 vol%**	**0.75 vol%**	**1.0 vol%**
1.4%	1.2%	1.2%	1.1%

Table 6.2: Uncertainty of the working fluids at a Re = 1 000

A possible reason for the decrease in the heat transfer coefficient for the *MWCNT-water* nanofluids can be explained by Figure 6.3. Shown in Figure 6.3 is the local heat transfer coefficient at various axial distances for *MWCNT-water* nanofluids compared to distilled water at a Reynolds number of 1 000. Up to an axial distance of 40 tube diameters the local heat transfer coefficient is approximately the same. The local heat transfer for the distilled water reaches a minimum at an axial distance of approximately 57 tube diameter after which it increases. A similar trend is seen for the *MWCNT-water* nanofluids, only that the minimum is shifted further along the tube as the volume concentration increases, indicating that the addition of particles delays the development of the thermal boundary layer. A possible reason for the dip in the local heat transfer coefficient could be due to a imposed bell-mouth inlet. In such a case, the boundary layer along the tube wall is at first laminar and then changes through a transition region to the turbulent condition, causing the dip in the results. The length of the dip decreases with the increase of the turbulent Reynolds number (Tam and Ghajar, 1998). This is shown in Figure

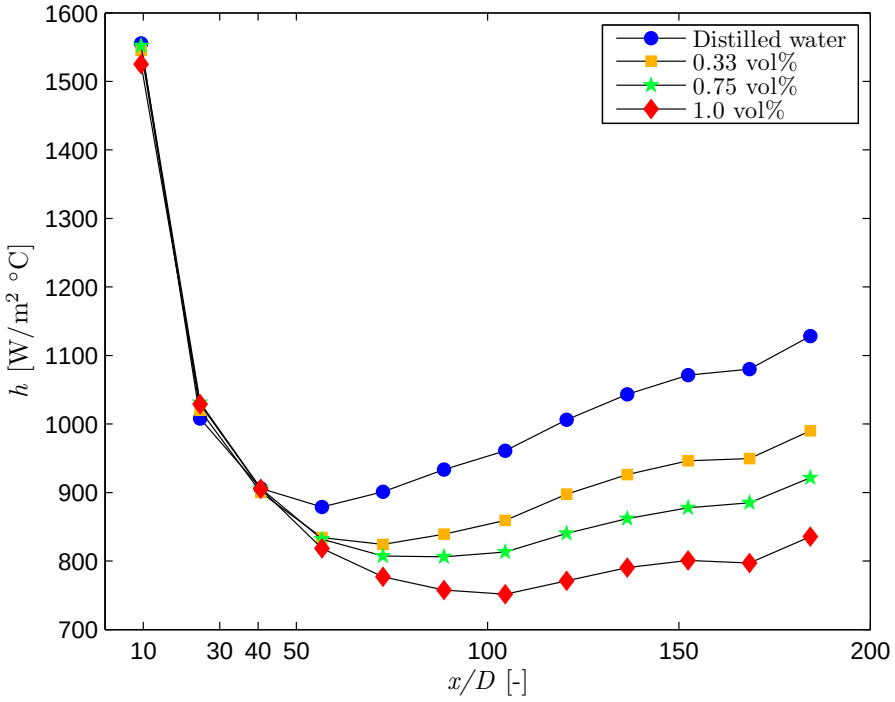

Figure 6.3: Axial profiles of heat transfer coefficients for *MWCNT-water* nanofluids compared to water at a Reynolds number of 1 000

6.4, where the dip decreases as the Reynolds number is increased. At a Reynolds number of a 2 000, the heat transfer is reduced by 1.6% when using the 0.33 vol% *MWCNT-water* nanofluid, enhanced by 2.2% and 2.3% when using the 0.75 vol% and 1.0 vol% *MWCNT-water* nanofluid respectively. Figure 6.4 shows that the *MWCNT-water* nanofluids for volume concentrations of 0.75% and 1.0% enhance the heat transfer up to an axial distance of approximately 120 tube diameters. The 0.33 vol% *MWCNT-water* only enhances the heat transfer between 25 and 90 tube diameters. The dip is still present for the distilled water and 0.33 vol% *MWCNT-water* nanofluid (there is a 10% and 6% increase in the heat transfer coefficient after the dip for distilled water and 0.33 vol% *MWCNT-water* nanofluid respectively) but has nearly vanished for the 0.75 vol% and 1.0 vol% *MWCNT-water* nanofluids. The addition of nanoparticles into the base fluid seems to suppress the bell-mouth inlet effect. This then results in a decrease in the heat transfer coefficient for the current nanofluids in laminar flow.

Shown in Table 6.3 are the experimental uncertainties compared to that of distilled water at a Reynolds number of 2 000. The uncertainty remains the same as the nanoparticle volume increase and is very close to the decrease/increase in the convective heat transfer coefficient. Hence one cannot say with certainty that there is enhancement or a decrease in the convective heat transfer coefficient.

Distilled water	**0.33 vol%**	**0.75 vol%**	**1.0 vol%**
1.2%	1.2%	1.2%	1.2%

Table 6.3: Uncertainty of the working fluids at a Re = 2 000

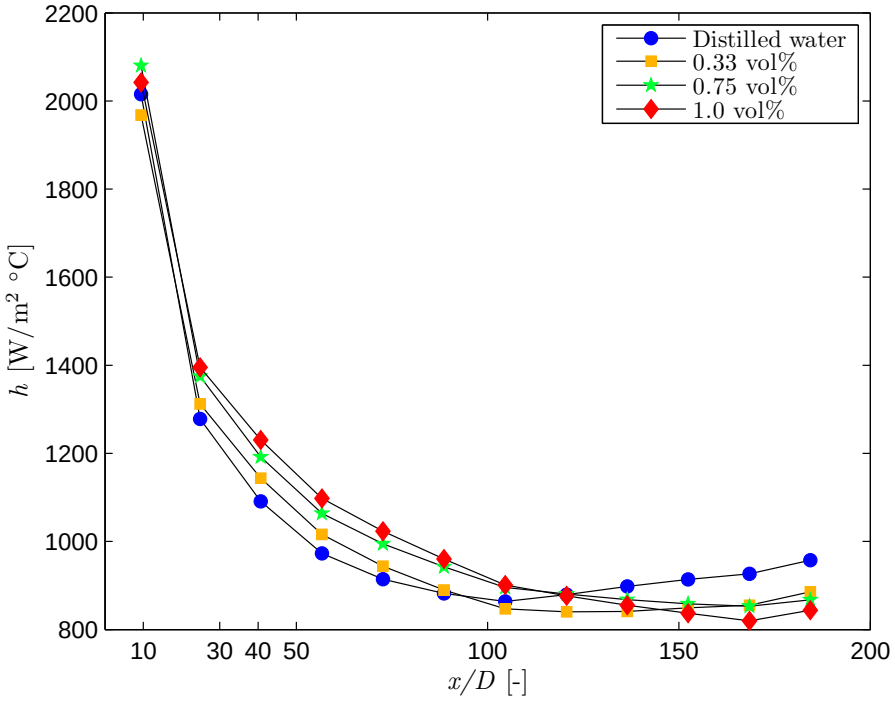

Figure 6.4: Axial profiles of heat transfer coefficients for *MWCNT-water* nanofluids compared to water at a Reynolds number of 2 000

6.3.2 Comparison of results to existing heat transfer correlations

Due to the increase in viscosity the *MWCNT-water* nanofluid results shifted to lower Reynolds numbers (see Figure 6.1), hence the results were compared to correlations developed for water by substituting the nanofluid properties for the water properties. Comparing nanofluid results to developed correlations for water was also done by Yu *et al.* (2009), Williams *et al.* (2008) and Liu and Liao (2010). The correlation by Ghajar and Tam (1994) was used for comparison purposes in the laminar and turbulent flow regime and Equation 4.19 was used for comparison purposes in the transitional flow regime.

Modified laminar correlation:

$$Nu_{nf} = 1.24\left[Gz_{nf} + 0.025 \cdot (Gr_{nf} \cdot Pr_{nf})^{0.75}\right]^{1/3} \cdot \left(\frac{\mu_{nf}}{\mu_w}\right)^{0.14} \tag{6.1}$$

where

$$Gz_{nf} = \frac{Re_{nf} \cdot Pr_{nf} \cdot D}{L}$$

and β in the Grashof number is calculated using water properties

Modified turbulent correlation:

$$Nu_{nf} = 0.023 \cdot Re_{nf}^{0.8} \cdot Pr_{nf}^{0.385} \cdot \left(\frac{L}{D}\right)^{-0.0054} \cdot \left(\frac{\mu_{nf}}{\mu_w}\right)^{0.14} \tag{6.2}$$

Modified transition correlation:

$$Nu_{nf} = Nu_{lam} + \left[e^{\frac{Re_{trans}-Re}{36}} + Nu_{turb}^{-0.935}\right]^{-0.935} \tag{6.3}$$

Heat transfer in the laminar flow regime

Shown in Figure 6.5 is the ratio of the predicted (Equation 6.1) to measured Nusselt numbers as a function of the laminar Reynolds numbers. The results for all three volume concentrations of *MWCNT-water* nanofluids are predicted to within 10%. For the 0.33 vol% *MWCNT-water* nanofluid the data is over predicted by 1.8% with a maximum deviation of 4%, the 0.75 vol% *MWCNT-water* nanofluid is over predicted by 3.5% with a maximum deviation of 1.8% and the 1.0 vol% *MWCNT-water* nanofluid is over predicted by 8.6% with a maximum deviation of 2.4%.

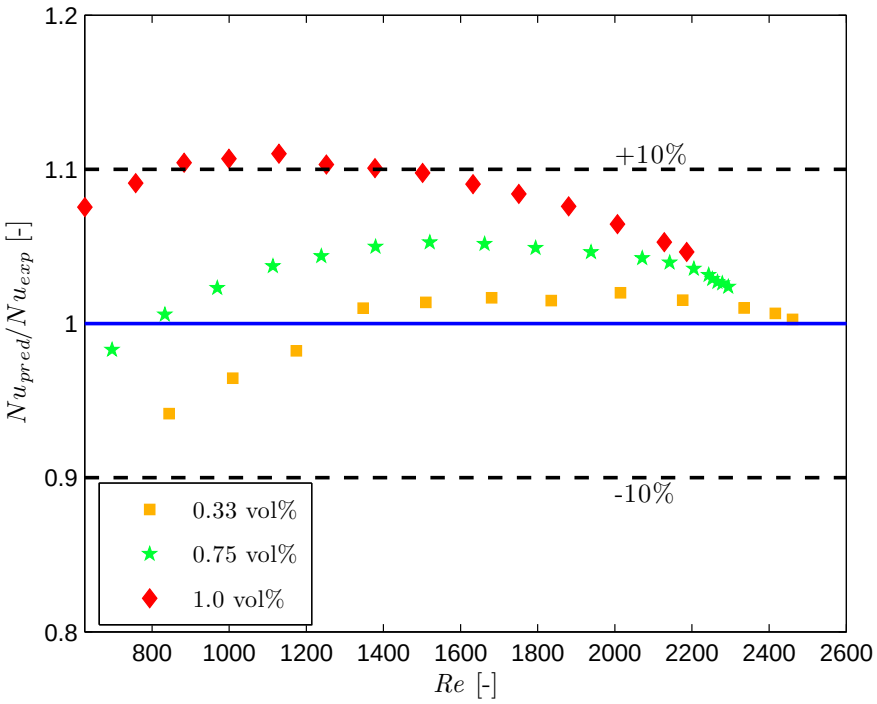

Figure 6.5: Ratio of the predicted (Equation 6.1) to measured Nusselt numbers as a function of the laminar Reynolds number

Heat transfer in the turbulent flow regime

Shown in Figure 6.6 is the ratio of the predicted (Equation 6.2) to measured Nusselt numbers as a function of the turbulent Reynolds numbers. The results for all three volume concentrations of *MWCNT-water* nanofluids are predicted to within 10%. For the 0.33 vol% *MWCNT-water* nanofluid the data is under predicted by 3.8% with a maximum deviation of 1.9%, the 0.75 vol% *MWCNT-water* nanofluid is under predicted by 5.8% with a maximum deviation of 2.2% and the 1.0 vol% *MWCNT-water* nanofluid is over predicted by 5.5% with a maximum deviation of 4.4%.

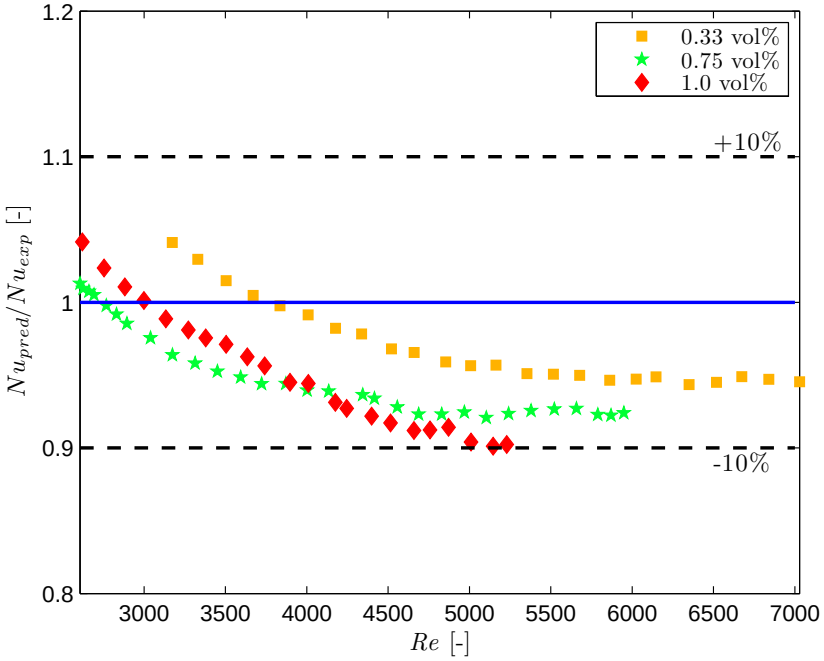

Figure 6.6: Ratio of the predicted (Equation 6.2) to measured Nusselt numbers as a function of the turbulent Reynolds number

Heat transfer in the transitional flow regime

Shown in Figure 6.7 is the ratio of the predicted (Equation 6.3) to measured Nusselt numbers as a function of the transitional Reynolds numbers. The results for all three volume concentrations for the *MWCNT-water* nanofluids are largely outside the 10% boundary. For the 0.33 vol% *MWCNT-water* nanofluid the data is over predicted by 16% with a maximum deviation of 84%, the 0.75 vol% *MWCNT-water* nanofluid is over predicted by 9.2% with a maximum deviation of 91% and the 1.0 vol% *MWCNT-water* nanofluid is over predicted by 12% with a maximum deviation of 88%.

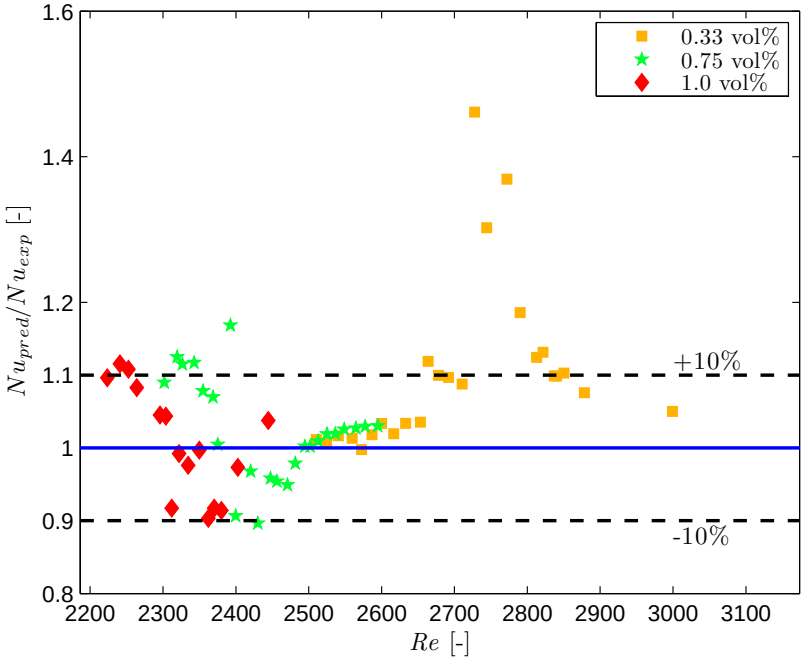

Figure 6.7: Ratio of the predicted (Equation 6.3) to measured Nusselt numbers as a function of the transitional Reynolds numbers

Shown in Figure 6.8 is the transitional region for the 0.33 vol% *MWCNT-water*. The Reynolds number at which transition starts is at approximately 2 500 and the transition region is approximately 500 Reynolds numbers long. Equation 6.3 predicts the data fairly well, up until a Reynolds number of 2 700, after which there is a large scatter in data. This scatter is also shown in Figure 6.7, which results in a large deviation in data.

The onset of transition for the 0.75 vol% *MWCNT-water* nanofluid starts at a Reynolds number of approximately 2 300 and is approximately 300 Reynolds numbers long and is shown in Figure 6.9. The data is predicted by Equation 6.3 from the critical Reynolds number up until 2 600.

Figure 6.10 shows the transitional region for the 1.0 vol% *MWCNT-water* nanofluid. Transition starts at a Reynolds number of approximately 2 200 and is approximately 300 Reynolds numbers long. The data is predicted by Equation 6.3 fairly well, however, there is a large scatter in results. This could be due to the chaotic movement of the particles in the transitional flow regime.

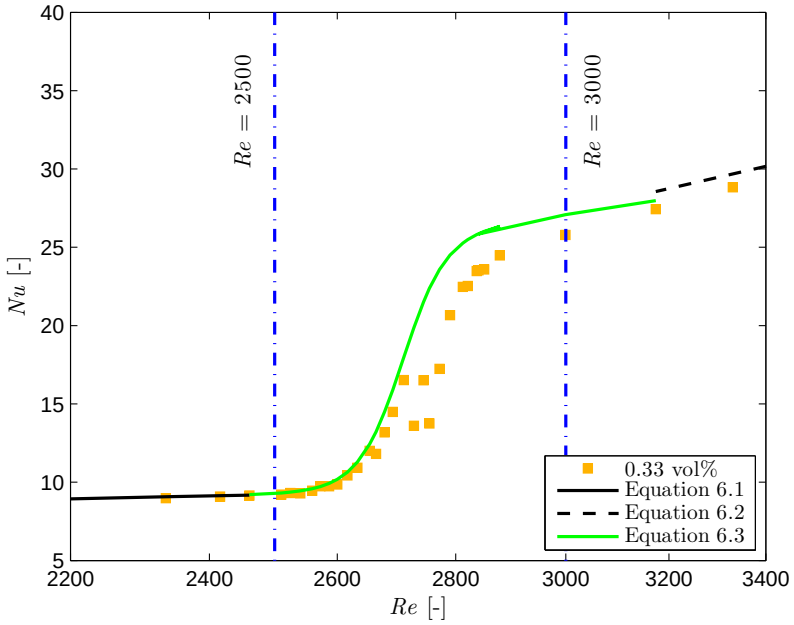

Figure 6.8: Nusselt number as a function of the transitional Reynolds number for the 0.33 vol% *MWCNT-water* nanofluid

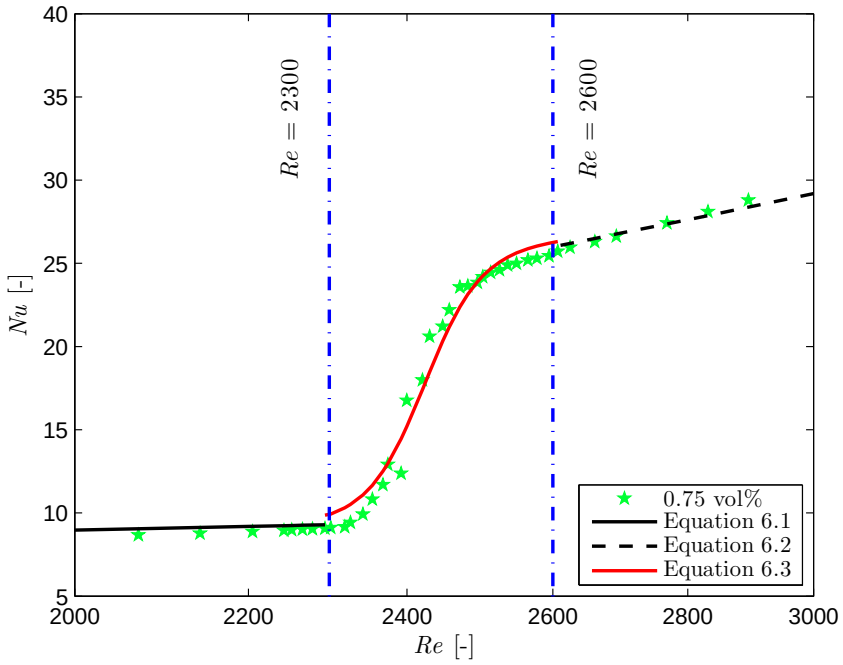

Figure 6.9: Nusselt number as a function of the transitional Reynolds number for the 0.75 vol% *MWCNT-water* nanofluid

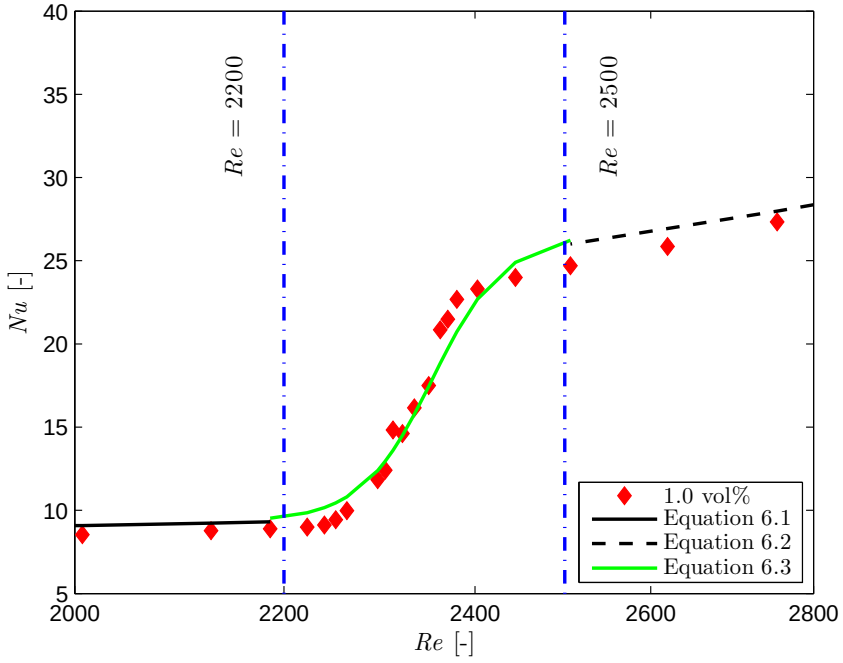

Figure 6.10: Nusselt number as a function of the transitional Reynolds number for the 1.0 vol% *MWCNT-water* nanofluid

6.4 Friction factor and pressure drop results

The pressure drop of the 0.33 vol% and 0.75 vol% *MWCNT-water* nanofluid are compared to the pressure drop of water. The reason for not showing the results of the 1.0 vol% *MWCNT-water* nanofluid is that the small pressure ports became blocked and pressure readings could not be taken. This is due to the high nanoparticle concentration in the distilled water and with the pH of the solution being to close to the iso-electric point (see Figure 5.1) the nanoparticles agglomerated.

Shown in Figure 6.11 are the friction factors for the 0.33 vol%, 0.75 vol% *MWCNT-water* nanofluids and distilled water for the entire flow range. The results are compared to the Poiseuille equation for laminar flow and the correlation by Allen and Eckert (1964) for turbulent flow.

In the turbulent flow regime at a Reynolds number of 5 000 the friction factor for the 0.33 vol% *MWCNT-water* nanofluid is 0.8% higher and for the 0.75 vol% *MWCNT-water* nanofluid it is 2.5% lower than that of distilled water. In the laminar flow regime at a Reynolds number of 2 000 the friction factor for the 0.33 vol% *MWCNT-water* nanofluid is 0.7% lower and the 0.75 vol% *MWCNT-water* nanofluid is 20% lower than that of distilled water. The friction factors of the 0.33 vol% *MWCNT-water* nanofluid are very similar to that of the water, this is most likely due to the low concentration of nanoparticles in the base fluid. As in the case of heat transfer results, the experimental friction factor data shifts to lower Reynolds numbers, this is due to the higher viscosity of the *MWCNT-water* nanofluids.

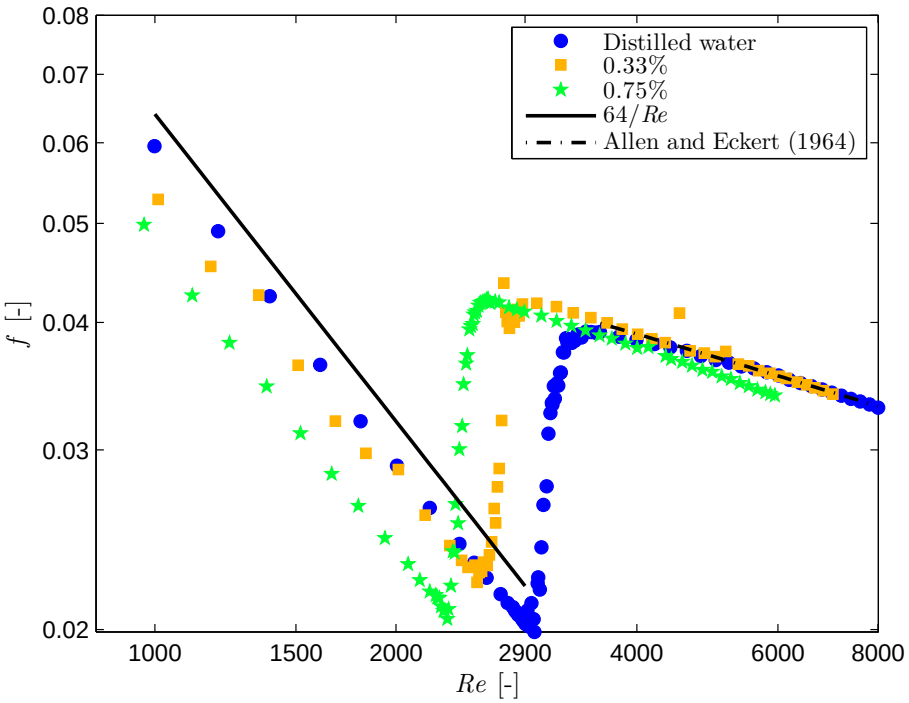

Figure 6.11: Friction factor of the *MWCNT-water* nanofluids compared to distilled water

Due to the shift in the experimental data the pressure drop of the *MWCNT-water* nanofluids

is compared to distilled at the average velocity. Shown in Figure 6.12 are the measured pressure drops across the test section for the 0.33 vol%, 0.75 vol% *MWCNT-water* nanofluid and of distilled water for the entire flow range. The pressure drop increases with increasing average velocity. There is a slight increase in pressure drop for an increasing nanoparticle concentration. In the turbulent flow regime, $\Delta P_{nf}/\Delta P_{bf} = 1.03$ for both *MWCNT-water* nanofluids and in the laminar flow regime, $\Delta P_{nf}/\Delta P_{bf} = 1.1$ for the 0.33 vol% *MWCNT-water* nanofluid and $\Delta P_{nf}/\Delta P_{bf} = 1.2$ for the 0.75 vol% *MWCNT-water* nanofluid.

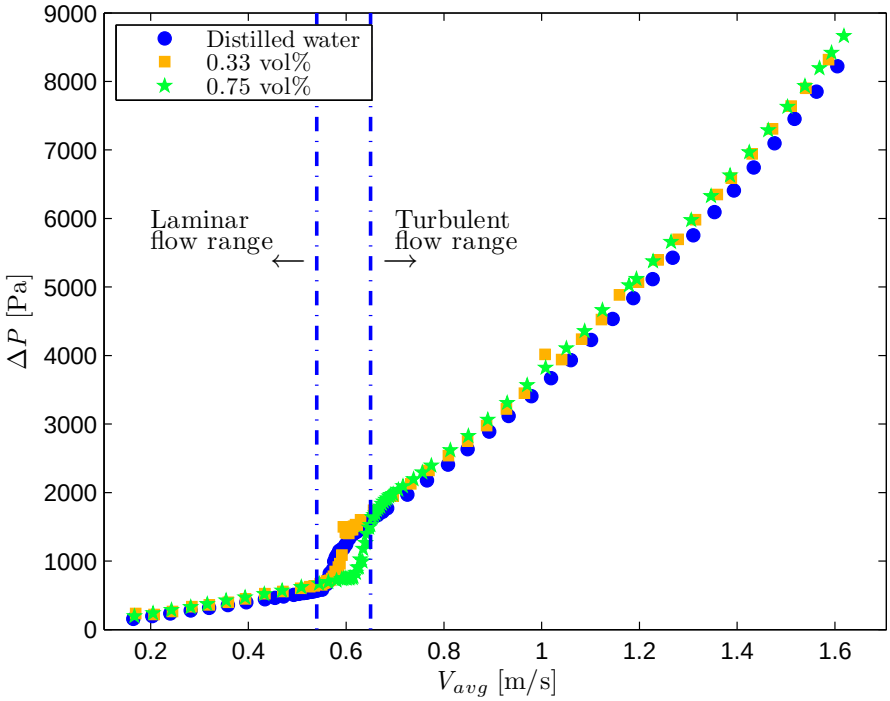

Figure 6.12: Pressure drop of the *MWCNT-water* nanofluids compared to water

6.5 Performance evaluation of the *MWCNT-water* nanofluids

Experimental results indicate that there is enhancement in heat transfer using nanofluids when comparing the results using a Reynolds number and Nusselt number plot. This is only due to the increase in viscosity of the nanofluids which shift the results to the left. When plotting the results for the average velocity, nanofluids do not show enhancement in heat transfer.

Prasher *et al.* (2006b) challenged the idea whether there is any benefit using nanofluids as heat transfer fluids. They considered the conservative case where $h_{nf} = h_{bf}$ and developed the design equation for nanofluids, given in Equation 6.4.

$$\frac{\Delta P_{nf}}{\Delta P_{bf}} = \left(\frac{\mu_{nf}}{\mu_{bf}}\right) \cdot \left(\frac{k_{bf}}{k_{nf}}\right)^4 \cdot \left(\frac{Nu_{bf}}{Nu_{nf}}\right)^4 \tag{6.4}$$

If $\Delta P_{nf}/\Delta P_{bf} > 1$ then the nanofluid is worse as a heat transfer fluid than the base fluid, however, if it is $\Delta P_{nf}/\Delta P_{bf} < 1$, then it is a better heat transfer fluid. In the previous section where

$\Delta P_{nf}/\Delta P_{bf}$ was investigated, it was shown that in the turbulent flow regime, $\Delta P_{nf}/\Delta P_{bf} \approx 1$ and in the laminar flow regime $\Delta P_{nf}/\Delta P_{bf} > 1$. Hence this indicates that in the current study, nanofluids are better suited for the turbulent flow regime due to the shear thinning behaviour that they exhibit. In the laminar flow regime, they are worse heat transfer fluids than the base fluid, which was also indicated by the heat transfer coefficient reduction in Section 6.3.

Equation 6.4 shows that ΔP is more sensitive to changes in k and Nu when compared with the viscosity. The thermal conductivity and viscosity can be represented in the following form for low volume concentrations:

$$\frac{k_{nf}}{k_{bf}} = 1 + C_k \cdot \phi \tag{6.5}$$

$$\frac{\mu_{nf}}{\mu_{bf}} = 1 + C_\mu \cdot \phi \tag{6.6}$$

where C_k and C_μ depend on experimental data

For the conservative case of $Nu_{nf} = Nu_{bf}$, desiring that ΔP_{nf} not exceed ΔP_{bf} and substituting Equation 6.5 and 6.6 into Equation 6.4. Assuming that $C_k \cdot \phi$ is very small compared to 1 (which is a good approximation for small values of ϕ (Prasher et al., 2006b)), Equation 6.4 then reduces to the following form:

$$C_\mu = 4 \cdot C_k \tag{6.7}$$

This shows that in order to have a beneficial heat transfer fluid, the increase in viscosity may not be more than four times the increase in thermal conductivity. In the current case C_μ equals 60, which is more than four times C_k and which equals 7.

Ferrouillat *et al.* (2011) used energetic performance evaluation criterion (PEC) to evaluate their nanofluids. It is defined as the ratio of heat transferred to the required pumping power in the test section:

$$PEC = \frac{\dot{m} \cdot c_p \cdot (T_e - T_i)}{(\dot{m}/\rho) \cdot \Delta P} \tag{6.8}$$

Shown in 6.13 is the PEC of the *MWCNT-water* nanofluids compared to distilled water. For the turbulent flow regime PEC of the *MWCNT-water* nanofluids is almost that of water which indicates that energy budget of the *MWCNT-water* nanofluids equals nearly that of distilled water. In the laminar flow regime the PEC for the 0.33 vol% *MWCNT-water* nanofluid is 12% lower than that of distilled water and for the 0.75 vol% *MWCNT-water* nanofluid is 15% lower hence the energy budget is unfavourable. For the transitional flow regime the PEC for the 0.33 vol% *MWCNT-water* nanofluid is 18% larger than that of the distilled water and for the 0.75 vol% *MWCNT-water* nanofluid it is 52% larger, which makes the energy budget favourable for the nanofluids. Even though the viscosity of the nanofluid is four times greater than that of the thermal conductivity it is more favourable to run nanofluids in the transition and high turbulent flow regime since the energy budget is better than that of the distilled water.

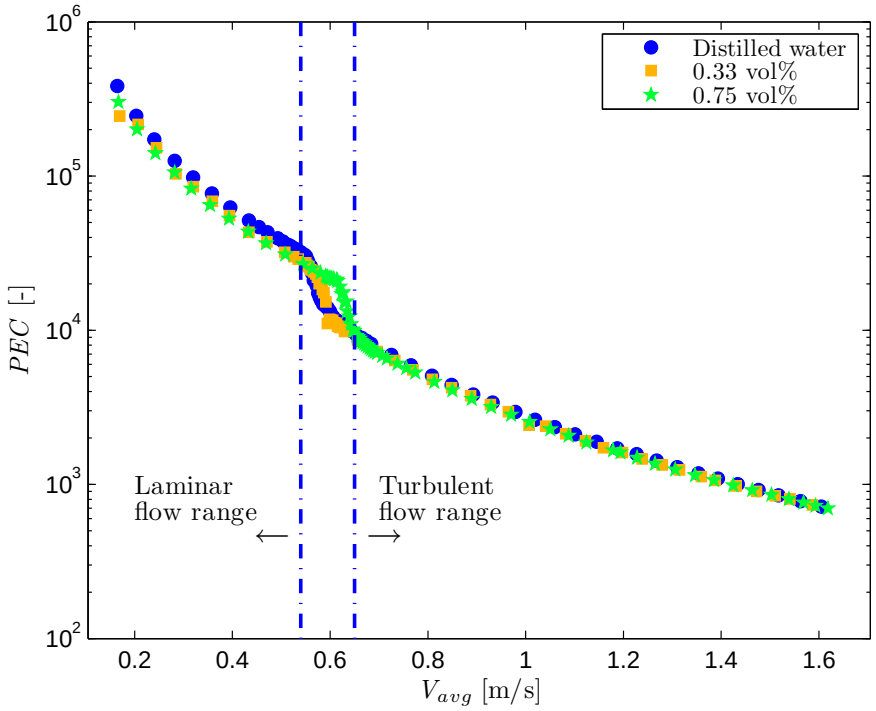

Figure 6.13: The PEC as a function of average velocity for *MWCNT-water* nanofluids and distilled water

6.6 Conclusion

Three different *MWCNT-water* nanofluid volume concentrations were tested for the late laminar, transition and early turbulent flow regimes. Heat transfer and pressure drop measurements were taken from a Reynolds number of a 1 000 to about 8 000 and compared with those of distilled water.

For the turbulent flow regime, all three nanofluids showed enhancement in the convective heat transfer coefficient, with the 1.0 vol% showing the highest enhancement and the 0.33 vol% the least. When comparing the heat transfer coefficients with each other at the same fluid velocity, the nanofluids showed a decrease in heat transfer performance when compared with water. This was due to the fact that *MWCNT-water* nanofluids have a larger viscosity than water and the data shifted lower Reynolds numbers which resulted in transitional flow starting sooner. For the laminar flow regime the *MWCNT-water* nanofluids showed only a slight enhancement in heat transfer. This was attributed to the fact that the distilled water showed an imposed bell-mouth inlet condition, which resulted in a higher local heat transfer coefficient than compared with the nanofluids.

Due to the shift of the nanofluids to lower Reynolds numbers, it was considered to compare the data with correlations, developed for water, found in literature. The correlation were modified for nanofluids and it was found that the modified correlations predicted the results in the turbulent and laminar flow regime to within ±10% and in the transitional flow regime the 0.75

vol% and 1.0 vol% the data was predicted within ±10% whereas the 0.33 vol% was not. This was attributed to the large scatter in the data.

Pressure drop measurements were only taken for the 0.33 vol% and 0.75 vol% *MWCNT-water* nanofluids since the pressure ports got clogged with the 1.0 vol% *MWCNT-water* nanofluid. The clogging of the pressure ports was attributed to the nanoparticles of the 1.0 vol% *MWCNT-water* nanofluid agglomerating since its pH was to close to the iso-electric point.

Results indicated that with increasing volume concentration the pressure drop increases which can be attributed to the increase in viscosity. A performance evaluation on the *MWCNT-water* nanofluids was done and results indicated that the increase in viscosity exceeds four times the amount of increase in thermal conductivity of the nanofluids, which is the conservative case where the heat transfer of the nanofluids equals that of the base fluid. When considering the energetic performance evaluation criterion of the *MWCNT-water* nanofluids it can be concluded that it is more favourable to run nanofluids in the transition and high turbulent flow regime since the energy budget is better than that of the distilled water.

Chapter 7

Summary, conclusions and recommendations for future work

7.1 Summary

Currently there is an exponential growth in electronic technologies. With their decrease in size and increase in the rate of operation, problems arise with the their thermal management. Research is being done on enhancing the heat removal of these systems by using nanofluids. Numerous papers in literature report on the enhanced heat transfer rate using nanofluids compared with conventional fluids such as water. Most of the papers reported in literature tested nanofluids in either the fully turbulent flow regime or laminar flow regime and only a few reported on the transitional flow regime with even fewer using MWCNT as their nanofluids.

An experimental system was developed in order to test different volume concentrations of *MWCNT-water* nanofluids. The test setup consisted out of a single tube, heated via a constantine wire creating a constant heat flux boundary condition. The test section was 1 m long with a mixer attached to the end and a 0.5 m inlet section attached to the inlet of the test section to ensure hydrodynamically developed flow at the test section. Three different volume concentrations of *MWCNT-water* nanofluid were tested for the laminar-transition-turbulent flow regimes. The results of the nanofluids were compared with that of distilled water and then to developed correlation for water, where the water properties were replaced by the nanofluid properties. The results are summarised in the following section.

7.2 Conclusions

The conclusions are divided in two parts. The first part is a conclusion on the results using water as test fluid and the second part using *MWCNT-water* nanofluids as the testing fluid

7.2.1 Water conclusions

The heat transfer coefficient for water was determined and the results were validated against published results in literature. Validation was done for flow in the laminar and turbulent flow

regime, and results show that the experimental data is under predicted by 5.2% in the laminar flow regime and by 2.4% in the turbulent flow regime when comparing to literature. This showed good agreement in the laminar and turbulent flow regimes and hence it was concluded that it should give good results in the transitional flow regime. The uncertainties in the heat transfer coefficient are 1.4% for the lowest flow rate and 2.5% for the highest. In the transitional flow regime a new correlation was developed based on the works by Ghajar and Tam (1994), the reason being that only fully developed inlet condition was used throughout the experimental process.

For validating the friction factor only the adiabatic results are used in order to eliminate any density and viscosity variations due to the heating of the tube. The friction factors were compared with Poiseuille flow in laminar flow and Blasius in turbulent flow. The experimental data is under predicted on average by 3.3% in laminar flow and 0.2% in turbulent flow. The uncertainties in the friction factor are between 2% and 10%.

7.2.2 Nanofluid conclusions

Results show that for the turbulent flow regime all three nanofluids showed enhancement in the convective heat transfer coefficient, with the 1.0 vol% showing the highest enhancement and the 0.33 vol% the least. When comparing the heat transfer coefficients to each other at the same fluid velocity, the nanofluids showed a decrease in heat transfer performance when compared with water. This was due to the fact that *MWCNT-water* nanofluids have a larger viscosity than water and the data shifted to lower Reynolds numbers which resulted in the early transition of the *MWCNT-water* nanofluids. For the laminar flow regime the *MWCNT-water* nanofluids showed only a slight enhancement in heat transfer. This was attributed to the fact that the distilled water showed an imposed bell mouth inlet condition, which resulted in a higher local heat transfer coefficient than compared with the nanofluids.

Due to the shift of the nanofluids to lower Reynolds numbers it was considered to compare the data with correlations, developed for water, found in literature. The correlation were modified for nanofluids and it was found that the modified correlations predicted the results in turbulent and laminar flow regime to within ±10% and in the transitional flow regime the 0.75 vol% and 1.0 vol% the data was predicted within ±10% whereas the 0.33 vol% was not. This was attributed to the large scatter in the data.

Pressure drop measurement were only taken for the 0.33 vol% and 0.75 vol% *MWCNT-water* nanofluids since the pressure ports got clogged with the 1.0 vol% *MWCNT-water* nanofluid. The clogging of the pressure ports was attributed to the nanoparticles of the 1.0 vol% *MWCNT-water* nanofluid agglomerating since its pH was to close to the iso-electric point.

Results indicated that with increasing volume concentration the pressure drop increases which can be attributed to the increase in viscosity. A performance evaluation on the *MWCNT-water* nanofluids was done and results indicated that the increase in viscosity exceeds four times the amount of increase in thermal conductivity of the nanofluids, which is the conservative case where the heat transfer of the nanofluids equals that of the base fluid. When considering the energetic performance evaluation criterion of the *MWCNT-water* nanofluids it can be concluded that it is more favourable to run nanofluids in the transition to turbulent flow regime since the

energy budget is better than that of the distilled water.

7.3 Future work

A very broad spectrum of work was covered surrounding nanofluids, hence not every aspect could be covered in detail and thus some questions are still unanswered. Therefore, future recommended work should include the following:

- The preparation of nanofluids is a critical part, if not the most important part, when wanting the optimal heat transfer performance. In a poorly prepared nanofluid the nanaparticles settle out of suspension, which leads to a large increase in viscosity due to the agglomeration of the nanoparticles. Most preparation methods found in literature are for metallic nanoparticles and very few exist for non-metallic. Hence an intensive study should investigate the proper preparation technique for MWCNT nanofluids.

- After a proper prepared nanofluid an investigation on the thermal conductivity and viscosity should be done. There exists numerous correlations for the thermal conductivity and viscosity but they are all study specific, in that they can only be used for that specific nanofluid. Hence a study on the thermal conductivity and viscosity for MWCNT nanofluids of different nanoparticle should be performed in order to get unified correlations.

- In this study only MWCNT nanofluids were investigated, hence different types of CNT nanofluids should be investigated.

References

S.I. Abu-Eishah. Correlations for the thermal conductivity of metals as a function of temperature. *International Journal of Heat and Mass Transfer*, 22(6):1855–1868, 2001.

R.W. Allen and E.R.G. Eckert. Friction and heat-transfer measurements to turbulent pipe flow of water (Pr = 7 and 8) at uniform wall heat flux. *Journal of Heat Transfer*, 86:301–310, 1964.

A. Amrollahi, A.M. Rashidi, R. Lotfi, M.E. Meibodi, and K. Kashefi. Convection heat transfer of functionalized mwnt in aqueous fluids in laminar and turbulent flow at the entrance region. *International Communications in Heat and Mass Transfer*, 37:717–723, 2010.

K.B. Anoop, T. Sundararajan, and S.K. Das. Effect of particle size on the convective heat transfer in nanofluid in the developing region. *International Journal of Heat and Mass Transfer*, 52(11):2189–2195, 2009.

Y. A. Çengel. *Heat and mass transfer - A practical approach*. McGraw Hill, 2nd edition, 2006.

S.K. Das and S.U.S. Choi. A review of heat transfer in nanofluids. In T.F. Irvine and J.P. Hartnett, editors, *Advances in Heat Transfer*, volume 41 of *Advances in Heat Transfer*, pages 81–197. Elsevier, 2009.

S.K. Das, S.U.S. Choi, and H.E. Patel. Heat transfer in nanofluids - A review. *Heat Transfer Engineering*, 27(10):3–19, 2006.

W. Daungthongsuk and S. Wongwises. A critical review of convective heat transfer of nanofluids. *International Journal of Thermal Sciences*, 11(5):797–817, 2007.

W. Daungthongsuk and S. Wongwises. An experimental study on the heat transfer performance and pressure drop of $TiO_2 - water$ nanofluids flowing under turbulent flow regime. *International Journal of Heat and Mass Transfer*, 53(1-3):334–344, 2010.

Y. Ding, H. Alias, D. Wen, and R. A. Williams. Heat transfer of aqueous suspensions of carbon nanotubes (CNT nanofluids). *International Journal of Heat and Mass Transfer*, 49(1-2):240–250, 2006.

F. Durst, S. Ray, B. Unsal, and O.A. Bayoumi. The development lengths of laminar pipe and channel flows. *Journal of Fluids Engineering*, 127(6):1154–1160, 2005.

S. Ferouillat, A. Bontemps, J.-P. Ribeiro, J.-A. Gruss, and O. Soriano. Hydraulic and heat transfer study of $SiO_2 - water$ nanofluids in horizontal tubes with imposed wall temperature boundary conditions. *International Journal of Heat and Fluid Flow*, 32(2):424–439, 2011.

O.S. Galaktionov, P.D. Anderson, G.W.M. Peters, and H.E.H. Meijer. Analysis and optimization of kenics static mixers. *International Polymer Processing*, 2(18):138–150, 2003.

P. Garg, J. L. Alvardo, C. Marsh, T. A. Carlson, D. A. Kessler, and K. Annamalai. An experimental study on the effect of ultrasonication on viscosity and heat transfer performance of multi-wall carbon nanotube-based aqueous nanofluids. *International Journal of Heat and Mass Transfer*, 52(29):5090–5101, 2009.

A.J. Ghajar and L.-M. Tam. Heat transfer measurements and correlations in the transition region for a circular tube with three different inlet configurations. *Experimental Thermal and Fluid Science*, 8(1):79–90, 1994.

A.J. Ghajar and L.-M. Tam. Flow regime map for a horizontal pipe with uniform wall heat flux and three inlet configuration. *Experimental Thermal and Fluid Science*, 10(3):287–297, 1995.

A.J. Ghajar, C.C. Tang, and W.L. Cook. Experimental investigation of friction factor in the transition region for water flow in minitubes and microtubes. *Heat Transfer Engineering*, 31 (6):646–657, 2010.

V. Gnielinski. New equations for heat and mass transfer in turbulent pipe and channel flow. *International Chemical Engineering*, 16(2):359–367, 1976.

S.Z. Heris, S. Gh. Etemad, and M.N. Esfahany. Experimental investigation of oxide nanofluids laminar flow convective heat transfer. *International Communications in Heat and Mass Transfer*, 33(4):529–535, 2006.

S.Z. Heris, M.N. Esfahany, and S. Gh. Etemad. Experimental investigation of convective heat transfer of $Al_2O_3 - water$ nanofluid in circular tube. *International Journal of Heat and Fluid Flow*, 28:203–210, 2007.

P.C. Hiemenz. *Principles of colloid and surface chemistry*, volume 9. Marcel Dekker, Inc., 2 edition, 1986.

S.P. Jang and S.U.S Choi. Role of brownian motion in the enhanced thermal conductivity of nanofluids. *Applied Physics Letters*, 84(21):4316–4318, 2004.

S. Kakaç and A. Pramuanjaroenkij. Review of convective heat transfer enhancement with nanofluids. *International Journal of Heat and Mass Transfer*, 52(13-14):3187–3196, 2009.

P. Keblinski, S.R. Phillpot, S.U.S. Choi, and J.A. Eastman. Mechanisms of heat flow in suspensions of nano-sized particles (nanofluids). *International Journal of Heat and Mass Transfer*, 45(4):855–863, 2002.

D. Kim, Y. Kwon, Y. Cho, C. Li, S. Cheong, Y. Hwang, J. Lee, D. Hong, and S. Moon. Convective heat transfer characteristics of nanofluids under laminar and turbulent flow conditions. *Current Applied Physics*, 9(2):119–123, 2009.

G.H. Ko, K. Heo, K. Lee, D.S. Kim, C. Kim, Y. Sohn, and M. Choi. An experimental study on the pressure drop of nanofluids containing carbon nanotubes in a horizontal tube. *International Heat and Mass Transfer*, 50(23-24):4749–4753, 2007.

S.W. Lee, S.D. Park, S. Kang, I.C. Bang, and J.H. Kim. Investigation of viscosity and thermal conductivity of SiC nanofluids for heat transfer applications. *International Journal of Heat and Mass Transfer*, 54(1-3):433–438, 2011.

Q. Li and Y. Xuan. Convective heat transfer and flow characteristics of $cu - water$ nanofluid. *Science in China*, 45(4):408–416, 2002.

D. Liu and L. Yu. Single-phase thermal transport of nanofluids in a minichannel. *Journal of Heat Transfer*, 133(3):031009(11 pages), 2011.

Z.-H. Liu and L. Liao. Forced convective flow and heat transfer characteristics of aqueous drag-reducing fluid with carbon nanotubes added. *International Journal of Thermal Sciences*, 49: 2331–2338, 2010.

S.E.B. Maiga, C.T. Nguyen, N. Galanis, G. Roy, T. Mare, and M. Coqueux. Heat transfer enhancement in turbulent tube flow using Al_2O_3 nanoparticle suspension. *International Journal of Numerical Methods for Heat and Fluid Flow*, 16(3):275–292, 2006.

B. Metais and E.R.G. Eckert. Forced, mixed and free convection regimes. *Transactions of the ASME Journal of Heat Transfer*, 10:295–296, 1964.

J.P. Meyer and J.A. Olivier. Transitional flow inside enhanced tubes for fully developed and developing flow with different types of inlet disturbances: Part I - Adiabatic pressure drop. *International Journal for Heat and Mass Transfer*, 54(7-8):1587–1598, 2011a.

J.P. Meyer and J.A. Olivier. Transitional flow inside enhanced tubes for fully developed and developing flow with different types of inlet disturbances: Part II - Heat transfer. *International Journal for Heat and Mass Transfer*, 54(7-8):1598–1607, 2011b.

R.J. Moffat. Describing the uncertainties in experimental results. *Experimental Thermal and Fluid Science*, 1(1):3–17, 1988.

S.M.S Murshed, K.C. Leong, C. Yang, and N.-T. Nguyen. Convective heat transfer characteristics of aqueous TiO_2 nanofluid under laminar flow conditions. *International Journal of Nanoscience*, 7(6):325–331, 2008.

S.M.S Murshed, C.A.N de Castro, M.J.V Lourenço, M.L.M Lopes, and F.J.V Santos. A review of boiling and convective heat transfer with nanofluids. *Renewable and Sustainable Energy Reviews*, 15(5):2342–2354, 2011.

C.-W. Nan, Z. Shi, and Y. Lin. A simple model for thermal conductivity of carbon nanotube-based composites. *Chemical Physics Letters*, 375(5-6):666–669, 2003.

M.J. O'Connell. *Carbon nanotubes - Properties and applications.* Taylor and Francis., 2006.

J.A. Olivier. *Single-phase heat transfer and pressure drop of water cooled at a constant wall temperature inside horizontal circular smooth and enhanced tubes with different inlet configurations in the transitional flow regime.* PhD thesis, University of Pretoria, August 2009.

J.A. Olivier and J.P. Meyer. Single-phase heat transfer and pressure drop of the cooling of water inside smooth tubes for transitional flow with different inlet geometries (RP-1280). *HVAC and R*, 16(4):471–496, 2010.

B.C. Pak and Y.I. Cho. Hydrodynamic and heat transfer study of dispersed fluids with submicron metallic oxide particles. *Experimental Heat Transfer*, 11(2):151–170, 1998.

C.O. Popiel and J. Wojtkowiak. Simple formulas for thermophysical properties of liquid water for heat transfer calculations. *Heat Transfer Engineering*, 19(3):87–101, 1998.

R. Prasher, P.E. Phelan, and P. Bhattacharya. Effect of aggregation kinetics on the thermal conductivity of nanoscale colloidal solutions (Nanofluid). *Nano Letters*, 6(7):1529–1534, 2006a.

R. Prasher, D. Song, J. Wang, and P.E. Phelan. Measurements of nanofluids viscosity and its implications for thermal applications. *Applied Physics Letters*, 89(13):1–3, 2006b.

R.E. Rayle. An investigation of the influence of orifice geometry on static pressure measurements. Master's thesis, Massachusetts Institute of Technology, October 1949.

B. Shome and M.K. Jensen. Mixed convection laminar flow and heat transfer of liquids in isothermal horizontal circular ducts. *International Journal of Heat and Mass Transfer*, 38 (11):1945–1956, 1995.

E.N. Sieder and G.E. Tate. Heat transfer and pressure drop of liquids in tubes. *Industrial and Engineering Chemistry*, 28(12):1429–1435, 1936.

L.-M. Tam and A.J. Ghajar. Effect of inlet geometry and heating on the fully developed friction factor in the transition region of a horizontal tube. *Experimental Thermal and Fluid Science*, 15(1):52–64, 1997.

L.-M. Tam and A.J. Ghajar. The unusual behaviour of local heat transfer coefficient in a circular tube with a bell-mouth inlet. *Experimental Thermal and Fluid Science*, 16(3):187–194, 1998.

V. Trisaksri and S. Wongwises. Critical review of heat transfer characteristics of nanofluids. *Renewable and Sustainable Energy Reviews*, 11(3):512–523, 2007.

X.-J. Wang and X.-F. Li. Influence of ph on nanofluids viscosity and thermal conductivity. *Chinese Physics Letters*, 26(5):1–4, 2009.

X.Q. Wang and A.S. Mujumdar. Heat transfer characteristics of nanofluids: A review. *International Journal of Thermal Sciences*, 46(1):1–19, 2007.

R.L. Webb and N.H. Kim. *Principles of enhanced heat transfer*. Taylor and Francis Group, 3rd edition, 2005.

D. Wen and Y. Ding. Experimental investigation into convective heat transfer of nanofluids at the entrance region under laminar flow conditions. *International Journal of Heat and Mass Transfer*, 47(24):5181–5188, 2004.

W. Williams, J. Buongiorno, and L.-W. Hu. Experimental investigation of turbulent convective heat transfer and pressure loss of alumina/water and zirconia/water nanoparticle colloids (nanofluids) in horizontal tubes. *Journal of Heat Transfer*, 130(4):042412(7 pages), 2008.

H. Xie, H. Lee, W. Youn, and M. Choi. Nanofluids containing multiwalled carbon nanotubes and their enhanced thermal conductivities. *Journal of Applied Physics*, 94(8):4967–4971, 2003.

Y. Xuan and Q. Li. Heat transfer enhancement of nanofluids. *International Journal of Heat and Fluid Flow*, 21(1):58–64, 2000.

Y. Xuan and Q. Li. Investigation on convective heat transfer and flow features of nanofluids. *Journal of Heat Transfer*, 125(1):151–155, 2003.

Y. Xuan and W. Roetzel. Conceptions for heat transfer correlation of nanofluids. *International Journal of Heat and Mass Transfer*, 43(19):3701–3707, 2000.

Q.Z. Xue. Model for thermal conductivity of carbon nanotube-based composites. *Physica B*, 368(1-4):302–307, 2005.

Y. Yang, Z.G. Zhang, E.A. Grulke, W.B. Anderson, and G. Wu. Heat transfer properties of nanoparticles-in-fluid dispersions (nanofluids) in laminar flow. *International Journal of Heat and Mass Transfer*, 48(6):1107–1116, 2005.

W. Yu, D.M. France, D.S. Smith, D. Singh, E.V. Timofeeva, and J.L. Routbort. Heat transfer to silicon carbide/water nanofluid. *International Journal of Heat and Mass Transfer*, 52(15-16): 3606–3612, 2009.

Appendix A

Experimental setup's used in literature

In order to perform tests, an experimental set-up has to be built. From the various set-ups that have been considered at in literature, the current test set-up has been designed accordingly. Due to the fact that nanofluids are quite expensive, the set-up has been kept as small as possible. Shown below are different setups that where previously used.

A.1 Pak and Cho

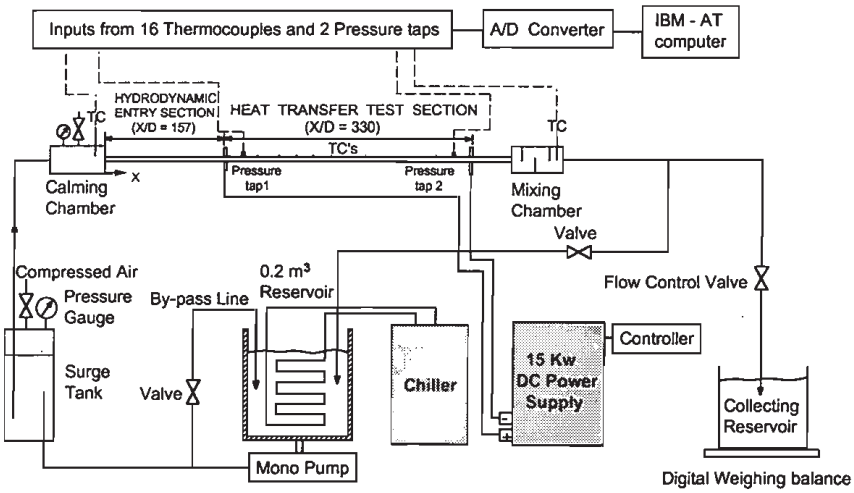

Figure A.1: Test setup used by Pak and Cho (1998)

Shown in Figure A.1 is the test setup used by Pak and Cho (1998). The test section consists out of a calming chamber, a hydrodynamic entry section, a heat transfer test section and a mixing chamber. The hydrodynamic entry section and the heat transfer test section where manufactured out of a seamless, stainless steel tube (type 304) of which the inside diameter was 10.66 mm and the total length 4 800 mm. In total 16 thermocouples and 2 pressure taps were attached to the test section. The experiments were run at a constant heat-flux boundary

condition. This was achieved by heating the test section electrically with constant DC power supply capable of delivering a maximum of 15 kW at 15 V.

A.2 Li and Xuan

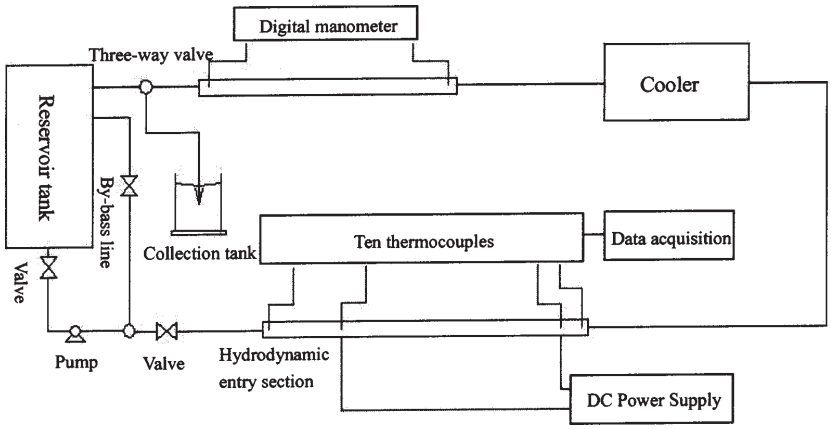

Figure A.2: Test setup used by Li and Xuan (2002) and, Xuan and Li (2003)

Shown in Figure A.2 is the test setup used by Li and Xuan (2002) and, Xuan and Li (2003). The test section consists out of a hydrodynamic entry section and a heat transfer test section. The heat transfer test section is a straight brass tube with an inner diameter of 10 mm and a length of 800 mm. 10 thermocouples are mounted at different places on the heat transfer test section to measure the wall and fluid bulk temperature. The flow loop also contains pressure drop test section of 1 m length and 12 mm internal diameter where two pressure taps are mounted. The tests were done under a constant heat-flux boundary condition. This was achieved by heating the test section electrically with a DC power supply capable of delivering a maximum of 3.5 kW.

A.3 Wen and Ding

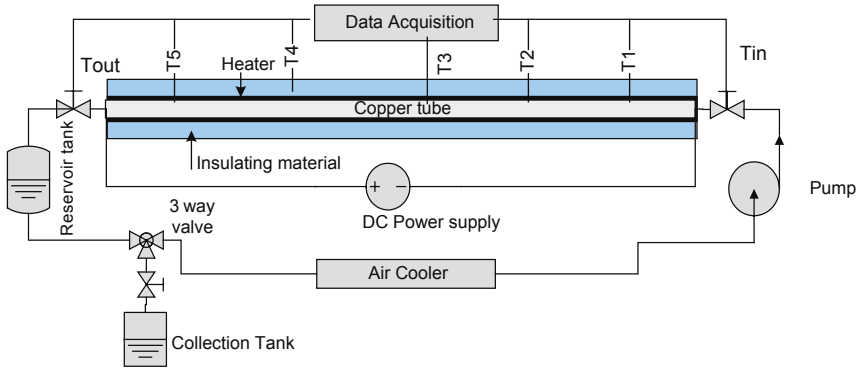

Figure A.3: Test setup used by Wen and Ding (2004) and Ding *et al.* (2006)

Shown in Figure A.3 is the test setup used by Wen and Ding (2004) and, Ding *et al.* (2006). The test section consists out of a straight copper tube with a 970 mm length and a 4.5 ±0.02 mm inner diameter. In order to achieve a constant heat-flux boundary condition the test section was heated by a silicon rubber flexible heater linked to a DC power supply of maximum 300 W power. 5 thermocouples were mounted on the test section to measure the wall temperature distribution and two further thermocouples were inserted into the flow at the inlet and exit to measure the bulk temperatures of the nanofluid.

A.4 Yang

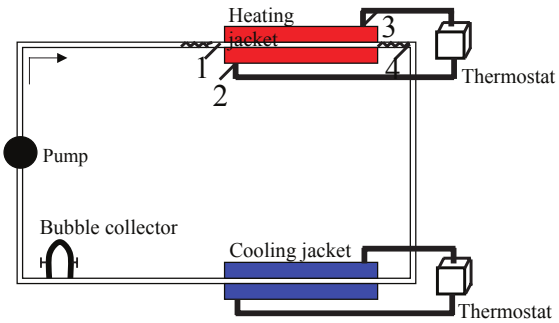

Figure A.4: Test setup used by Yang *et al.* (2005)

Shown is Figure A.4 is the test setup used by Yang *et al.* (2005). The test setup up is a small flow loop (∼ 100 ml) where the test section is thermally insulated from the loop by plastic fittings. The test section consists out of a straight 457 mm pipe with an inside diameter of 4.57 mm. The fluid was heated by a counter-current flow heating jacket in which water was used as the heating fluid. Four thermocouples were used, two of which were placed at the inlet and outlet of the test section and the other two at the inlet and outlet of the heating jacket. A cooling jacket was used to cool down the whole system.

A.5 Garg

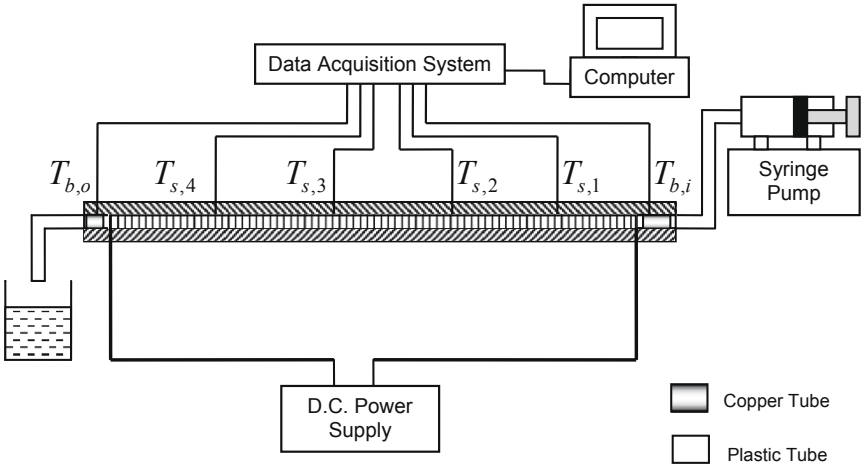

Figure A.5: Test setup used by Garg *et al.* (2009)

Shown in Figure A.5 is the test setup used by Garg *et al.* (2009).The test section consists out of a straight copper tube of 914.4 mm in length and 1.55 mm inner diameter. Tests were done under constant heat flux conditions, were the section was heated by nichrome wire which was connected to a 1.5 kW power supply. Four thermocouples were mounted to the test section and an additional two thermocouples were mounted at the inlet and outlet to measure the fluid bulk temperatures.

Appendix B

Uncertainty analysis

B.1 Introduction

In order to obtain the desired objectives of the current study, it is necessary to obtain heat transfer and friction factors for a constant heat flux boundary condition. In order to determine the accuracy of these two parameters an uncertainty analysis is performed as well as for the non-dimensional parameters such as the Reynolds and Nusselt numbers. In the case of the heat transfer parameter, the uncertainty of the heat transferred, the energy balance obtained, mass flow rates, inlet, outlet and wall temperatures will be analysed. For the friction factors the uncertainty of the differential pressure transducer, mass flow rates and dimensions of the test section will be analysed.

B.2 Theory

The result R of the experiment is calculated from a set of measurements using a group of equations. The result R is a function of several variables and is given by Moffat (1988) as:

$$R = fcn(x_1, x_2, ..., x_n) \tag{B.1}$$

Hence the effect of the uncertainty in a single measurement on the calculated result, if only that one measurement were in error would be:

$$\delta R = \frac{\partial R}{\partial x_i} \cdot \delta x_i \tag{B.2}$$

The partial derivative of R with respect to x_i is the sensitivity coefficient for the result R with respect to the measurement x_i. For several independent variables, the uncertainty of R can be found by a root-sum-square method. Hence for several independent variables the uncertainty of R is described by Moffat Moffat (1988) as:

$$\delta R = \left[\Sigma_{i=1}^{n} \left(\frac{\partial R}{\partial x_i} \cdot \delta x_i \right)^2 \right]^{0.5} \tag{B.3}$$

Terms in the uncertainty equations that 3 times smaller than the largest term are suppressed by the root-sum-square method. Hence small terms have very small effects Moffat (1988).

B.3 Uncertainties

B.3.1 Uncertainties of the instrumentation

Instrumentation that is used in the current study include thermocouples, Coriolis flow meters, pressure transducers and the power supply. Shown in Table B.1 are the uncertainties of each instrument used in the study. The uncertainty falls within the 95% confidence region.

Instrument	**Range**	**Uncertainty**
Thermocouple		
Inlet/Outlet	-200 - 350 ℃	0.1 ℃
Station	-200 - 350 ℃	0.1 ℃
Coriolis flow meter	0 - 0.07 kg/s	0.1 %
Pressure transducer	0 - 17 kPa	0.16 %
Power supply	0 - 320 V	0.33 V
	0 - 12.5 A	0.04 A

Table B.1: Ranges and accuracies of instruments used

B.3.2 Analysis

In the analysis the extremities of the flow rate are considered. The lowest flow rate corresponding to a Reynolds number of a 1 000 and the highest a Reynolds number of 8 000. First, the heat transfer uncertainties are calculated. These include all the uncertainties of the measuring equipment and the dimensionless properties. Secondly the uncertainties of the dimensionless parameters are determined and lastly, the uncertainty of the friction factor is calculated.

Heat transfer uncertainties

In- and outlet and station temperatures Since only one thermocouple was used to measure inlet temperature and one thermocouple to measure the outlet thermocouple the uncertainty of the measurement remains 0.1℃. For the stations also only one thermocouple was used and here the uncertainty is 0.1℃.

Fluid properties All fluid properties and their uncertainties were calculated from the formulations obtained by Popiel and Wojtkowiak (1998). The uncertainties of the properties are given in Table B.2

Property	**Uncertainty**
Density	0.003%
Specific heat	0.04%
Thermal conductivity	2%
Dynamic viscosity	1%

Table B.2: Uncertainties of fluid properties

Heat transfer coefficient The heat transfer coefficient is calculated from

$$h(x) = \frac{\dot{q}}{T_s(x) - T_m(x)} \tag{B.4}$$

with its uncertainty given by

$$\delta h(x) = \left[\left(\frac{\partial h(x)}{\partial \dot{q}} \cdot \delta \dot{q} \right)^2 + \left(\frac{\partial h(x)}{\partial T_s} \cdot \delta T_s \right)^2 + \left(\frac{\partial h(x)}{\partial T_m} \cdot \delta T_m \right)^2 \right]^{0.5}$$

$$\begin{aligned} \delta h(x) = \Bigg[& \left(\frac{\delta \dot{q}}{T_s(x) - T_m(x)} \right)^2 + \left(\frac{-\dot{q}}{(T_s(x) - T_m(x))^2} \cdot \delta T_s \right)^2 \\ & + \left(\frac{-\dot{q}}{(T_s(x) - T_m(x))^2} \cdot \delta T_m \right)^2 \Bigg]^{0.5} \end{aligned} \tag{B.5}$$

The wall temperatures are measured at 13 stations, and between each station the local heat transfer coefficient is calculated. The average heat transfer coefficient was obtained by adding all the local heat transfer coefficients and then dividing the result by 12.

$$h_{avg} = \frac{1}{n} \cdot (h(x_1) + ... + h(x_n)) \tag{B.6}$$

$$\delta h_{avg} = \left[\left(\frac{\partial h_{avg}}{\partial h(x_1)} \cdot \delta h(x_1) \right)^2 + ... + \left(\frac{\partial h_{avg}}{\partial h(x_n)} \cdot \delta h(x_n) \right)^2 \right]^{0.5}$$

hence the uncertainty of the average heat transfer coefficient is determined by equation B.7

$$\delta h_{avg} = \frac{1}{n} \cdot (\delta h(x_1)^2 + ... + \delta h(x_n)^2)^{0.5} \tag{B.7}$$

Fluid mean temperature The fluid mean temperature is calculated from

$$T_m(x) = T_i + \frac{\dot{q} \cdot x \cdot P}{\dot{m} \cdot c_p} \tag{B.8}$$

with its uncertainty given by

$$\begin{aligned} \delta T_m(x) = \Bigg[& \left(\frac{\partial T_m}{\partial T_i} \cdot \delta T_i \right)^2 + \left(\frac{\partial T_m}{\partial \dot{q}_{in}} \cdot \delta \dot{q}_{in} \right)^2 + \left(\frac{\partial T_m}{dx} \cdot \delta x \right)^2 \\ & + \left(\frac{\partial T_m}{\partial P} \cdot \delta P \right)^2 + \left(\frac{\partial T_m}{\partial \dot{m}} \cdot \delta \dot{m} \right)^2 + \left(\frac{\partial T_m}{\partial c_p} \cdot \delta c_p \right)^2 \Bigg]^{0.5} \end{aligned}$$

$$\begin{aligned} \delta T_m(x) = \Bigg[& (\delta T_i)^2 + \left(\frac{x \cdot P}{\dot{m} \cdot c_p} \cdot \delta \dot{q}_{in} \right)^2 + \left(\frac{\dot{q}_{in} \cdot P}{\dot{m} \cdot c_p} \cdot \delta x \right)^2 \\ & + \left(\frac{\dot{q}_{in} \cdot x}{\dot{m} \cdot c_p} \cdot \delta P \right)^2 + \left(-\frac{\dot{q}_{in} \cdot x \cdot P}{\dot{m}^2 \cdot c_p} \cdot \delta \dot{m} \right)^2 + \left(-\frac{\dot{q}_{in} \cdot x \cdot P}{\dot{m} \cdot c_p^2} \cdot \delta c_p \right)^2 \Bigg]^{0.5} \end{aligned} \tag{B.9}$$

Heat flux The heat flux is calculated from

$$\dot{q}_{in} = \dot{Q}_{in}/A_s \tag{B.10}$$

with its uncertainty given by

$$\delta\dot{q}_{in} = \left[\left(\frac{\partial\dot{q}_{in}}{\partial\dot{Q}_{in}}\cdot\delta\dot{Q}_{in}\right)^2 + \left(\frac{\partial\dot{q}_{in}}{\partial A_s}\cdot\delta A_s\right)^2\right]^{0.5}$$

$$\delta\dot{q}_{in} = \left[\left(\frac{\delta\dot{Q}_{in}}{A_s}\right)^2 + \left(-\frac{\dot{Q}_{in}}{A_s^2}\cdot\delta A_s\right)^2\right]^{0.5} \tag{B.11}$$

Heat transfer The input heat transfer uncertainty is calculated from

$$\dot{Q} = V\cdot I \tag{B.12}$$

with the uncertainty given by

$$\delta\dot{Q} = \left[\left(\frac{\partial\dot{Q}}{\partial V}\cdot\delta V\right)^2 + \left(\frac{\partial\dot{Q}}{\partial I}\cdot\delta I\right)^2\right]^{0.5}$$

$$\delta\dot{Q} = \left[(I\cdot\delta V)^2 + (V\cdot\delta I)^2\right]^{0.5} \tag{B.13}$$

Heat transfer area The heat transfer area is calculated from

$$A_s = \pi\cdot D\cdot L \tag{B.14}$$

with its uncertainty given by

$$\delta A_s = \left[\left(\frac{\partial A_s}{\partial D}\cdot\delta D\right)^2 + \left(\frac{\partial A_s}{\partial L}\cdot\delta L\right)^2\right]^{0.5}$$

$$\delta A_s = \left[(\pi\cdot L\cdot\delta D)^2 + (\pi\cdot D\cdot\delta L)^2\right]^{0.5} \tag{B.15}$$

Perimeter of test section The perimeter of the test section is calculated from

$$P = \pi\cdot D \tag{B.16}$$

with its uncertainty given by

$$\delta P = \left[\left(\frac{\partial P}{\partial D}\cdot\delta D\right)^2\right]^{0.5}$$

$$\delta P = \pi\cdot\delta D \tag{B.17}$$

Dimensionless parameters

Since all fluid flow and heat transfer equations are in terms of dimensionless parameters, the uncertainties of these parameters are determined. The Nusselt, Reynolds and Prandtl number are mainly used in the study of heat transfer their respective uncertainties are shown below.

$$Nu_{avg} = \frac{h_{avg} \cdot D}{k} \tag{B.18}$$

with its uncertainty given by

$$\delta Nu_{avg} = \left[\left(\frac{\partial Nu_{avg}}{\partial h_{avg}} \cdot \delta h_{avg} \right)^2 + \left(\frac{\partial Nu_{avg}}{\partial D} \cdot \delta D \right)^2 + \left(\frac{\partial Nu_{avg}}{\partial k} \cdot \delta k \right)^2 \right]^{0.5}$$

$$\delta Nu_{avg} = \left[\left(\frac{D}{k} \cdot \delta h_{avg} \right)^2 + \left(\frac{h_{avg}}{k} \cdot \delta D \right)^2 + \left(-\frac{h_{avg} \cdot D}{k^2} \cdot \delta k \right)^2 \right]^{0.5} \tag{B.19}$$

$$Re = \frac{4 \cdot \dot{m}}{\mu \cdot D \cdot \pi} \tag{B.20}$$

with its uncertainty given by

$$\delta Re = \left[\left(\frac{\partial Re}{\partial \dot{m}} \cdot \delta \dot{m} \right)^2 + \left(\frac{\partial Re}{\partial \mu} \cdot \delta \mu \right)^2 + \left(\frac{\partial Re}{\partial D} \cdot \delta D \right)^2 \right]^{0.5}$$

$$\delta Re = \left[\left(\frac{4}{\mu \cdot D \cdot \pi} \cdot \delta \dot{m} \right)^2 + \left(-\frac{4 \cdot \dot{m}}{\mu^2 \cdot D \cdot \pi} \cdot \delta \mu \right)^2 + \left(-\frac{4 \cdot \dot{m}}{\mu \cdot D^2 \cdot \pi} \cdot \delta D \right)^2 \right]^{0.5} \tag{B.21}$$

Friction factor uncertainties

The friction factors are calculated from its simplified definition

$$f = \frac{\Delta P \cdot \rho \cdot \pi^2 \cdot D^5}{8 \cdot L \cdot \dot{m}^2} \tag{B.22}$$

with its uncertainty given by

$$\delta f = \left[\left(\frac{\partial f}{\partial \Delta P} \cdot \delta \Delta P \right)^2 + \left(\frac{\partial f}{\partial \rho} \cdot \delta \rho \right)^2 + \left(\frac{\partial f}{\partial D} \cdot \delta D \right)^2 + \left(\frac{\partial f}{\partial L} \cdot \delta L \right)^2 + \left(\frac{\partial f}{\partial \dot{m}} \cdot \delta \dot{m} \right)^2 \right]$$

$$\begin{aligned} \delta f = \Bigg[& \left(\frac{\rho \cdot \pi^2 \cdot D^5}{8 \cdot L \cdot \dot{m}^2} \cdot \delta \Delta P \right)^2 + \left(\frac{\Delta P \cdot \pi^2 \cdot D^5}{8 \cdot L \cdot \dot{m}^2} \cdot \delta \rho \right)^2 + \left(\frac{\Delta P \cdot \rho \cdot \pi^2 \cdot 5 \cdot D^4}{8 \cdot L \cdot \dot{m}^2} \cdot \delta D \right)^2 \\ & + \left(-\frac{\Delta P \cdot \rho \cdot \pi^2 \cdot D^5}{8 \cdot L^2 \cdot \dot{m}^2} \cdot \delta L \right)^2 + \left(-\frac{\Delta P \cdot \rho \cdot \pi^2 \cdot D^5}{4 \cdot L \cdot \dot{m}^3} \cdot \delta \dot{m} \right)^2 \Bigg]^{0.5} \end{aligned} \tag{B.23}$$

B.4 Summary

The uncertainties of all the values discussed are given in Table B.3.Values for the low Reynolds number ($\approx$ 1 000) and high Reynolds number ($\approx$ 8 000) are given.

Property	**Low *Re***	**High *Re***
$\dot{m}$	1.99 %	0.20 %
T_m	0.11 ℃	0.1 ℃
$\dot{q}_{in}$	3.49 %	3.49 %
h	1.35 %	2.45 %
Nu	2.45 %	3.19 %
Re	2.26 %	1.09 %
ΔP	17.5 %	0.3 %
f	18 %	2.0 %

Table B.3: Uncertainties of the equations used

Appendix C

Preparation of nanofluids

The preparation of the nanofluid is an important process. A proper prepared nanofluid has an even, durable and stable suspension, low agglomeration of particles and no chemical change of the fluid (Trisaksri and Wongwises, 2007). Due to their size nanoparticles can stay suspended for much longer but they have the tendency to form agglomerates that can be of micrometer in size and settle out of the suspension much quicker. Hence dispersing the nanoparticles with no or very little agglomeration, giving the fluid the nano-effect, is very important (Das and Choi, 2009). The sedimentation rate can be calculated from Stokes-Einstein theory (Hiemenz, 1986) as

$$\upsilon = \frac{2r_p^2|\rho_p - \rho_f|g}{9\mu_f} \tag{C.1}$$

where r_p is the radius of the particle, ρ_p is the density of the particle, ρ_f is the density of the fluid, μ_f is the viscosity of the fluid and g is the gravitational acceleration. This means that in order to have a stable suspension the density difference has to be low, small particles and a high viscosity. According to Equation C.1 the key to stable suspension is a small particle size, since a larger viscosity is not desired due to the adverse affect it has on heat transfer and in the case of CNT nanofluids the density difference is low.

There are two methods used in producing nanofluids, the single-step and the two-step method:

In the single-step process metallic vapour is directly condensed into nanoparticles by contact with a flowing low-vapour-pressure. The method is called direct evaporation condensation (DEC) and has the advantages that nanoparticle agglomeration is minimised and there is excellent control over particle size and gives stable nanofluids (Das and Choi, 2009). But a disadvantage is that only low-vapour-pressure fluids are compatible with such a process (Wang and Mujumdar, 2007; Das and Choi, 2009).

In the two-step process nanoparticles are first produced and then dispersed into the base fluid through mechanical or ultrasonification dispersion. Mechanical dispersion is the technique were agglomerates are broken by high shear mixing. Ultrasonification is the method were an elastic wave is sent giving mechanical and thermal interaction. Ultrasonic vibration is found to be the better option for nanofluids (Das and Choi, 2009) and the time under sonification was found to be important, since a to long sonication time can reduce the aspect ratio of nanopar-

ticles. Garg *et al.* (2009) discovered that there is an optimum sonication time were you get an increase in heat transfer.

Another part of the two-step process is the chemical-dispersion method. This method is aimed at disrupting the long-range attractive Van der Waals forces (Das and Choi, 2009). This is done by electrostatic, steric dispersion or functional group coating technique.

The electrostatic method is to charge particles with similar charges and create the repulsive electrostatic forces that oppose the long-range Van der Waals forces. This is done by changing the pH of the suspension, since it controls the properties of the nanoparticle surface. At the optimal pH of the solution the surface charge of the nanoparticle increases because of the more frequent attacking of the surface hydroxyl groups (H^+ and OH^-) by potential-determining ions. This leads to an increase of the electrostatic repulsion force between the particles which results in a stable suspension with reduced agglomeration (Wang and Li, 2009). Xie it et al. (2003) investigated the effect of pH on MWCNT. The purchased MWCNT were treated with Nitric and nitric/sulphuric acid in order to modify the surface of the CNT. The treated CNT showed no aggregates and entanglements whereas the untreated CNT were entangled and aggregated when viewed under a transmission electron microscope. The treated surface of the CNT particles changes the iso-electric point of the fluid due to the hydoxyl groups formed on the particles surface. The iso-electric point is the point were the nanoparticle carries no net electrical charge and will form agglomerations since there are no sufficient repulsive forces between the nanoparticles (Lee et al., 2011). For the untreated CNT the iso-electric point was at a pH of 7.3 whereas for the treated CNT the iso-electric point was at a pH of less than 2. Ding *et al.* (2006) had a pH of 6 and 10.5 for their *MWCNT-water* nanofluid, but reported no significant difference in convective heat transfer for the different pH values. This is due to the fact that their pH of their nanofluids was far from the iso-electric point which is at a pH of 7.3.

Steric stabilisation is the process by which a surfactant is added to prevent agglomeration. Some examples of previously tested surfactants are sodium laurate (SL), sodium dodecyl benzene sulfonate (SDBS), sodium dodecyl sulfate (SDS) and Gum Arabic (GA) (Ding et al., 2006). It was found that SDBS failed at elevated temperatures (Ding et al., 2006). GA was found to stabilise the suspension best as compared to the other surfactants (Garg et al., 2009) when considering CNT. Due to the hydrophobic nature of CNT they cannot be dispersed in water under normal conditions (Garg et al., 2009), which makes dispersing of CNT in water very challenging. In order to disperse the CNT into the base fluid properly, a chemical surfactant in conjunction with a mechanical method has to be used. This includes the ultrasonification of the CNT under dry conditions (Ding et al., 2006) or ultrasonification of the solution with CNT already dispersed in the base fluid (Garg et al., 2009). After the sonification of CNT and adjusting the suspension to a preset pH level, Ding *et al.* (2006) treated the mixture with a high shear homogeniser. CNT nanofluids made in this way were found to be very stable for months without visually observable sedimentation (Ding et al., 2006).

Functionalization generally involves treating the nanoparticle with acids at high temperature. This results in addition of polar groups like $-COOH$ or $-OH$ at defect sites on the nanoparticle surface, thus making nanoparticles more hydrophilic in nature. Functionalization can however, damage the nanoparticles (Garg et al., 2009). Ko *et al.* (2007) used two different methods in preparing their CNT nanofluids. The first method was to use a surfactant. SDS was first dissolved in distilled water after which the mixture of CNTs and SDS solution was sonicated to

make a well-dispersed and homogenous suspension. The other method was to attach hydrophilic groups onto the surfaces of CNTs. Nitric/sulphuric acid mixture was used to modify the surfaces of the CNTs. The treated CNTs were then added to distilled water and the solution was sonicated producing well-dispersed and homogenous suspension. It was found that the second method produced CNT nanofluid had a lower viscosity compared to the first method. This was due to the acid treatment that soften the CNTs making the nanotubes more flexible which may reduce the friction drag under low shear rate conditions.

Appendix D

Thermal properties of the testing fluids

D.1 Properties of water

Simple formula's, which are shown below, that were developed by Popiel and Wojtkowiak (1998) are used to calculate the properties of the water:

D.1.1 Density of saturated liquid water

$$\rho = a + bT + cT^2 + dT^{2.5} + eT^3 \tag{D.1}$$

where
$a = 999.79684$, $b = 0.068317355$, $c = -0.010740248$, $d = 0.00082140905$ and
$e = -2.3030988 \cdot 10^{-5}$. The estimated uncertainty for Equation D.1 is $\pm 0.002\%$ to $\pm 0.004\%$.

D.1.2 Specific heat of water at constant pressure

$$c_p = a + bT + cT^{1.5} + dT^2 + eT^{2.5} \tag{D.2}$$

where
$a = 4.2174356$, $b = -0.0056181625$, $c = 0.0012992528$, $d = -0.00011535353$ and
$e = 4.14964 \cdot 10^{-6}$. The estimated uncertainty for Equation D.2 is $\pm 0.04\%$.

D.1.3 Thermal conductivity of water

$$k = a + bT + cT^{1.5} + dT^2 + eT^{0.5} \tag{D.3}$$

where
$a = 0.5650285$, $b = 0.0026363895$, $c = -0.00012516934$, $d = -1.5154918 \cdot 10^{-6}$ and
$e = -0.0009412945$. The estimated uncertainty for Equation D.3 is $\pm 2\%$.

D.1.4 Dynamic viscosity of water

$$\mu = \frac{1}{a + bT^1 + cT^2 + dT^3} \tag{D.4}$$

where
$a = 557.82468$, $b = 19.408782$, $c = 0.1360459$, $d = -3.1160832 \cdot 10^{-4}$. The estimated uncertainty for Equation D.4 is $\pm 1\%$.

D.2 Properties of the nanofluid

In this section the correlations that follow are from literature. The density and specific heat correlations can be used for any type of nanofluid where as the thermal conductivity and viscosity are nanofluid type dependent and have to be determined experimentally.

D.2.1 Density of the nanofluid

From literature (Pak and Cho, 1998; Maiga et al., 2006; Heris et al., 2006; Liu and Yu, 2011) the following correlation was used to estimate the density of the nanofluid:

$$\rho_{nf} = \phi \cdot \rho_p + (1 - \phi) \cdot \rho_{bf} \tag{D.5}$$

D.2.2 Specific heat of the nanofluid

From literature (Xuan and Roetzel, 2000; Heris et al., 2006; Yu et al., 2009; Liu and Yu, 2011) the following correlation was used to estimate the specific heat of the nanofluid:

$$(c_p)_{nf} = \frac{\phi \cdot (\rho c_p)_p + (1 - \phi) \cdot (\rho c_p)_{bf}}{\rho_{nf}} \tag{D.6}$$

Pak and Cho (1998) and Maiga *et al.* (2006) used a slightly different correlation to predict the specific heat of the nanofluid:

$$(c_p)_{nf} = \phi \cdot (c_p)_p + (1 - \phi) \cdot (c_p)_{bf} \tag{D.7}$$

Equation D.7 is used throughout literature the most and is also used in the current study.

D.2.3 Thermal conductivity of the nanofluid

Xue (2005) developed a numerical model for the effective thermal conductivity of CNT nanofluids based on the Maxwell theory. The model shows that the aspect ratio and the space distribution of the CNTs can largely affect the thermal conductivity of nanofluids and that a low volume concentration can result in a large enhancement of the effective thermal conductivity. Shown in Equation D.8 is the model for the effective thermal conductivity for CNT nanofluids:

$$k_{eff} = k_{bf} \frac{1 - \phi + 2\phi \frac{k_p}{k_p - k_{bf}} ln \frac{k_p + k_{bf}}{2k_{bf}}}{1 - \phi + 2\phi \frac{k_{bf}}{k_p - k_{bf}} ln \frac{k_p + k_{bf}}{2k_{bf}}} \tag{D.8}$$

Nan *et al.* (2003) developed correlation for the thermal conductivity of CNT composites. The used various effective medium approach (EMA) like the Maxwell-Garnett approximation to determine the effective thermal conductivity of different composite structures. The MG-EMA model for CNT is valid for matrix-based composites in which the nanotubes are surrounded by the matrix. The correlation is shown in Equation D.9:

$$k_{eff} = \frac{3k_{bf} + \phi k_p}{3 - 2\phi} \tag{D.9}$$

D.2.4 Dynamic viscosity of the nanofluids

The viscosity of dilute suspensions (< 5 vol%) of small and rigid spherical particles was treated by Einstein in 1906 and is given by Equation D.10 (Hiemenz, 1986):

$$\mu_{nf} = \mu_{bf}(1 + 2.5\phi) \tag{D.10}$$

The equation can be extended to include ellipsoidal particles (Prasher et al., 2006b; Ferouillat et al., 2011):

$$\mu_{nf} = \mu_{bf}(1 + C_\mu \phi) \tag{D.11}$$

where C_μ depends on the ratio of the revolution ellipsoid axes and is equal to 2.5 for spherical particles.

Appendix E

Uncertainty analysis of the *MWCNT-water* nanofluids

E.1 Introduction

A similar procedure is followed as that of the uncertainty analysis of water. Only the uncertainty of the nanofluid properties are discussed here since the uncertainty of the heat transfer and friction factor use the same equations as discussed in Appendix B. First the uncertainty of the density and specific heat are discussed using the equations found in Appendix D. To calculate the uncertainty of the thermal conductivity and viscosity of the nanofluids, Equation 5.1 and Equation 5.4 are respectively used. The chapter ends with the heat transfer and friction factor uncertainties for the *MWCNT-water* nanofluids.

E.2 Uncertainty of the *MWCNT-water* nanofluid properties

E.2.1 Density

The density of the nanofluid is calculated from

$$\rho_{nf} = \phi \cdot \rho_p + (1 - \phi) \cdot \rho_{bf} \tag{E.1}$$

with the uncertainty given by

$$\delta\rho_{nf} = \left[\left(\frac{\partial \rho_{nf}}{\partial \rho_{bf}} \cdot \delta\rho_{bf} \right)^2 \right]^{0.5}$$

$$\delta\rho_{nf} = (1 - \phi) \cdot \delta\rho_{bf} \tag{E.2}$$

E.2.2 Specific heat

The specific heat of the nanofluid is calculated from

$$(c_p)_{nf} = \phi \cdot (c_p)_p + (1 - \phi) \cdot (c_p)_{bf} \tag{E.3}$$

with the uncertainty given by

$$\delta(c_p)_{nf} = \left[\left(\frac{\partial(c_p)_{nf}}{\partial(c_p)_{bf}} \cdot \delta(c_p)_{bf}\right)^2\right]^{0.5}$$

$$\delta(c_p)_{nf} = (1-\phi) \cdot \delta(c_p)_{bf} \tag{E.4}$$

E.2.3 Thermal conductivity

The thermal conductivity of the nanofluid is calculated from

$$k_{nf} = k_{bf} \cdot (1 + C_k \cdot \phi) \tag{E.5}$$

with the uncertainty given by

$$\delta k_{nf} = \left[\left(\frac{\partial k_{nf}}{\partial k_{bf}} \cdot \delta k_{bf}\right)^2 + \left(\frac{\partial k_{nf}}{\partial C_k} \cdot \delta C_k\right)^2\right]^{0.5}$$

$$\delta k_{nf} = \left[((1 + C_k \cdot \phi) \cdot \delta k_{bf})^2 + (k_{bf} \cdot \phi \cdot \delta C_k)^2\right]^{0.5} \tag{E.6}$$

where the uncertainty of C_k, with a confidence level of 95%, is 10%.

E.2.4 Viscosity

The viscosity of the nanofluid is calculated from

$$\mu_{nf} = \mu_{bf} \cdot (1 + C_\mu \cdot \phi) \tag{E.7}$$

with the uncertainty given by

$$\delta\mu_{nf} = \left[\left(\frac{\partial \mu_{nf}}{\partial \mu_{bf}} \cdot \delta\mu_{bf}\right)^2 + \left(\frac{\partial \mu_{nf}}{\partial C_\mu} \cdot \delta C_\mu\right)^2\right]^{0.5}$$

$$\delta\mu_{nf} = \left[((1 + C_\mu \cdot \phi) \cdot \delta\mu_{bf})^2 + (\mu_{bf} \cdot \phi \cdot \delta C_\mu)^2\right]^{0.5} \tag{E.8}$$

where the uncertainty of C_μ, with a confidence level of 95%, is 1%.

E.3 Uncertainties of the *MWCNT-water* nanofluid properties compared to that of water

Table E.1 compares the nanofluid properties to that of water. The uncertainty of the density and the specific heat for the nanofluid are the same as that of the water, since they largely only depend on the uncertainty of the water properties. There is slight change in the thermal conductivity of the 0.75 vol% and 1.0 vol% of the *MWCNT-water* nanofluid compared to water where as there is a bigger change when comparing the viscosity. This could be due to the coefficient of Equation 5.4 being significantly larger than that of Equation 5.1.

Property	**Water**	**0.33 vol%**	**0.75 vol%**	**1.0 vol%**
Density	0.003%	0.003%	0.003%	0.003%
Specific heat	0.04%	0.04%	0.04%	0.04%
Thermal conductivity	2%	2%	2.1%	2.1%
Viscosity	1%	1.2%	1.5%	1.6%

Table E.1: Uncertainties of properties for water and *MWCNT-water* nanofluid

E.4 Heat transfer and friction factor uncertainties

Table E.2 up to Table E.4 list the uncertainties of the heat transfer and friction factors for the *MWCNT-water* nanofluids. Shown are the uncertainties of the mass flow rate, mean temperature of the fluid, heat flux, heat transfer coefficient, Nusselt number, Reynolds number, pressure drop and friction factor at lowest and highest Reynolds number tested. For the 0.33 vol% *MWCNT-water* nanofluid the lowest Reynolds number tested was approximately 850 and the highest approximately 7 000. For the 0.75 vol% *MWCNT-water* nanofluid the lowest Reynolds number tested was approximately 700 and the highest approximately 6 000. For the 1.0 vol% *MWCNT-water* nanofluid the lowest Reynolds number tested was approximately 600 and the highest approximately 5 200.

Property	**Low *Re***	**High *Re***
$\dot{m}$	1.92%	0.21%
T_m	0.1 °C	0.1 °C
$\dot{q}_{in}$	3.49%	3.49%
h	1.28%	2.44%
Nu	2.45%	3.20%
Re	2.30%	1.28%
ΔP	11.5%	0.33%
f	12.3%	2.01%

Table E.2: Uncertainties of the 0.33 vol% *MWCNT-water* nanofluid

Property	**Low *Re***	**High *Re***
$\dot{m}$	1.94%	0.20%
T_m	0.1 °C	0.1 °C
$\dot{q}_{in}$	3.49%	3.49%
h	1.27%	2.40%
Nu	2.49%	3.22%
Re	2.46%	1.51%
ΔP	14.1%	0.31%
f	14.7%	2.01%

Table E.3: Uncertainties of the 0.75 vol% *MWCNT-water* nanofluid

Property	**Low *Re***	**High *Re***
$\dot{m}$	1.94%	0.21%
T_m	0.1 °C	0.1 °C
$\dot{q}_{in}$	3.49%	3.49%
h	1.22%	2.33%
Nu	2.5%	3.19%
Re	2.55	1.66%
ΔP	-	-
f	-	-

Table E.4: Uncertainties of the 1.0 vol% *MWCNT-water* nanofluid